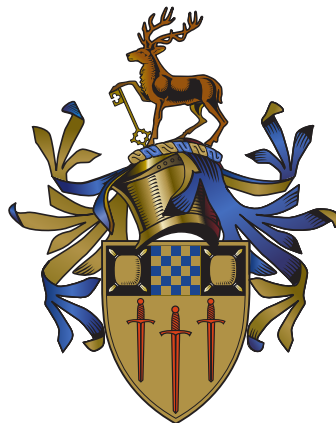


MEASUREMENT UNCERTAINTY IN NONLINEAR
BEHAVIOURAL MODELS OF MICROWAVE AND
MILLIMETRE-WAVE AMPLIFIERS

Laurence Stant



This thesis is submitted for the degree of Doctor of Philosophy

Department of Electrical and Electronic Engineering
Faculty of Engineering and Physical Sciences
University of Surrey

Principal Supervisor: Dr. Peter H. Aaen
Collaborative Supervisor: Prof. Nick M. Ridler (NPL)

©Laurence Stant
September 2019

Declaration of Authorship

This thesis and the work to which it refers are the results of my own efforts. Any ideas, data, images or text resulting from the work of others (whether published or unpublished) are fully identified as such within the work and attributed to their originator in the text, bibliography or in footnotes. This thesis has not been submitted in whole or in part for any other academic degree or professional qualification. I agree that the University has the right to submit my work to the plagiarism detection service TurnitinUK for originality checks. Whether or not drafts have been so assessed, the University reserves the right to require an electronic version of the final document (as submitted) for assessment as above.

Laurence Stant (Author)

Date

“What error drives our eyes and ears amiss? Until I know this sure uncertainty I’ll entertain the offered fallacy.”

William Shakespeare, The Comedy of Errors

“That’s right!” shouted Vroomfondel, “we demand rigidly defined areas of doubt and uncertainty!”

Douglas Adams, The Hitchikers Guide to the Galaxy

Abstract

To support the responsible implementation of next-generation wireless communications networks such as 5G, the efficiency of power amplifiers located in both base-stations and mobile handsets must be improved. This improvement will also benefit other areas of wireless innovation such as satellite communications, military and civilian short-range radar (automotive and gesture tracking), and future submillimetre-wave communications. Significant efficiency gains can be obtained by using nonlinear amplifier techniques, however these cause undesired distortion to the signal. Methods used to mitigate these effects rely on accurate models extracted from the internal transistors, which circuit simulators interrogate to predict the performance of new amplifier designs. This thesis presents the first evaluation of measurement uncertainty propagated into a nonlinear behavioural model, X-parameters, and used within a circuit simulator to provide confidence in the results. This uncertainty evaluation can also reveal the relative uncertainty contributions from different aspects of the measurement setup, the knowledge of which can be used to make informed improvements in manufacturing test laboratories. The evaluation was tested on a millimetre-wave amplifier designed for communications use, which showed encouraging results when simulated in a test circuit to provide figures for gain and PAE. During development of this uncertainty evaluation, a standard guidance document was reviewed and found to contain ambiguities which significantly affect scattering-parameter measurements commonly used in RF laboratories. This ambiguity is highlighted to inform those working on revisions that is must be addressed. Finally, traditional uncertainty evaluation techniques for vector network analyser measurements in coaxial transmission lines are applied to rectangular metallic waveguide setups to investigate their success. Waveguide concerning frequencies up to 750 GHz are considered, covering E-band and higher which are being developed for future high-bandwidth communications. Although the uncertainty evaluation techniques work well for most waveguides tested, mechanical issues in WR-1.5 prohibits the feasibility of the technique.

Research Outcomes

Publications

- [1] H. Votsi, L. T. Stant, M. J. Salter, C. Li, N. M. Ridler, and P. H. Aaen, “An interferometric characterization technique for extreme impedance microwave devices,” in *94th ARFTG Microw. Meas. Conf.*, San Antonio, TX, USA, Jan. 2020 (accepted).
- [2] M. J. Salter, L. T. Stant, K. Buisman, and T. Nielsen, “An inter-laboratory comparison of NVNA measurements,” in *Workshop on Integr. Nonlinear Microw. and Millimetre-Wave Circuits*, Brive, France, Jul. 2018.
- [3] L. T. Stant, M. J. Salter, N. M. Ridler, D. F. Williams, and P. H. Aaen, “Propagating measurement uncertainty to microwave amplifier nonlinear behavioural models,” *IEEE Trans. Microw. Theory Techn.*, vol. 67, no. 2, pp. 815–821, Nov. 2018.
- [4] L. T. Stant, P. H. Aaen, and N. M. Ridler, “Evaluating residual errors in waveguide VNAs from microwave to submillimetre-wave frequencies,” *IET Microw. Antennas Propag.*, vol. 11, no. 3, pp. 324–329, Feb. 2017.
- [5] ——, “Comparing methods for evaluating measurement uncertainty given in the JCGM ‘evaluation of measurement data’ documents,” *Measurement*, vol. 94, pp. 847–851, Dec. 2016.
- [6] ——, “Evaluating residual errors in waveguide network analysers from microwave to submillimetre-wave frequencies,” in *IET Colloq. on Millimetre-Wave and Terahertz Eng. & Technol.*, London, U.K.: Institution of Engineering and Technology (IET), Mar. 2016.

Presentations

- [1] L. T. Stant, “Comparing methods for evaluating measurement uncertainty given in the JCGM ‘evaluation of measurement data’ documents,” 2nd NPL Postgraduate Institute Annual Conference, Teddington, UK, Oct. 2017 (Oral & Poster).
- [2] ——, “Comparing methods for evaluating measurement uncertainty given in the JCGM ‘evaluation of measurement data’ documents,” Faculty of Engineering and Physical Sciences Annual Festival of Research, University of Surrey, Jun. 2017 (Poster).
- [3] ——, “Evaluating measurement uncertainty in microwave and terahertz frequency metrology,” 6th Annual Postgraduate Research Conference, University of Surrey, Apr. 2016 (Oral).
- [4] L. T. Stant, P. H. Aaen, and N. M. Ridler, “Evaluating residual errors in waveguide network analysers from microwave to submillimetre-wave frequencies,” in *IET Colloq. on Millimetre-Wave and Terahertz Eng. & Technol.*, London, U.K.: Institution of Engineering and Technology (IET), Mar. 2016 (Oral).

Acknowledgements

I would like to thank my supervisory team: Peter Aaen, Nick Ridler and Marian Florescu. Peter and Nick gave me many opportunities throughout the project and were especially helpful and encouraging when problems arose. Marian took over as my primary supervisor while writing this dissertation and offered great advice and support to help me complete my work.

Martin Salter at the National Physical Laboratory (NPL), Teddington, who learned about nonlinear behavioural models and their extraction alongside me, always provided fruitful discussions and these helped me a great deal in my understanding of the science and mathematics. Martin also assisted with or performed some of the measurements in our publications.

I would also like to thank Daniel Stokes and other scientists in the electromagnetic measurements labs at NPL, who provided training and access to use their equipment, including the National primary standards for impedance in a variety of coaxial and waveguide media. Their welcoming and friendly nature also made every trip to NPL interesting, even when the schedule consisted entirely of repeated measurements!

I must extend huge thanks to Dylan Williams and his group at the National Institute for Standards and Technology (NIST) in Boulder, CO, USA. When I made contact with Dylan in regards to extending his existing software uncertainty framework he was immediately helpful and encouraging. He extended his upcoming UK trip to European Microwave Week and stayed at the university for an additional week to work with me expanding his software. The following year he invited me to visit NIST for three weeks to spend more time integrating behavioural model extraction into his software, and to characterise phase references used in my experiments. Both Dylan and his colleagues were excellent hosts and it was really exciting to work in an office with so much knowledge and experience. Special thanks also to Gustavo Avolio who performed the characterisation of our phase references, and also reviewed my final publication.

Away from my desk, my mother has provided me with a lot of support during my studies and put up with my various complaints. She has never stopped believing that I could finish my project and must feel quite vindicated now!

I am enormously grateful to my colleague and friend throughout my entire university career, Sean Gillespie. Together we were Peter's first PhD students at the University of Surrey, and experienced all the ups and downs of starting a new lab. We saw the university change a lot over the previous nine years, and I'm sure we will both look back in future with very fond memories of it.

Finally, last but not least, I would like to thank my fellow students and staff at the Advanced Technology Institute at the University of Surrey: Haris, Gemma, Jonas, Morgan, Steve, Matei, Tony, John, Grace, Julian, Jose, Kostis, Scott, James, Bob - the list goes on. Together they made my time as a postgraduate thoroughly enjoyable and I will miss them all!

Contents

	Page
List of Figures	viii
List of Tables	x
List of Abbreviations	xi
1 Introduction	1
1.1 Motivation	1
1.2 Prior Research	4
1.3 Objectives	6
1.4 Contributions	7
1.5 Thesis Structure	7
2 Radio Frequency and Microwave Measurements	9
2.1 Introduction	9
2.2 Electromagnetic Wave Parameters	10
2.2.1 Wave Definitions	10
2.2.2 Derived Metrics and Figures of Merit	11
2.3 Measurements of Nonlinear Devices	14
2.4 Vector Network Analysers	16
2.4.1 Architecture	16
2.4.2 Error Models	19
2.4.3 Calibration	22
2.5 Nonlinear Vector Network Analysers	24
2.5.1 Absolute Eight-Term Error Model	25
2.5.2 Power Meter Calibration	25
2.5.3 Phase Reference	26
2.6 Conclusions	27
3 Measurement Uncertainty	28
3.1 Introduction	28
3.2 The Measurement Process	33
3.2.1 Modelling the Measurement	33
3.2.2 Evaluating Standard Uncertainty of Input Quantities	34
3.2.3 Evaluating Combined Standard Uncertainty	44
3.2.4 Expanded Uncertainty and Coverage Intervals	47
3.3 Sensitivity Analysis	48

3.4	Conclusions	49
4	Evaluating Uncertainty in VNA Measurements	51
4.1	Introduction	51
4.2	VNA Measurement Model Input Quantities	52
4.2.1	Calibration Standards	52
4.2.2	Noise	56
4.2.3	Repeatability	58
4.2.4	Drift	58
4.3	Simplified Residual Model for VNA Uncertainty Evaluation	59
4.3.1	Method	59
4.3.2	Application to Waveguide VNAs	65
4.4	Rigorous Models for VNA Uncertainty Evaluation	71
4.4.1	Method	71
4.4.2	Keysight PNA-X Dynamic S-parameter Uncertainty	71
4.4.3	METAS VNA Tools II	73
4.4.4	NIST Microwave Uncertainty Framework	73
4.5	NVNA Uncertainty Evaluation	75
4.5.1	Phase Reference	75
4.5.2	Power Meter	77
4.5.3	Propagation of Uncertainties	79
4.6	Conclusion	81
5	Prop. Meas. Unc. To Nonlinear Behavioural Models	85
5.1	Introduction	85
5.2	Nonlinear Behavioural Models	86
5.2.1	The Volterra “VIOMAP” Model	86
5.2.2	Scattering Functions	87
5.2.3	Hot S-parameters	87
5.2.4	X-Parameters	88
5.2.5	The Cardiff Model	91
5.3	X-Parameter Extraction Procedure	91
5.3.1	Method	92
5.3.2	Implementation	96
5.4	Evaluation of the Combined Standard Uncertainty of X-Parameters Extracted from Measurement Data	100
5.4.1	X-Parameter Uncertainties	102
5.4.2	Sensitivity Analysis for X-parameter Uncertainties	105
5.5	Propagation of Uncertainty from X-Parameters into Circuit Simulations	105
5.6	Conclusions	107
6	Conclusion	111
6.1	Future Work	113
References		113
Appendix A		126
Appendix B		136

List of Figures

1.1	The past and predicted trends of global mobile subscribers [1].	2
1.2	A typical packaged RF power transistor [7].	3
2.1	The frequency dependence of a bandstop filter.	12
2.2	An illustration of gain compression.	14
2.3	Intermodulation products from two interacting tones.	16
2.4	Structure of a one-port reflectometer.	17
2.5	Structure of a two-source mixer-based VNA.	18
2.6	The three-term VNA error model.	19
2.7	The eight-term VNA error model.	21
2.8	The power calibration of an NVNA.	26
2.9	The phase calibration of an NVNA.	27
3.1	Egyptian royal cubit rod of Maya.	29
3.2	An illustration of measurement traceability.	30
3.3	Propagation of measurement uncertainty.	36
3.4	Scaling factor to convert from a GUM standard uncertainty to a GUM Supplement.	38
3.5	Plot of minimum observations for valid GUM Supplement uncertainty evaluation.	42
3.6	Propagation of probability distributions used in GUM Supplement 1.	45
3.7	Sensitivity analysis example results.	49
4.1	Structure of VNA uncertainty evaluation.	53
4.2	A graphical representation of the ripple extraction technique, including a possible failure mechanism.	61
4.3	Measurements of residual directivity performed in coaxial transmission line.	63
4.4	Measurements of residual TPM performed in coaxial transmission line.	64
4.5	Magnitude of the reflection measurement of a matched load and a short-circuit offset by a length of coaxial line.	66
4.6	Test port setup used for residual directivity measurements in WR-1.5 waveguide.	68
4.7	Phase plot for a residual directivity evaluation performed in WR-1.5 waveguide using an SOSLT calibration.	69
4.8	Time domain representation of the pulse train which creates the harmonic comb in the frequency domain.	77
4.9	Results of the phase reference characterisation performed at NIST for unit MY51256113 displayed using the MUF measurement viewer software.	78
4.10	A chart showing dominant uncertainty contributions within the power meter measurement.	79

4.11	An example sensitivity analysis showing the effect of power meter uncertainties on an X-parameter measurement.	80
4.12	The NVNA measurement model used in [16]. Here, Polyharmonic Distortion (PHD) Modeling can be substituted for X-parameters or alternative nonlinear behavioural models.	82
4.13	The LSNA calibration tab of the MUF VNA Uncertainty Calculator application.	83
5.1	Device-under-test model representation.	86
5.2	Performance of hot S-parameter models with different <i>hotS22</i> definitions.	89
5.3	The harmonic superposition principle.	89
5.4	Relationship of device output against input wave phase for different nonlinear behavioural models.	92
5.5	NVNA setup required for X-parameter measurements.	93
5.6	Offset-phase X-parameter extraction procedure.	94
5.7	X-parameter uncertainty processing flow.	98
5.8	The measurement setup used for extracting X-parameters from the DUT.	101
5.9	Histogram comparing the Monte Carlo and sequential perturbation uncertainty results for the DUT.	103
5.10	Estimates and standard uncertainties for the magnitude and phase of a sample of the extracted X-parameters.	104
5.11	Sensitivity analysis results for a sample of the extracted X-parameters.	106
5.12	An example circuit simulation schematic using an X-parameter model incorporating uncertainties in ADS.	108
5.13	Results from an ADS circuit simulation using an X-parameter model incorporating uncertainties in ADS.	109

List of Tables

1.1	Summary of prior research into RF vector network analyser measurement uncertainty.	6
3.1	GUM and GUM Supplement example values.	40
3.2	GUM and GUM supplement example results comparison.	40
3.3	GUM and GUM supplement demonstration S-parameter measurement results. .	41
4.1	Residual directivity and TPM values obtained for 3.5 mm coaxial line VNA calibrations as measured by the ripple extraction method.	66
4.2	Residual directivity and TPM values of WR-15 and WR-05 waveguide VNA calibrations as measured by the ripple extraction method.	66
4.3	Residual directivity and TPM values of WG25 and WG30 waveguide VNA calibrations as measured by the ripple extraction method.	67
4.4	Residual directivity and TPM values of two WR-1.5 waveguide VNA calibrations as measured by the ripple extraction method.	68
5.1	Nominal values and standard uncertainties for the TRL coaxial line standards. .	101
5.2	Standard uncertainties for power meter uncertainty contributions derived in [110]	102
5.3	Nominal phase and standard uncertainty for harmonic phase reference at calibration frequencies	102

List of Abbreviations

5G Fifth-Generation (cellular network technology)

AC Alternating Current

ACPR Adjacent Channel Power Ratio

ADS Advanced Design System

ANAMET Automatic Network Analyser Metrology

BER Bit Error Rate

BIPM International Bureau of Weights and Measures

CFEr Calibration Factor Error

DC Direct Current

DUT Device Under Test

EURAMET European Association of National Metrology Institutes

EVM Error Vector Magnitude

GUM Guide to the Expression of Uncertainty in Measurement

IEC International Electrotechnical Commission

IEEE Institute of Electrical and Electronics Engineers

IFBW Intermediate Frequency Bandwidth

IFCC International Federation of Clinical Chemistry and Laboratory Medicine

ILAC International Laboratory Accreditation Cooperation

InsE Instrumentation Error

ISO International Organisation for Standardisation

IUPAC International Union of Pure and Applied Chemistry

- IUPAP** International Union of Pure and Applied Physics
- LPU** Law of Propagation of Uncertainty
- LSNA** Large Signal Network Analyser
- LSOP** Large Signal Operating Point
- METAS** (Swiss) Federal Institute of Metrology
- MUF** Microwave Uncertainty Framework
- NIST** (US) National Institute of Standards and Technology
- NMDG** Network Measurement and Description Group
- NMI** National Metrology Institute
- NPL** (UK) National Physical Laboratory
- NVNA** Nonlinear Vector Network Analyser
- OIML** International Organisation of Legal Metrology
- PAE** Power-Added Efficiency
- PHD** Polyharmonic Distortion
- RF** Radio Frequency
- ROMM** Reference Oscillator Mismatch
- ROPU** Reference Oscillator Power Uncertainty
- SI** International System of Units
- SOL** Short-Open-Load
- SOLR** Short-Open-Load-Reflect
- SOLT** Short-Open-Load-Thru
- SOSLT** Short-Offset-Short-Load-Thru
- TRL** Thru-Reflect-Line
- TPM** Test Port Match
- UKAS** United Kingdom Accreditation Service
- VIM** International Vocabulary of Metrology
- VIOMAP** Volterra Input-Output Map
- VNA** Vector Network Analyser
- ZCOE** Zero Carryover Error
- ZSEr** Zero Set Error

1 Introduction

1.1 Motivation

Telecommunications underpins our modern world. Both business and leisure activities rely on the connectivity of digital devices, and telecoms increasingly relied upon for safety-critical services in emergencies. The use of mobile devices continues to rise year-on-year at a rate such that it is predicted there will be 8.4 billion mobile broadband internet subscriptions by 2024 [1], as shown in Figure 1.1. To achieve the bandwidth and access needs for this demanding challenge requires continuous technological development. The next iteration of technology to be deployed, the fifth-generation cellular network technology (5G), involves substantial hardware innovations to satisfy these requirements. One of the most significant proposed additions for 5G networks is a dramatic increase in the number of base stations required to serve mobile devices. This is a cause for concern due to the energy efficiency of the high power amplifiers in the final stage of the base station, which amplify the output of the network to drive the antennas. In addition, the efficiency of the amplifiers in mobile devices is important due to the billions of them in use.

We are increasingly aware of the effects of climate change and our responsibility to reduce our impact on the environment. Energy consumption is a key area where this can be addressed, so it is desirable to improve the efficiency of new cellular amplifiers, especially if many more will soon be deployed. In addition to mobile communications, the same efficiency gains will benefit satellite links, radar and future generation wireless systems. From a communications perspective, the ideal choice is a linear amplifier, however the efficiency of such amplifiers is limited to 50% [2]. Alternatively, amplifiers operated in the nonlinear regime can use methods which are not fundamentally limited in their efficiency, with recent performance as high as 70% [3], [4]. The problem with using nonlinear amplifiers for communications is that they distort the signal, causing errors in the received data. To obtain both good linearity and high efficiency,

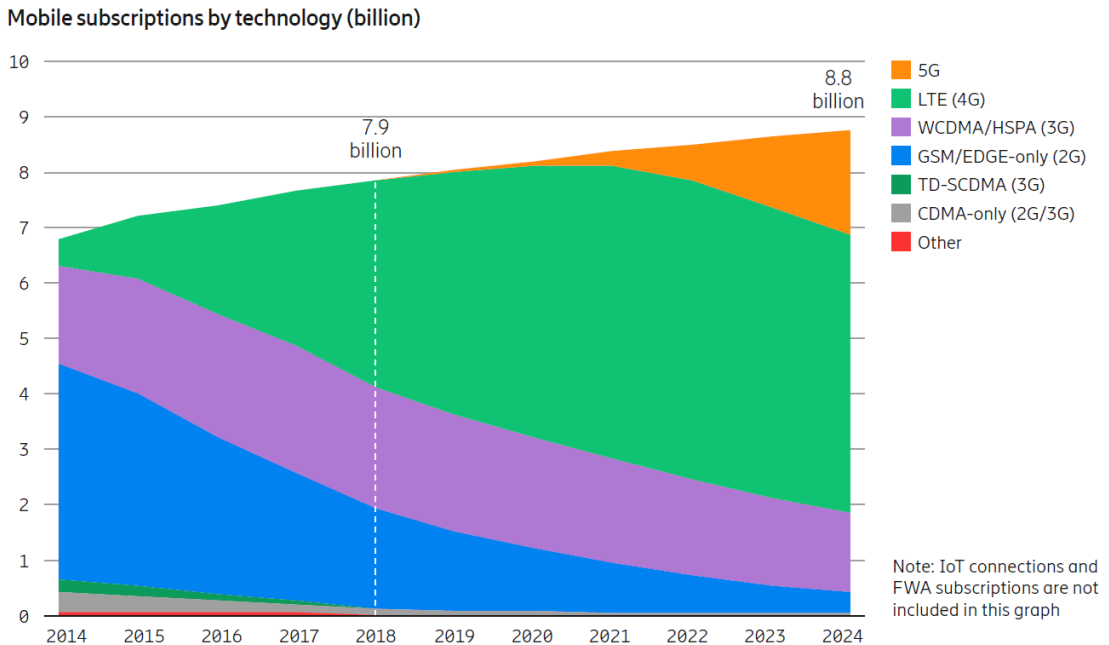


Figure 1.1: The past and predicted trends of global mobile subscribers [1].

innovative designs are used such as Doherty configurations with deeply backed-off nonlinear amplifiers [5]. In addition, digital pre-distortion (DPD) and filtering can be applied to correct for remaining nonlinear effects in the output. To design advanced amplifiers such as these, engineers rely on accurate models of the active device (a radio-frequency (RF) power transistor), an example of which is shown in Figure 1.2. These models are a critical part of the amplifier design process and many large-scale manufacturers have a dedicated team of engineers devoted to developing them. There are three main categories of model in use [6]:

- *Physical models* are defined by the physics-based equations which describe the internal structure and materials of the transistor. They can be used in the early stages of the design process when the transistor die itself is developed and also during integration into the package. Due to their computational complexity they are not used in later packaged amplifier or system simulation stages.
- *Compact models* represent the transistor as an equivalent-circuit of lumped components. The parameters of the model are found during extraction, where various measurements are made of the device and the model is fitted to the results. Compact models can be used in circuit simulators to integrate transistors into full amplifier systems, which can contain



Figure 1.2: A typical packaged RF power transistor [7].

multiple transistors and passive components.

- *Behavioural models* are entirely measurement based and their formulation does not vary with the internal structure of the device. This “black-box” approach is very attractive to industry as it minimises the intellectual property which must be shared with users of their product. In addition, less time is spent when compared to validating a custom compact model. However, more advanced effects like temperature dependency can be more difficult to integrate than with physical and compact models. Like compact models, behavioural models are used in circuit simulators at the amplifier design stage.

Between the foundry, transistor manufacturer and amplifier designer, all three categories of model may be used for a particular product. It is important in this competitive industry for fast time-to-market and therefore first-pass design success is always a target for amplifier designers. To enable this, transistor models must be as accurate as possible to ensure the simulated performance matches the physical reality. Measurements of transistors are critical to both compact and behavioural models, which means the quality and confidence of those measurements are a significant factor in increasing device performance. In addition, functional testing at the end of manufacture relies on measurements of these devices to provide quality assurance to their customers.

To provide confidence in measurements, an evaluation of any uncertainty in their result is required. All measurements have sources of error which contribute to uncertainty, and the sci-

ence of metrology is concerned with quantifying and minimising these uncertainties. Due to the prevalence of measurement in science and commerce, National Metrology Institutes (NMIs) exist, such as the National Physical Laboratory (NPL) in the UK, to improve confidence in measurements via traceability to national standards and the development of new measurement methods. The recent challenges from next-generation cellular technologies presents opportunities for new metrology. These include increasing the upper frequency of advanced measurement techniques to millimetre-wave and beyond for 5G network back-haul applications, developing an understanding of measurement uncertainties in nonlinear device measurements, and incorporating these uncertainties into compact and behavioural models of nonlinear amplifiers. The latter point has significant benefits to the amplifier design community. Firstly, confidence in the extraction of the model can be quantified. This allows the designer to decide if the model is suitable and if first-pass design success is likely when compared with their tolerances and requirements [8]. If the sensitivities to different sources of error are propagated into the model, then it is possible to make informed investments to improve the accuracy of relevant measurement instrumentation. Secondly, both compact and behavioural models do not recreate the device response perfectly, typically ignoring some higher-order effects. If measurement uncertainty from the model extraction is propagated into the model itself, then any unaccounted error between the model and the device measurements must be attributed to model inaccuracies [9]. The research in this dissertation evaluates traditional NMI metrology at higher frequencies and introduces a method to incorporate measurement uncertainty into behavioural models of power amplifiers for use with 5G.

1.2 Prior Research

Vector network analyser (VNA) metrology has been prevalent at NMIs for decades, resulting in the publication of guidance documents for laboratory use [10], [11]. However, rigorous evaluations of VNA measurement uncertainty, which include all significant sources of error and propagates their uncertainties into the result, have only occurred relatively recently. These evaluations can support either of two different propagation techniques (or both): Numerical propagation, implemented using either Monte Carlo or finite-difference methods, requires only the knowledge of equations describing the measurement (the “measurement model”). Analytical propagation is typically implemented using the Law of Propagation of Uncertainty (LPU) [12], which requires the first-order derivatives of the measurement model to be derived. Although faster than nu-

merical propagation, it cannot easily produce accurate probability distributions for the results of complicated measurement models which Monte Carlo methods can. For VNA measurements, rigorous uncertainty evaluations using numerical propagations has been demonstrated in [13], and the popular software framework “VNA Tools II” from the Swiss NMI METAS provides a free easy-to-use implementation [14]. Analytical propagation is also provided by this software package using automatic differentiation techniques, and an explicit derivation can be found in [15].

Nonlinear Vector Network Analysers (NVNAs) are used to perform the measurements required to extract compact and behavioural models of nonlinear amplifiers, and these instruments can be based on a modified version of a VNA. Recent research has built upon the knowledge of VNA metrology in order to adapt uncertainty evaluations to support NVNA measurements. Lin and Zhang provided the first uncertainty evaluation using analytical propagation in 2012 [16], which has been followed by the Microwave Uncertainty Framework (MUF) software tool from the US NMI, the National Institute for Standards and Technology (NIST), providing numerical propagation methods [17], [18].

The only propagation of measurement uncertainty into a nonlinear model of a microwave amplifier prior to the work covered in this dissertation was by Cheron et al. in 2018 [9]. This evaluation of uncertainty used a numerical propagation provided by [17] and extended the framework to include the extraction of parameters for a compact model. To date, there has been no published work regarding uncertainty evaluations for extracted behavioural models of nonlinear microwave amplifiers.

A concise view of prior research is shown in Table 1.1. Further detail of the work summarised here is given in subsequent chapters.

Measurement	Numerical Propagation	Analytical Propagation
VNA (S-parameters)	[13], [14]	[14], [15]
NVNA (power waves)	[17], [18]	[16]
Compact model	[9], [19]	None
Behavioural model	None	None

Table 1.1: A brief summary of prior research in the area of RF vector network analyser measurement uncertainty. Work shown provides a rigorous evaluation of uncertainty using either numerical or analytical uncertainty propagation methods.

1.3 Objectives

This research has explored three main objectives:

1. Review existing RF and microwave metrology practice to prepare foundations for the development of a new uncertainty evaluation later in the project. This will include procedures defined in guidance documents such as the ISO Guide to the Expression of Uncertainty in Measurement [12] and EURAMET Guidelines on the Evaluation of Vector Network Analysers [11].
2. Investigate how microwave measurement uncertainty evaluations can be applied at higher frequencies. This includes millimetre-wave for use in 5G communications, and above [20]. At higher frequencies the small wavelengths can become comparable to the dimensions of test equipment components, which may cause uncertainty evaluation methods proven at lower frequencies to be invalidated. Using resources available at a National Metrology Institute, attempt to apply best practices to higher frequencies and observe if they are applicable.
3. Development of a software framework, or extension of a suitable existing one, to enable a rigorous evaluation of measurement uncertainty in nonlinear behavioural models. This framework must include all significant sources of error in nonlinear measurements required for the behavioural model extraction. The uncertainty should be stored with the extracted model in such a way that it can be used in circuit simulators to aid the amplifier design process.

1.4 Contributions

This project has contributed the following key results:

1. A technical review [21] of the treatment of input quantities in uncertainty evaluations as prescribed in [12] and its supplements [22], [23]. This work addresses an ambiguity between two current guidance documents which can cause major discrepancies in results, especially when applied to RF measurements.
2. An evaluation of the effectiveness of the “ripple technique” used to measure residual error and quantify uncertainty in VNA calibrations, when applied in rectangular metallic waveguide up to submillimetre-wave frequencies (750 GHz) [24]. Similar waveguide is being used in 5G back-haul development at E-band frequencies (60–90 GHz), and data links around 300 GHz are also being investigated [25], so reliable metrology in this transmission medium is important.
3. A new uncertainty evaluation of nonlinear behavioural models, based on the NIST Microwave Uncertainty Framework [17]. This framework provides a rigorous uncertainty evaluation including over 300 sources of error, and preserves all correlations between input quantities. An implementation of the X-parameter model has been demonstrated with two examples: a microwave and a millimetre-wave amplifier [26]. Information about the uncertainty in these models is stored with them and can be imported and used within circuit simulators.

Part of the work to develop this evaluation required modification of the existing framework, for which I was given an invited secondment to NIST in Boulder, CO, USA. I worked alongside Dylan Williams [27] (IEEE MTT-S president during that year) and his team in the High-Speed Measurements Group to provide significant speed enhancements and new features for the software, not limited to behavioural model capabilities.

1.5 Thesis Structure

This chapter has described the motivation for this work, along with the derivation of its objectives by studying prior research. The following chapter, Chapter 2, provides a foundation in the RF and microwave measurement background and introduces VNA and NVNA theory.

Chapter 3 defines the role of uncertainty and traceability in measurements and presents a review of the GUM document [21]. Chapter 4 explains VNA and NVNA uncertainty methods and presents the results of the investigation into the application of existing RF metrological practices in millimetre- and submillimetre-wave waveguide [24]. Chapter 5 describes nonlinear behavioural models and introduces the software framework developed to propagate measurement uncertainty into them [26]. Finally, conclusions and opportunities for future work are covered in Chapter 6.

2 Radio Frequency and Microwave Measurements

2.1 Introduction

To characterise nonlinear behavioural models, the radio frequency (RF) response of a device to electromagnetic wave stimuli must be measured. When compared with DC (and low frequency) measurements, RF and microwave measurements present significant additional challenges. For DC systems, it is desirable to propagate voltages through a circuit with minimal loss in amplitude. To achieve this effectively, components are typically designed with high input impedance and low output impedance to ensure there is ample power to drive connected components. With RF systems, circuit components and interconnects can be of the order of a quarter-wavelength in length, and therefore signals must be treated as electromagnetic waves to account for different behaviour at these frequencies. When a travelling electromagnetic wave encounters a discontinuity in impedance, such as a cable connector or on-wafer structure, some of the power in the wave is reflected. The amount of reflected power depends on the impedance mismatch between each side of the discontinuity. Hence for most RF systems, because the transmission of power is the focus of the circuit designer the impedance is carefully maintained, typically at $50\text{-}\Omega$. The measurement of power flowing through a transmission line is complicated by three key factors. Firstly, because the waves are travelling, the instantaneous voltage at any point on the transmission line will vary between the peak-to-peak values of the wave. Secondly, waves travel in both directions along the transmission line and must be measured separately. Finally, the power of the wave is a complex quantity consisting of both magnitude and phase. To perform these measurements a vector network analyser (VNA) can be used. In this chapter, the concepts and measurements associated with this instrument are introduced, which will be used later in the

thesis to understand the uncertainty contributions from measurements to nonlinear behavioural models.

2.2 Electromagnetic Wave Parameters

2.2.1 Wave Definitions

To describe the propagation of electromagnetic waves within transmission lines, the terminology that follows is defined. Information presented in this section has been obtained from [28]–[32].

2.2.1.1 Travelling Waves

Travelling waves are a solution to Maxwell's equations along a transmission line. They are physical and measurable via slotted line experiments or “thru-reflect-line” calibrations (explained later in this Chapter). Travelling waves are defined by the total transverse electric and magnetic fields \mathbf{E}_t and \mathbf{H}_t of a single propagating mode at each frequency:

$$\mathbf{E}_t = c^+ e^{-\gamma z} \mathbf{e}_t + c^- e^{+\gamma z} \mathbf{e}_t, \quad \mathbf{H}_t = c^+ e^{-\gamma z} \mathbf{h}_t - c^- e^{+\gamma z} \mathbf{h}_t \quad (2.1)$$

where, following the notation of [32], \mathbf{e}_t and \mathbf{h}_t are the un-normalized electric and magnetic fields of the modal solution of Maxwell's equations in transmission line, $\gamma = a + jb$ is the complex propagation constant of the mode, z is the direction of propagation, and c^+ and c^- are complex quantities representing the un-normalized forward and backward amplitude of the mode, respectively.

2.2.1.2 Equivalent-Circuit Voltage and Current

To represent travelling waves as equivalent low frequency circuit parameters such as voltage and current, a normalisation is chosen to derive a characteristic impedance for the transmission line. This normalisation takes the form:

$$\mathbf{E}_t(z) = \frac{v(z)}{v_0} \mathbf{e}_t, \quad \mathbf{H}_t(z) = \frac{i(z)}{i_0} \mathbf{h}_t, \quad (2.2)$$

where v_0 and i_0 are normalisation constants that allow v and i to take units of root-mean-square voltage and current, respectively [32].

2.2.1.3 Pseudowaves

Equivalent voltages and currents cannot be conveniently used when modelling lossy transmission lines where the electric and magnetic fields are out of phase [33]. To account for this and provide a solution which can be used with conventional circuit design methodologies (e.g. Smith chart techniques [34]) and simulators, pseudowaves can be used. This representation is defined with a reference impedance, Z_{ref} , which can be chosen by the user, but is typically 50Ω in conventional measurements. The forward and backward pseudowaves a and b can be written as:

$$a(Z_{\text{ref}}) = \left[\frac{|v_0|}{v_0} \frac{\sqrt{\Re(Z_{\text{ref}})}}{2|Z_{\text{ref}}|} \right] (v + iZ_{\text{ref}}), \quad b(Z_{\text{ref}}) = \left[\frac{|v_0|}{v_0} \frac{\sqrt{\Re(Z_{\text{ref}})}}{2|Z_{\text{ref}}|} \right] (v - iZ_{\text{ref}}) \quad (2.3)$$

2.2.1.4 Power Waves

Finally, power waves are defined so that the relationship $P = |a|^2 - |b|^2$ is true for any reference impedance, where P is the power transmitted through the transmission line and a and b are the forward and backward power waves, respectively. They are defined as:

$$a(Z_i) = \frac{v + iZ_i}{2\sqrt{\Re(Z_i)}}, \quad b(Z_i) = \frac{v - iZ_i^*}{2\sqrt{\Re(Z_i)}}. \quad (2.4)$$

where Z_i is the impedance seen at port i . Data taken from Keysight instruments used later in this work is presented in power wave format, with units of square-root Watts. To convert these values into decibels referenced to 1 milliwatt, the following formula is used:

$$P(\text{dBm}) = 10 \log_{10}(P(\sqrt{W})^2) + 30 \quad (2.5)$$

2.2.2 Derived Metrics and Figures of Merit

The behaviour of a linear microwave device can be completely defined by the ratio of electromagnetic waves which are scattered at each port to those which are incident at each port. The combinations of these ratios constitutes the scattering parameters (S-parameters) of a microwave device and are used extensively in the design and measurement of microwave systems [35]. The formal definitions of the S-parameters for a two-port device are:

$$S_{11} = \left. \frac{b_1}{a_1} \right|_{a_2=0}, \quad S_{12} = \left. \frac{b_1}{a_2} \right|_{a_1=0}, \quad S_{21} = \left. \frac{b_2}{a_1} \right|_{a_2=0}, \quad S_{22} = \left. \frac{b_2}{a_2} \right|_{a_1=0}, \quad (2.6)$$

where both a and b can be expressed in either pseudowave or power wave representation. The term “scattered” can be interchanged with “transmitted” and “reflected” depending on if the scattered wave is output on a different port, or the same port, to the incident wave, respectively.

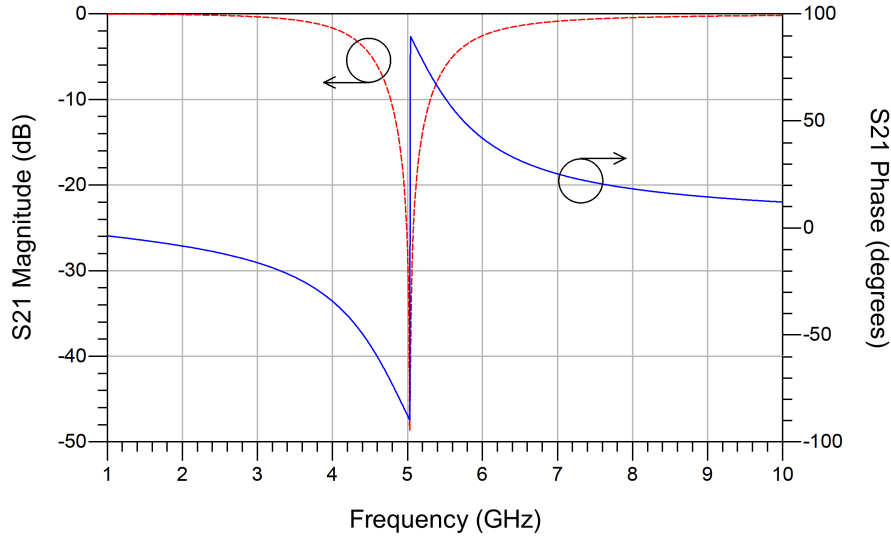


Figure 2.1: The frequency dependence of the magnitude (red dotted trace) and phase (blue solid trace) of S_{21} for a bandstop filter.

The S-parameters of all microwave devices will exhibit some degree of frequency dependence. This effect originates from physical processes occurring in the device and can either be a benefit or hindrance to a design. Most passive components (including cables) will have a usable bandwidth which is an unwanted limitation, whereas microwave filters are a ubiquitous component where the same fixed bandwidth is the main purpose of the device. To capture this frequency dependence, S-parameters are measured across a frequency range and stored in a table. An example of the frequency dependence of a filter is shown in Figure 2.1. For a device operating in the linear regime, if multiple stimuli at different frequencies are incident on the device, they will not interact with each other. The scattered waves will have the same frequency components as if the stimulus at each frequency was applied separately and the outputs combined. This is called the frequency superposition principle and it does not apply to nonlinear devices, which will be discussed later in this chapter.

Scattering parameters are often expressed in matrix form, where the column index is the scattered port, and the row index is the incident port. For a two-port device, the S-parameter

matrix is:

$$S = \begin{bmatrix} S_{11} & S_{12} \\ S_{21} & S_{22} \end{bmatrix} \quad (2.7)$$

The most useful characteristic of a two-port microwave device is often the effect which it has on a transmitted wave in the forward direction (S_{21}). If the device increases the magnitude of the incident signal this metric is called gain, otherwise it is called insertion loss. Typically gain is associated with active devices (those which are powered from an external source separate to the incident microwave signals) such as amplifiers, and insertion loss is associated with passive devices (those with no external power source) such as attenuators, splitters and mixers. The power gain (operating gain) and insertion loss relating to S_{21} can be calculated using:

$$\text{Power Gain} = 10 \log_{10} |S_{21}|^2 \text{ dB}, \quad (2.8)$$

and:

$$\text{Insertion Loss} = -10 \log_{10} |S_{21}|^2 \text{ dB}, \quad (2.9)$$

respectively.

Optimal transmission in microwave systems requires impedance matching between components, and it is inevitable that this matching will not be perfect and so some power will be reflected in a two-port device. Therefore, the match of a device is another important measurement, which is dependent on the voltage reflection coefficient (Γ) of the device and can be related to the impedance of a source (Z_S) and load (Z_L) by:

$$\Gamma_{xx} = S_{xx} = \frac{Z_L - Z_S}{Z_L + Z_S}, \quad (2.10)$$

where x is a port index. For a two-port device, Γ includes any effect from the impedance terminating the other port, and for the case of input reflection coefficient is calculated as:

$$\Gamma_{11} = S_{11} + \frac{S_{12}S_{21}\Gamma_L}{1 - S_{22}\Gamma_L}, \quad (2.11)$$

where Γ_L is the voltage reflection coefficient of the load connected to the device.

For active devices, such as amplifiers, it can also be useful to consider the power reflected at the input when calculating the power gain of the device. The transducer gain of a device accounts for this potential loss of power at the input and provides a more portable metric which is not dependent on the impedance of the measurement setup. It is defined as:

$$G_T = \frac{1 - |\Gamma_S|^2}{1 - |\Gamma_{in}\Gamma_S|^2} |S_{21}|^2 \frac{1 - |\Gamma_L^2|^2}{1 - |S_{22}\Gamma_L|^2}, \quad (2.12)$$

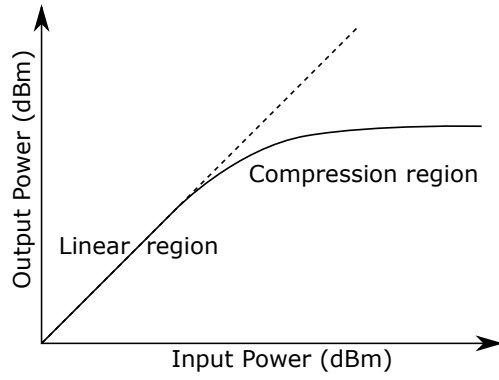


Figure 2.2: Gain compression occurs when an amplifier is driven into a nonlinear operating regime.

where Γ_{in} is the input match of the device.

For all devices operating in the linear regime, any reflected or transmitted wave will have a frequency equivalent to that incident to the device. In addition, the stimulus power that was used to measure the S-parameters is not important as the ratio of scattered to incident wave magnitude is not dependent on this quantity. However, when microwave devices operate in the nonlinear regime, these conditions no longer apply, and S-parameters cannot be used to capture the full behaviour of the device.

2.3 Measurements of Nonlinear Devices

Microwave devices operating in the nonlinear regime exhibit three differences from their linear counterparts which are significant.

Firstly, the amplitude of electromagnetic waves scattered from the device are not linearly dependent on the amplitude of waves incident. This is the cause of features such as gain compression and gain expansion in amplifiers. Some of these effects are solely due to nonlinear effects inside the device, while others include the response of the power supply. A typical gain compression curve is shown in Figure 2.2.

Secondly, the frequency superposition principle does not apply, and instead the frequency spectrum of scattered waves contains components at frequencies other than those incident upon

it. Incident tones are multiplied with each other (frequency mixing), as shown by:

$$b = c_0 + c_1 a + c_2 a^2 + c_3 a^3 + \dots , \quad (2.13)$$

$$\alpha = \beta = 2\pi\omega t, \quad (2.14)$$

$$a(t) = A \cos(\alpha), \quad (2.15)$$

$$\cos(\alpha) \cos(\beta) = \frac{1}{2}(\cos(\alpha + \beta) + \cos(\alpha - \beta)), \quad (2.16)$$

$$a^2(t) = \frac{1}{2}A^2[\cos(2\pi(2\omega)t) + 1], \quad (2.17)$$

$$a^3(t) = \frac{1}{4}A^3[\cos(2\pi(3\omega)t) + 3\cos(2\pi\omega t)]. \quad (2.18)$$

Here, a and b are the incident and scattered waves for the device, c_i are coefficients of the device's nonlinear transfer function, and $a(t)$ is a wave in the time domain with amplitude A and frequency ω . For stimuli with a single frequency ($\alpha=\beta$, as above), integer multiples of that frequency will be scattered from the device (harmonics). For stimuli with multiple tones ($\alpha \neq \beta$), additional products from combinations of the incident tone frequencies will be scattered (intermodulation). If the nonlinear device is incident with a fixed bandwidth of frequencies, such as the case for communications signals, then sidebands will be produced around the harmonics of the oscillator frequencies. This effect can be troublesome when the undesired sidebands overlap with the useful microwave signal, causing distortion. For this reason, it is important for designers to be able to accurately measure and characterise this nonlinear effect. Figure 2.3 shows example spectra of these effects.

Finally, the amplitude of scattered waves when incident waves at multiple ports and harmonics is nonlinearly dependent on the phase of incident waves. This was not the case while the superposition principle held in the linear regime, but this nonlinear relationship can have significant effects on the amplitude of scattered waves. Designers must consider this when building efficient nonlinear amplifiers, which leads to the practice of accurately terminating scattered harmonic frequencies at an optimum phase - a process called "waveform engineering". This will be covered in more detail in Chapter 5 when we discuss nonlinear device models.

The result of these differences is that the measurement requirements for nonlinear devices are considerably larger than for linear devices. The nonlinear dependencies on stimulus power and phase means that ratioed measurements no longer fully capture the device response, and absolute measurements of the magnitude and phase of both the incident and scattered waves are required. The production of scattered waves at frequencies different to those in the stimulus demands an additional dimension of measurements. These complications must be met with changes to both

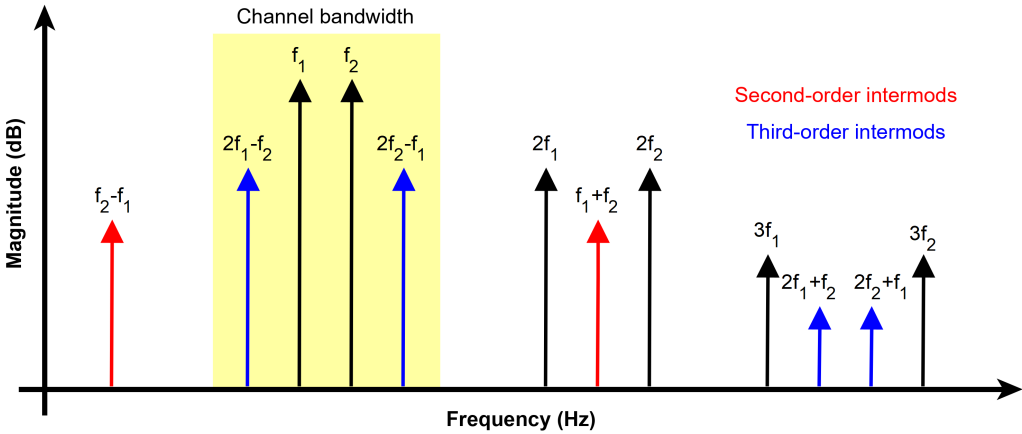


Figure 2.3: Intermodulation products from two tones within the cellular channel bandwidth f_1 and f_2 . The second order products, and upper third order products, can be easily filtered out. However, the lower third order products $2f_1 - f_2$ and $2f_2 - f_1$ are located within the channel bandwidth and interact with the useful data, increasing error vector magnitude (EVM) and bit error rate (BER).

the measurement system and the method of storing the results.

2.4 Vector Network Analysers

To measure the incident and scattered waves for a device and calculate the S-parameters as in (2.6), a vector network analyser (VNA) is typically used. Due to the challenging nature of measurements at these frequencies, it is a complicated instrument with many internal parts. This section explains how the VNA functions and the procedures behind its calibration. For a good history of VNA architecture and product development please refer to [36]–[38].

2.4.1 Architecture

The origin of the VNA lies in an early instrument called a reflectometer. Designed in 1947 by Parzen and Yalow [39], it became an invaluable tool for characterising transmission lines used in telecommunication systems. Shown in Figure 2.4, the incident signal is generated by a swept signal source and passes through the directional coupler before arriving at the device-under-test

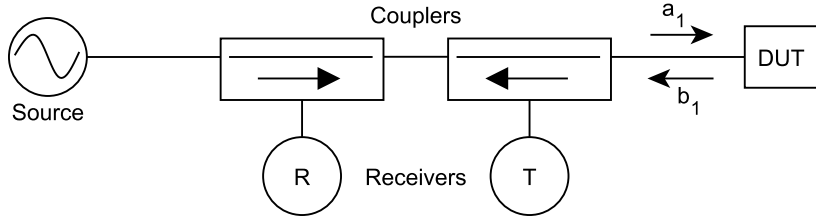


Figure 2.4: A one-port simple reflectometer. a_1 is the incident wave generated by the source, which is admitted to the DUT while also being sampled by the directional coupler and sent to the reference receiver, R. The reflected wave, b_1 , is also sampled by another directional coupler and sent to the test receiver, T, with the remaining power dissipated at the matched source.

(DUT). The voltage reflection coefficient of the DUT will cause an amount of incident power to be reflected, which passes back through the coupler before being absorbed by the source (which has very low reflection). The directional couplers allow the waves travelling between the source and the DUT to be sampled by complex receivers, filtering the two waves by their direction of travel thus allowing the incident and scattered waves to be separated for measurement.

The limitation of a single reflectometer is that it can only measure waves at one port of a DUT, therefore preventing transmission measurements. By adding a second reflectometer and synchronising the stimuli and measurements, it is possible to measure all S-parameters of a two-port device. This is the fundamental structure of a VNA, and most variations consist of changing the number of sources or receivers to optimise the instrument for cost or performance. Many older designs use an economical single source which is switched between both ports, whereas now the price of sources has fallen, there are instruments available with two independent sources, which allows more advanced methods such as two-tone measurements. These more versatile units often also expose more connections between internal components (e.g. the couplers and receivers) to allow the user to perform non-standard measurements or to add attenuation or preamplification for higher stimulus powers. Modern VNAs also offer the option of measuring more than two ports, which are referred to as “multi-port” measurements. Several manufacturers offer four-port instruments which include four reflectometers (with usually two sources), although with external switching networks it is possible to expand this up to 48 ports [40]. The basic block diagram of a modern two-port double-reflectometer VNA is shown in Figure 2.5. To measure both stimulus conditions for the two-port S-parameter equations in (2.6), the sources alternate

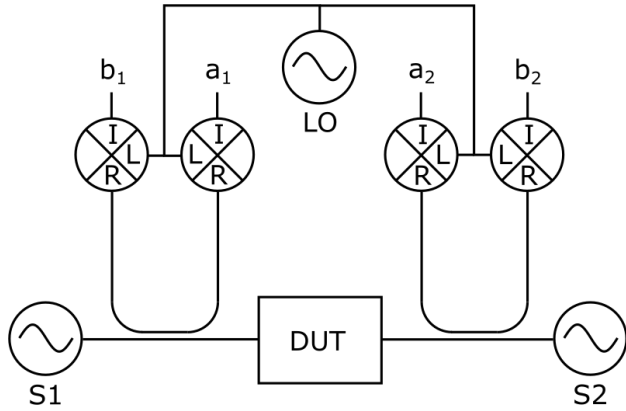


Figure 2.5: A modern two-source mixer-based VNA, which employs heterodyning to allow measurements at microwave frequencies. Two directional couplers are located between each source and the DUT and are connected back to back. These sample the waves travelling in both directions and are connected to mixers which downconvert the microwave frequencies (R) into intermediate frequencies (I) which can be sampled by the complex receivers. The shared local oscillator (LO) feeding the mixers preserves phase coherence between the receivers. This configuration is known as a two-port double-reflectometer VNA. Figure adapted by author from [41].

between delivering power and acting as a load for each measurement. As the source is swept the a and b waves for all ports are measured against frequency, from which the VNA software calculates the S-parameters. The receivers sampling the incident waves are known as the reference receivers and those sampling the scattered waves are called measurement or test receivers. The components in direct path between the source and the DUT (e.g. couplers) are historically called the test-set, which used to be interchangeable depending on the type of transmission line and test port connector family used.

To perform S-parameter measurements using a VNA, the user must set both the frequency span and number of frequency points. They may also change settings of intermediate frequency bandwidth (IFBW) and numerical averaging, both of which reduce measurement noise by applying digital filtering but can consequently increase acquisition time. The user will then perform a calibration, which corrects for any response present in the measurement setup that is not caused by the DUT. During calibration, physical “measurement planes” are defined at the closest interface to the DUT. All “corrected” measurements performed after the calibration will capture

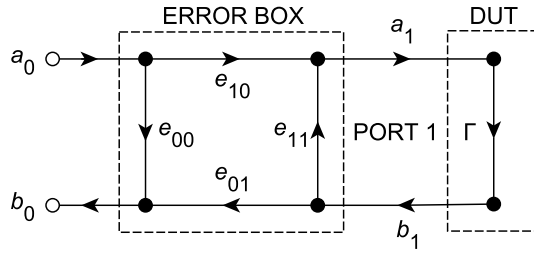


Figure 2.6: The three-term error model for a one-port measurement, which sits between the VNA receivers measuring a_0 and b_0 waves and the DUT with reflection coefficient Γ . The error box contains coefficients ($e_{00}, e_{10}, e_{01}, e_{11}$) which act like S-parameters, and captures unwanted effects from both the VNA internal components and and external test setup (e.g. cables and adapters).

the S-parameter response between these planes, including any adapters or other components between them and the DUT. After calibration, it is good practice to check that it was successful by measuring some known devices (verification [42]), or to use techniques such as ripple extraction (discussed in Chapter 4) to measure the residual uncertainty. This process characterises any remaining error which the calibration failed to correct.

2.4.2 Error Models

The calibration process involves characterising an error model which represents the response of the test-set and any cables and adapters between the VNA and the DUT. These error models are stored in the memory of the VNA and are typically de-embedded from the raw measurements before the results are presented to the user (although the raw measurements can still be obtained for separate post-processing). Because the measurement setup response is frequency dependent, the error model coefficients are characterised across the measurement bandwidth and are either applied at each measurement frequency or linearly interpolated. A popular review of VNA error models is provided in [43] but two particular models, used in the work presented in this dissertation, will now be described.

2.4.2.1 One-Port Model

The classic one-port error model can be obtained through analysis of the signal flow diagram of a one-port VNA shown in Figure 2.6. One can write the relationship between the measured (Γ_m) and actual (Γ) reflection coefficients as:

$$\Gamma_m = \frac{b_0}{a_0} = \frac{e_{00} - \overbrace{(e_{00}e_{11} - e_{01}e_{10})\Gamma}^{\Delta}}{1 - e_{11}\Gamma}, \quad (2.19)$$

from which the actual reflection coefficient can be obtained using the measured value and three error coefficients using:

$$\Gamma = \frac{\Gamma_m - e_{00}}{e_{11}\Gamma_m - \Delta}. \quad (2.20)$$

The three coefficients relate to unwanted physical effects occurring between the VNA receivers and the DUT. Directivity (e_{00}) is caused by the nonideal operation of the directional couplers used to separate the incident and reflected waves inside the VNA. In practice, some amount of incident wave will travel into the test receiver port, reducing the measured gain of the device under test. Test port match (e_{11}) results from the impedance of the VNA test port (either the original test port or the extended measurement plane including any cables or other components in the setup) being different from the characteristic impedance of the measurement, which is typically $50\text{-}\Omega$. This effect will cause some of the incident wave to be reflected at the test port which is not due to the device response. Reflection tracking (Δ) characterises the insertion loss of the couplers and other measurement components between the reference receiver and the test receiver.

2.4.2.2 Eight-Term Model

Devices with two or more ports require transmission measurements in addition to the reflection measurements corrected using the one-port model. Historically, two-port VNAs used a single reference receiver and a test receiver for each channel. This meant that the reference receiver would be shared between ports one and two, requiring a separate error model for each configuration (“forward” and “reverse”) [44]. This resulted in the 12-term and 10-term models which were the standard two-port VNA error models implemented in firmware. More recently, VNAs have employed dedicated reference receivers for each measurement port. Because the calibrated signal path (reference receiver to DUT) does not change when the stimulus is switched between ports one and two, a simpler error model can be used. This model is called the eight-term

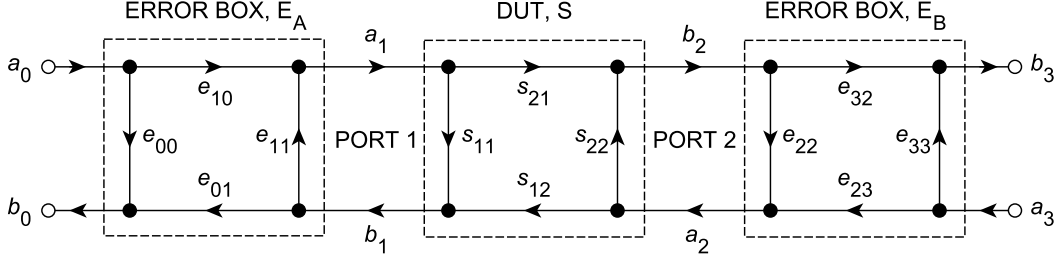


Figure 2.7: The eight-term error model for a two-port measurement. Similar to the three-term model for one-port measurements, an S-parameter model is used capture the error coefficients between the Port 1 receivers (a_0, b_0) and the DUT ($e_{00}, e_{10}, e_{01}, e_{11}$), and a separate model used between the Port 2 receivers (a_3, b_3) and the DUT ($e_{22}, e_{32}, e_{23}, e_{33}$).

model (or error box model) and is illustrated in Figure 2.7. The eight-term model also ignores error due to crosstalk between test ports, which is usually appropriate for coaxial and waveguide measurements but not for on-wafer measurements where the probes may couple. In this case the 16-term model provides greater accuracy [45].

The model defines two error boxes, \mathbf{E}_A and \mathbf{E}_B , associated with ports one and two, respectively:

$$\begin{bmatrix} b_0 \\ a_1 \end{bmatrix} = \underbrace{\begin{bmatrix} e_{00}^A & e_{01}^A \\ e_{10}^A & e_{11}^A \end{bmatrix}}_{\mathbf{E}_A} \begin{bmatrix} a_0 \\ b_1 \end{bmatrix} \quad (2.21)$$

$$\begin{bmatrix} b_3 \\ a_2 \end{bmatrix} = \underbrace{\begin{bmatrix} e_{33}^B & e_{32}^B \\ e_{23}^B & e_{22}^B \end{bmatrix}}_{\mathbf{E}_B} \begin{bmatrix} a_3 \\ b_2 \end{bmatrix}. \quad (2.22)$$

These error boxes can be rewritten as T-parameters (transfer parameters) [46, pp.12–14], which allow the error boxes to be cascaded using matrix multiplication with the DUT T-parameters to calculate the equivalent T-parameters of the three connected components:

$$\begin{bmatrix} b_0 \\ a_0 \end{bmatrix} = \underbrace{\begin{bmatrix} t_{00}^A & t_{01}^A \\ t_{10}^A & t_{11}^A \end{bmatrix}}_{\mathbf{T}_A} \underbrace{\begin{bmatrix} t_{11}^{\text{DUT}} & t_{12}^{\text{DUT}} \\ t_{21}^{\text{DUT}} & t_{22}^{\text{DUT}} \end{bmatrix}}_{\mathbf{T}_{\text{DUT}}} \underbrace{\begin{bmatrix} t_{33}^B & t_{23}^B \\ t_{32}^B & t_{22}^B \end{bmatrix}}_{\mathbf{T}_B} \begin{bmatrix} a_3 \\ b_3 \end{bmatrix} \quad (2.23)$$

$$\begin{bmatrix} b_0 \\ a_0 \end{bmatrix} = \mathbf{T}_A \mathbf{T}_{DUT} \mathbf{T}_B \begin{bmatrix} a_3 \\ b_3 \end{bmatrix} \quad (2.24)$$

$$\mathbf{T}_M = \mathbf{T}_A \mathbf{T}_{DUT} \mathbf{T}_B \quad (2.25)$$

The T-parameters of the DUT can therefore be calculated by multiplying those of the raw measurements by the inverse of the error boxes:

$$\mathbf{T}_{DUT} = \mathbf{T}_A^{-1} \mathbf{T}_M \mathbf{T}_B^{-1} \quad (2.26)$$

which can finally be converted to S-parameters to produce the result of the corrected measurement.

Like the three-term model (2.20), where e_{01} and e_{10} are always used as a product, the eight-term model contains redundant information in the transmission tracking coefficients e_{32} and e_{01} . Therefore, the eight-term model is commonly implemented as a 7-term model, but is still referred to by the eight-term name. For nonlinear measurements, as will be seen later in this section, the transmission tracking must be characterised per port and so all eight terms are used.

2.4.3 Calibration

To characterise the error models, impedance standards with known properties are measured. These properties can be prior measurements of reflection coefficients or S-parameters (data-based standards), polynomial model coefficients (a more compact representation of reflection coefficient), or realisable properties such as length and diameter which can be used in physical models to provide calibrations with good traceability (defined in Chapter 3). More explanation of the different types of calibration standard, along with a comparison of their contributions to measurement uncertainty, is provided in Chapter 4. Whichever type of standard is used, the calibration process (normally implemented in the VNA firmware) will obtain values for the actual S-parameters of the standard, which can be used together with the measured S-parameters and the error model to characterise the error coefficients. This is performed using linear least-squares techniques in typical implementations.

2.4.3.1 One-Port Model

For the three-term model used with one-port VNA measurements, there are three coefficients to solve. Therefore, “three-known-loads” must be measured in order to find a solution to the error

model. Of course, measurements of more standards can be made to reduce error in the knowledge or measurement of a single standard, but in doing so additional knowledge and measurements are introduced which may result in greater error. The three standards should present reflection coefficients at the extremes of possible values in order to provide the most accurate fit for the error coefficients. The most widely used choice is of a short-circuit, open-circuit and load (SOL). The standards are kept together along with their characterisation information in a calibration kit, or “cal-kit”.

To solve the three coefficients for the one-port model it is useful to rewrite (2.20) as:

$$e_{11} + e_{22}\Gamma\Gamma_m - \Delta\Gamma = \Gamma_m, \quad (2.27)$$

which can then be solved using a matrix least-squares estimator and measurements of the three standards:

$$\begin{bmatrix} 1 & \Gamma_1\Gamma_{m1} & -\Gamma_1 \\ 1 & \Gamma_2\Gamma_{m2} & -\Gamma_2 \\ 1 & \Gamma_3\Gamma_{m3} & -\Gamma_3 \end{bmatrix} \begin{bmatrix} e_{11} \\ e_{22} \\ \Delta \end{bmatrix} = \begin{bmatrix} \Gamma_{m1} \\ \Gamma_{m2} \\ \Gamma_{m3} \end{bmatrix} \quad (2.28)$$

to find values for e_{11} , e_{22} and Δ . These coefficients are then used with (2.20) to obtain the actual reflection coefficient of subsequent DUTs from the raw measurements.

2.4.3.2 Eight-Term Model

A great benefit of the eight-term model is the ability to characterise the error coefficients using standards which are only partially known - i.e. their S-parameters cannot be explicitly calculated. Reducing the amount of assumed knowledge of the standards also reduces the number of error sources and their impact on the accuracy of the calibration. Because the calibration fully characterises the VNA, the unknown parameters of the standards can even be calculated as a result, hence these calibrations are called “self-calibrations”. However, the eight-term model can also be calibrated using classic 12-port routines such as Short-Open-Load-Thru¹ (SOLT).

There are several variations of self-calibration, including Thru-Short-Delay, Thru-Reflect-Line, Line-Reflect-Line and Line-Reflect-Match. Each routine uses a different collection of standards as defined in their name. For coaxial transmission line, which is used for most studies presented in this dissertation, the Thru-Reflect-Line (TRL) calibration is most common.

¹The misspelling of through as “thru” is a convention in the network analyser community first introduced in [47].

TRL is the most accurate and widely supported two-port calibration routine implemented on VNAs. Not only does it require fewer parameters of the standards to be known than other non-self-calibrations, but the TRL parameters have excellent traceability because they are derived from physical measurements. This makes it the calibration of choice for National Metrology Institutes (NMIs) when working with primary standards (explained in Chapter 3). Of all three TRL standards, only parameters of the transmission line standard must be known, of which the characteristic impedance becomes the reference impedance of the calibrated VNA.

One notable limitation of the TRL calibration is that it has limited usable bandwidth due to resonance of the line at certain frequencies (when $e^{\gamma(l_L - l_T)} = 1$, where γ is the propagation constant and l_L and l_T are the line and thru length, respectively). For this reason, the multiline-TRL calibration was invented which uses several lines with overlapping usable bandwidths [48].

The mathematical method used for the TRL calibration of the eight-term error model is quite detailed and several resources provide good coverage of the derivation [36], [47].

2.5 Nonlinear Vector Network Analysers

To characterise devices which exhibit nonlinear behaviour, a nonlinear vector network analyzer (NVNA), also called a large signal network analyser (LSNA), is required. Compared with a standard VNA, these instruments allow the individual incident and scattered waves to be measured, rather than just their ratios. In addition, scattered waves at harmonics of the incident frequency can be measured.

There are two main architectures of NVNA - sampler-based and mixer-based. Sampler-based instruments use a real-time sampling oscilloscope connected to directional couplers [49]–[52], whereas mixer-based VNAs use a conventional VNA architecture with supplementary equipment [53], [54]. The oscilloscope system provides a large measurement bandwidth, which is useful for communications simulations, but because of this more noise and spurious content is also captured and reduced the dynamic range. In contrast, the mixer-based system must sweep between samples of small bandwidths (i.e. a single harmonic) and requires a longer measurement time. Additionally, on some mixer-based VNAs phase coherence is lost between measurements at different frequencies due to the source design, requiring a dedicated phase reference to be continuously measured on a separate test receiver channel.

The continued development of both technologies is reducing the limitations of each architecture and both are capable of performing a typical characterisation of a microwave power transistor

[55]. The mixer-based architecture was used for all experiments presented in this dissertation and will be explained in this section.

2.5.1 Absolute Eight-Term Error Model

The eight-term error model used for VNA calibration can be used to correct the raw measurements of individual waves (absolute measurements) instead of just their ratios (relative measurements). As mentioned in the previous section, the eight-term model reduces to seven terms for relative measurements, but for absolute measurements the value of each term in the transmission tracking product $e_{01}e_{32}$ must be known. This is required because the NVNA receiver and source are set at different frequencies while measuring harmonics and so calibrated ratio measurements are not possible. Instead, the power waves are directly measured, requiring each error box to be known independently and all eight error coefficients characterised.

To separate the transmission tracking terms, a single side of the error box must be measured. This cannot be done using passive standards and requires additional equipment - a power meter and phase reference. Typically the relative calibration, using VNA methods, is performed first, followed by the absolute calibration using the power meter and phase reference.

2.5.2 Power Meter Calibration

A calibrated power meter is connected to Port 1 of the NVNA and the source is enabled on that channel, providing the signal flow shown in Figure 2.8. The magnitude of e_{01} can be found by:

$$|e_{01}| = \frac{|a_0|}{\sqrt{P_{\text{meter}}}} \sqrt{|e_{11}\Gamma_{\text{PM}}^{\text{M}} - \Delta|^2 - |\Gamma_{\text{PM}}^{\text{M}} - e_{00}|^2} \quad (2.29)$$

where P_{meter} is the value read from the calibrated power meter and $\Gamma_{\text{PM}}^{\text{M}}$ is the raw reflection coefficient of the power meter (b_0/a_0) [16].

Although this example used Port 1, it is possible to connect the power meter to Port 2 and measure the magnitude of e_{32} instead. This can be desirable if the test port connectors are different, or a lot of attenuation is present on a particular port which may reduce calibration accuracy. Once the magnitude of one term has been found, the other can be calculated by dividing it from the product obtained during the relative calibration. Because the magnitude and phase are orthogonal, the two absolute calibration steps can be performed on different ports, although some NVNA firmwares do not allow this.

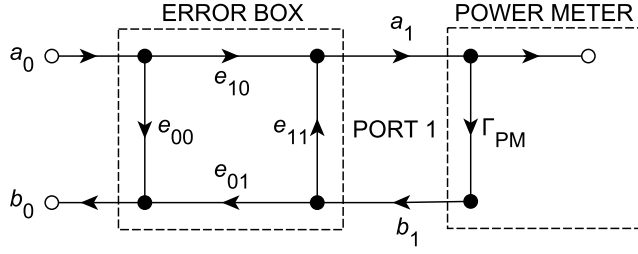


Figure 2.8: Signal flow for the power calibration of an NVNA. The power meter has reflection coefficient Γ_{PM} .

2.5.3 Phase Reference

To obtain the phase of e_{01} , a phase reference is connected to Port 1 as shown in Figure 2.9 and a measurement is made using the test receiver. This equipment produces a frequency comb with highly repeatable and known relative phases, driven from a reference controlled by the NVNA. The comb should contain frequency components (tones) at each of the harmonics which the NVNA is required to measure for the DUTs. More information on the phase reference is given in Chapter 4, Section 5.

The phase of e_{01} can be calculated using:

$$\varphi(e_{01}) = \varphi\left(\frac{a_0}{a_R} [\Gamma_{PR}^M - \Gamma_{PR}^M \Gamma_{PR} e_{11} - e_{00} + \Delta \Gamma_{PR}]\right) \quad (2.30)$$

$$= \varphi(a_0) + \varphi(\Gamma_{PR}^M - \Gamma_{PR}^M \Gamma_{PR} e_{11} - e_{00} + \Delta \Gamma_{PR}) - \varphi(a_R) \quad (2.31)$$

where a_R is the known signal from the phase reference, Γ_{PR}^M is the raw reflection coefficient of the phase reference (b_0/a_0) and Γ_{PR} is a previously measured and corrected reflection coefficient of the phase reference [16]. It can be seen from (2.31) that only the phases (relative to the fundamental driving tone) of the phase reference need to be known, and this information is supplied with the equipment.

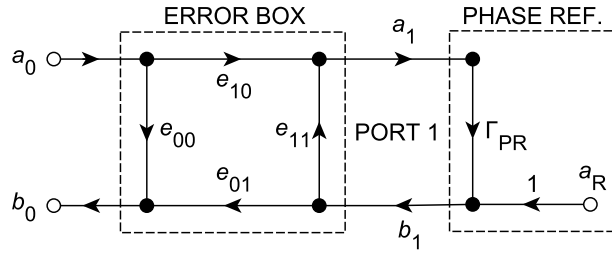


Figure 2.9: Signal flow for the phase calibration of an NVNA. The phase reference produces the broadband signal a_R and has reflection coefficient Γ_{PR} .

2.6 Conclusions

This chapter has introduced RF and microwave measurement techniques and given a brief overview of the theory behind VNA and NVNA measurements. Once it was established that electromagnetic wave measurements are not as straightforward as those performed with DC or even low frequency AC circuits, fundamental definitions were presented including the power waves used by VNA and NVNAs. Derived properties such as gain and insertion loss were expressed using S-parameters, which were shown to fully model the frequency-dependent response of a linear n -port device. By comparison, the additional measurement challenges required to characterise nonlinear devices could not be contained in the S-parameter model, and more capable solutions are required as covered in Chapter 5.

In the second half of the Chapter, the architecture and operation of the VNA was presented. Calibration models to correct for systematic errors in the instrument and test setup were explained along with the calibration methods used to characterise them. Finally, the NVNA was introduced as an instrument for measuring devices with a nonlinear response, namely microwave power amplifiers. Additional requirements for mixer-based NVNA calibration, in contrast with the VNA it is derived from, were described.

3 Measurement Uncertainty

3.1 Introduction

A measurement is an observation of a physical effect or quantity which provides useful information. This information, through the ages, has been used to facilitate advancement of both scientific knowledge and industrial development - from the production of standardised stone blocks to build the pyramids of ancient Egypt, to the production of standardised car parts to build Henry Ford's Model T. In the scientific realm, advanced measurement techniques at laboratories such as CERN are used to convince the world that new subatomic particles exist.

To communicate information about a measurement, the recipient needs to be able to either make or imagine a similar observation to that of the original measurer (or metrologist). The simplest way of doing this is to provide the recipient with the same physical effect or quantity for which to make their own observation (if you require a new nut for a bolt from a hardware shop, you might intuitively take the bolt with you), however, this can be inconvenient or impractical with larger objects, or if the recipient is located far away. Instead, you might substitute a more portable representation. For example, if you were to measure the size of a doorway to see if a new piece of furniture may fit through it, you might cut a piece of string to the same length and use this as the representation of the width of the item. However, this approach is very wasteful and also impractical for many physical effects (temperature, flow, pressure).

A solution widely thought to have been first established in the 3rd or 4th Millennium BC (see Figure 3.1), is a system of units. In such a system, a discretised value of a quantity is standardised and knowledge of its value is disseminated to all people who wish to use it. Typically, a range of discrete values are chosen, such that the system of units can be conveniently used to represent all measurements. Knowledge of the discretised values is obtained from a primary standard which becomes the definition of the unit and is used to create copies of the standard which can be



Figure 3.1: Egyptian royal cubit rod of Maya (treasurer of King Tutankhamun) 1336–1327 BC. The cubit is thought to be the earliest attested standard measure of length, first used in the 3rd or 4th Millennium BC.

given to users of the unit system to perform measurements with. The most common method of performing measurements with a unit system is to use a standard to calibrate a measuring instrument, which can then be used to measure an arbitrary value of a quantity in the units defined by the standard.

The introduction of a regulated system of units enables commerce, as traded goods can be reliably valued between merchants across cities. This application is encountered by all citizens, and so there is a high demand for standards to be produced from the primary standard and physically distributed. It becomes impractical to create all standards by copying the primary standard directly (in some cases because the value of the primary standard is perturbed each time it is measured), and so a tiered organisational structure of standards is used. In this structure, there is a tier consisting of a small number of standards which are created directly from measurements of the primary standard, followed by subsequent tiers of larger numbers of standards which are derived from measurements of those in the previous tier. For any standard produced, it should be possible to trace the lineage back to a measurement of the primary standard. This is referred to as a traceability chain (see Figure 3.2) and it is a fundamental tenet of metrology. Measurements with a shorter traceability chain are considered more traceable than those with longer chains.

Today, the primary standards are maintained in most countries by a National Measurement Institute (NMI) and co-ordinated by the Bureau of International Weights and Measures (BIPM). To accommodate international trade and compatibility, a routine process of inter-comparisons is undertaken to ensure that the values of the primary standards between countries are in agreement.

Secondary standards are also kept by the NMIs and are used to reduce excessive wear to

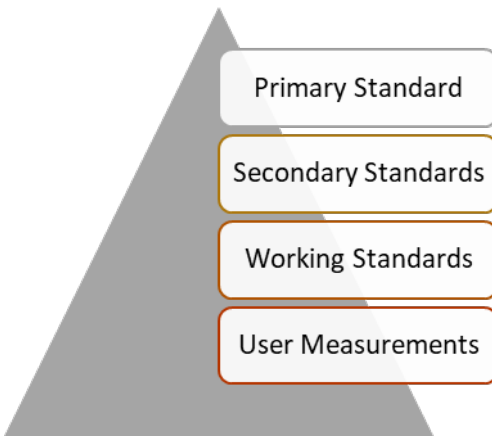


Figure 3.2: The traceability chain, where the pyramid shows the number of instances of standards in each tier. Secondary standards are held at NMIs and used to periodically calibrate working standards, which are sent by manufacturers and laboratories. User measurements are made using instruments calibrated with these working standards, so they number the greatest and are at the bottom of the traceability chain.

the primary standard caused by frequent measurements (and also to reduce bottlenecks caused by having a single standard). They are calibrated against the primary standard as infrequently as possible, again to reduce wear. Secondary standards are used by the NMI to characterise working standards which are sent to them by manufacturers and research institutes. Another important task of each NMI is to perform investigations to discover new and improved methods of measurement, which make use of secondary standards to better compare the accuracy of different methods.

Working standards are used, for example, by instrumentation manufacturers who may use them to calibrate their products before shipping to the customer, and more generally the standards can be used to calibrate test equipment to identify faulty products. Larger research institutes typically use working standards to recalibrate instrumentation prior to performing very sensitive measurements. To ensure that product specifications and scientific measurements are traceable and of high quality, accreditation services such as the United Kingdom Accreditation Service (UKAS) exist to certify manufacturers and laboratories that demonstrate good measurement practice and use traceable measurements [56].

The selection of quantities for which primary standards are kept is only a subset of those for which recognised units exist. This is because many units are derived quantities, where

their value can be obtained by calculation using definitions of other units. For example, the definition of the unit of resistance (R , ohms) can be derived from that of voltage (V , volts) and current (I , amperes), because $R = V/I$. The eight fundamental “base” units which make up the International System of Units (SI), are the metre, kilogram, second, ampere, kelvin, candela and mole. From these unit definitions, it is possible to define any other derived unit in use. NMIs will usually keep secondary standards of most derived quantities that users may wish to calibrate against, which are traceable to one or more primary standards of the base units. Although traditionally all primary standards were defined by physical artefacts (e.g. metallic weights, burning candles), these are being gradually replaced by definitions involving physical constants (e.g. Plank, Boltzmann), which do not degrade over time or use. The “Ninth SI Units” [57], a proposition recently accepted by the BIPM, covers the redefinition of four of the SI units (the ampere, the kilogram, the kelvin and the mole) which is scheduled for May 2019.

The crucial effect of traceability on measurements is the confidence in their results. Measurements with poor traceability (longer chains) will produce results which are likely to be less accurate than those with better traceability (shorter chains). The reason for this is measurement uncertainty, which will now be explained.

It is impossible to know the true value of a quantity being measured as many undesirable physical effects typically occur during the measurement process. These effects contribute error (an unwanted perturbation) to the measured value, causing a reduction in accuracy (the deviation of the measured value from the true value). Typical sources of error in measurement include thermal noise, imperfect calibration and drift of environmental conditions from those at which a measuring instrument was calibrated. In some cases, it is possible to quantify and correct for these errors, but there are often many sources (some of which contribute very small errors) which cannot be corrected for. This is because either the error cannot be quantified or the value of the error will change over the duration of the measurement process (random errors). Any source of error which cannot be removed from a measurement becomes a source of uncertainty, because the deviation of the measured value from the true value due to this source of error is uncertain. If it is possible to quantify the amount of uncertainty in a measurement, then a degree of confidence can be formed about its value. If every measurement has an associated uncertainty in its value, then any measurement involving the results of previous measurements will include uncertainty contributions from both measurements. Measurements with good traceability involve fewer sources of uncertainty than those with poor traceability, leading to a higher degree of confidence in the former. It is because of this fact that NMIs strive to reduce the uncertainties

in their primary standard definitions, which in turn reduces the uncertainty in all traceable measurements.

Because it is impossible to know the amount of error in a source of uncertainty, probability and statistical theories are used to instead describe the amount of uncertainty associated with it. By the nature of these theories there are often several methods which can be used to obtain a result, which sometimes provide different values. To ensure consistency and portability of uncertainty definitions, measurement guides were created in each industry and area of science, which specialised in processing the results of typical measurements. In addition, different guides were produced depending on the level of accuracy required - as more accurate measurements often require more effort to complete. Although this practice allowed suitable measurement comparisons within each field (e.g. chemistry, mechanical engineering), ambiguities still existed in uncertainty definitions between fields. To address this, a landmark document was published in 1993 by the International Organisation for Standardisation (ISO), the Guide to the Expression of Uncertainty in Measurement (GUM) [58]. This document was the work of representatives from seven international organisations: the BIPM, the International Organisation of Legal Metrology (OIML), the International Electrotechnical Commission (IEC), the ISO, the International Federation of Clinical Chemistry and Laboratory Medicine (IFCC), the International Union of Pure and Applied Chemistry (IUPAC), and the International Union of Pure and Applied Physics (IUPAP). The GUM, updated in 2008 [12], is still used today as a reference for the evaluation of measurement uncertainty in many laboratories and industries across the world. The seven original organisations which wrote the GUM, together with the International Laboratory Accreditation Cooperation (ILAC, of which UKAS is a member), form the Joint Committee for Guides in Metrology (JCGM), who maintain the GUM and subsequent additional documents. These additional documents consist of the International Vocabulary of Metrology (VIM) [59] and two supplements to the GUM [22], [23]: Supplement 1 covers the use of a Monte Carlo method [60] in uncertainty evaluation; Supplement 2 is used where more than one quantity is measured at the same time (multivariate).

Throughout this dissertation, the methodologies presented in the GUM will be used. The international authority of the guide, developed by seven international organisations (including the two global standardisation bodies IEC and ISO), gives strong motivation to use it as a basis for a framework to evaluate uncertainty in measurement.

This Chapter describes the evaluation of uncertainty prescribed in the GUM and highlights an inconsistency in the current version of the GUM and associated documents (which can have

a profound effect on electromagnetic measurements).

3.2 The Measurement Process

In contrast to basic evaluations of uncertainty, where only repeat measurements of the quantity of interest are analysed, the GUM prescribes a more rigorous approach, which defines a mathematical model of the measurement process (measurement model) and propagates uncertainty through that model to the result (measurands). This allows any uncertainties from previous measurements, including those involving standards in the traceability chain, to be included in the result. The measurement model can be simple, such as measuring resistance using input quantities of voltage and current, or complicated and multivariate, requiring many input quantities and producing many output quantities. In some cases, the measurement model may not be known and can be defined as a black box, but this has certain limitations discussed later with Monte Carlo methods.

The GUM defines a process that is to be followed when evaluating uncertainty in measurement. It consists of the following steps:

1. Modelling the measurement.
2. Evaluating standard uncertainty of input quantities.
3. Determining combined standard uncertainty of the measurands.
4. Determining expanded uncertainty of the measurands.

where standard uncertainty is an uncertainty expressed as a standard deviation and expanded uncertainty is used to define a coverage interval encompassing a large fraction of the distribution of values that could reasonably be attributed to the measurand.

3.2.1 Modelling the Measurement

The VIM document [59] defines a measurement model¹ as “a mathematical relation among all quantities known to be involved in a measurement”. In many cases, where an explicit relation can be written, it is possible to further define a measurement function. We can represent this

¹The definition of model used in “measurement model” is different to that used when describing models of amplifiers seen elsewhere in this dissertation.

generally as a set of measurands Y having a functional relationship, $f(\cdot)$, depending on N input quantities X_1, X_2, \dots, X_N :

$$Y = f(X_1, X_2, \dots, X_N) \quad (3.1)$$

The estimates of the measurands \bar{Y} can be found by evaluating the measurement model using the estimates of each input quantity $\bar{x}_1, \bar{x}_2, \dots, \bar{x}_N$:

$$\bar{Y} = f(\bar{x}_1, \bar{x}_2, \dots, \bar{x}_N) \quad (3.2)$$

Each input quantity could either be observed during the present measurement, a result from a previous measurement, or another source of information such as a datasheet or specification. An example of a measurement model could be for a temperature measurement, where the input quantities would include the value observed from the meter, the previously measured values of two calibration temperatures, and the assumed values of those calibration temperatures. Using this method, uncertainty from the calibration can be included in the evaluation. This is especially true for uncertainties caused by systematic errors, which do not vary during the measurement process and cannot be evaluated purely by performing repeat measurements.

3.2.2 Evaluating Standard Uncertainty of Input Quantities

Sources, or components, of uncertainty in measurement can be divided into two categories: Category A uncertainty components are those that are evaluated using statistical analysis of a series of observations (i.e. repeats); Category B components are those that are evaluated using other means, for example using information from datasheets.

The GUM presents methods that include the use of both Bayesian and classical probabilistic methods to evaluate the uncertainty in the input quantities for a measurement model. In particular, classical methods [61] are used for the treatment of Category A uncertainty components and Bayesian methods [62] are used for the treatment of Category B uncertainty components. This is a sensible assignment as classical (frequentist) methods work well for repeat observations and Bayesian inference can be used to incorporate alternative sources of knowledge. An informative discussion on these types of method can be found in [63]. Since the publication of the GUM, some authors have stated (for example, in [64]–[67]) that this combination of different probabilistic methods (i.e., Bayesian and classical) represents an inconsistency in the GUM methodology for evaluating measurement uncertainty. The author has published a paper considering the effects of

this inconsistency on electromagnetic wave measurements at radio frequencies [21], which forms the basis for this section of the chapter.

The supplements to the GUM [22], [23] resolve the above-mentioned inconsistency by introducing a method for treating the Category A uncertainties that follows a Bayesian approach [68]. Therefore, the two supplements no longer contain the inconsistency found in the original GUM document. However, as a consequence of this change, there is now inconsistency between the method used to evaluate uncertainty described in the GUM and that described in the two supplements. In many situations, these different methods do not have a significant impact on the overall uncertainty that is evaluated. For situations where a considerable number of input quantities are observed simultaneously, the two different approaches can produce significantly different values of uncertainty. Such situations often occur in the area of high-frequency electromagnetic metrology, which is the topic of this dissertation.

3.2.2.1 Category A Evaluation

GUM Method The classical statistical technique [61] applied to Category A uncertainties in the current GUM is based on a series of observations of a randomly varying input quantity. After n observations x_1, x_2, \dots, x_n , the best available estimate (arithmetic mean of measured values), \bar{x} , and standard deviation, s , of a randomly varying input quantity, X , is written as

$$\bar{x} = \frac{1}{n} \sum_{i=1}^n x_i, \quad (3.3)$$

$$s = \sqrt{\frac{1}{n-1} \sum_{i=1}^n (x_i - \bar{x})^2} \quad (3.4)$$

respectively, where x_i is the result of the i th observation. Importantly, a minimum of two observations must be made ($n = 2$) in order for \bar{x} and s to be defined. The standard uncertainty of the best estimate of X , $u(\bar{x})_{\text{GUM}}$ can be found by dividing s by the square root of the number of observations:

$$u(\bar{x})_{\text{GUM}} = \frac{s}{\sqrt{n}} \quad (3.5)$$

If there are correlated (mutually dependent) input quantities present in the measurement model, the covariances of each pair of input quantities must also be calculated before the propagation of uncertainty. Both the standard uncertainties and the covariances for N input quantities

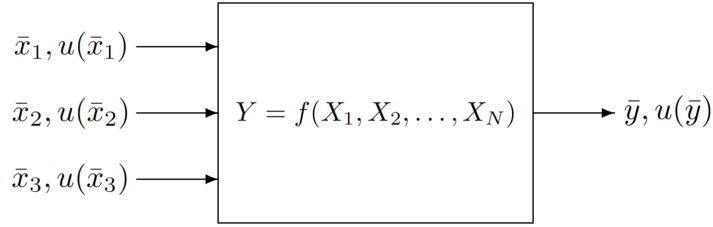


Figure 3.3: The propagation of measurement uncertainty through the measurement model, as specified in the GUM. Here, a single measurand Y is shown, but the model could include multiple measurands.

can be represented in a symmetric ($N \times N$) matrix containing the variance of each quantity (s^2) along the diagonal and the covariance between x_i and x_j in the i, j th element. This is called the “uncertainty matrix” in the GUM and the “measurement covariance matrix” in the GUM Supplement 2. An example given in the GUM and described later in this Chapter, demonstrates this scenario using the example of a simultaneous measurement of resistance and reactance with voltage, current and phase as correlated input quantities [12, Example H.2].

Once the uncertainties of the input quantities have been evaluated, they are propagated through the measurement model, as illustrated in Figure 3.3. This requires the sensitivities of the measurand to each input quantity to be calculated to at least a first order approximation (i.e. the partial derivatives of the measurement model known). The estimates of the input quantities are used in the measurement model to obtain the estimate of the measurand. The variances and covariances of the input quantities are combined with the sensitivity coefficients in order to obtain the variance of the measurand. The combined standard uncertainty of the measurand is equal to the positive square root of this value. The result of the measurement process is then presented as the measurand estimate and combined standard uncertainty. Alternatively, the combined standard uncertainty can be multiplied by a positive factor to form an expanded measurement uncertainty. From this value, a coverage interval can be derived which states a particular probability that the true value of the measurand is within that range. A more detailed description of propagating uncertainties through the measurement model and presenting the results will be given later in this Chapter, but a brief introduction was given here to help the reader understand research on input quantity uncertainties presented in the remainder of this section.

GUM Supplement Method Both GUM supplements (GUM-S1/S2) [22], [23] use a Bayesian approach [69] to assign a probability density function (PDF) to all input quantities. This approach results in the choice of a *t*-distribution to characterize Category A input quantities, in contrast to the Gaussian distribution used in the GUM [23, para. 5.3.2.1]. Of particular relevance is the inclusion of the degrees-of-freedom parameter, ν , in the definition of the standard uncertainty and covariances of a *t*-distribution. Whereas for the Gaussian distribution ν is used as a measure of reliability of the standard uncertainty, it is explicitly required when using the *t*-distribution in order to obtain the standard uncertainty, $u(\bar{x})_{\text{SUPP}}$:

$$u(\bar{x})_{\text{SUPP}} = \frac{s}{\sqrt{n}} \times \sqrt{\frac{\nu}{\nu - 2}}, \quad (3.6)$$

where $\nu = n - N$, with n being the number of observations and N being the number of input quantities. In the GUM-S1 only a univariate *t*-distribution is offered, which represents $N = 1$ input quantities. For this case (3.6) can be rewritten as:

$$u(\bar{x})_{\text{SUPP}} = \frac{s}{\sqrt{n}} \times \sqrt{\frac{n - 1}{n - 3}}. \quad (3.7)$$

Equation 3.7 is undefined if n is less than four, in which case the standard uncertainty cannot be calculated for a single input quantity according to the guidance given in the GUM-S1 (and the GUM-S2). Figure 3.4 illustrates the ratio between the standard uncertainty values calculated for different numbers of observations of a single Category A input quantity using the GUM and the GUM-S1/S2 approaches. It can be seen that when $n = 4$, $u(\bar{x})_{\text{SUPP}} = \sqrt{3} \times u(\bar{x})_{\text{GUM}}$, and as the number of observations increases the results from both approaches converge: If n tends to infinity, the *t*-distribution tends towards a Gaussian distribution. However, most commercial laboratories would avoid making large numbers of measurements as this is often time-consuming and therefore expensive.

For measurements involving multiple input quantities, such as the measurement of a vector quantity, a multivariate/joint distribution should be used as suggested in the GUM-S2. The variances and covariances between all pairs of input quantities are obtained using a matrix form of (3.6) ([23, Section 5.3.2]):

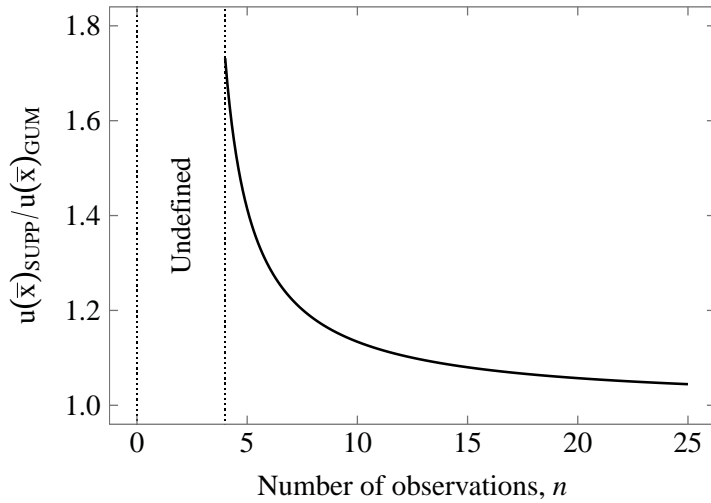


Figure 3.4: Scaling factor to convert from a GUM standard uncertainty to a GUM Supplement.

$$\mathbf{V}(\mathbf{X}) = \frac{\nu}{(\nu - 2)} \frac{\mathbf{S}(\mathbf{X})}{n} = \frac{1}{n(n - N - 2)} \sum_{i=1}^n (\mathbf{x}_i - \bar{\mathbf{x}})(\mathbf{x}_i - \bar{\mathbf{x}})^\top \quad (3.8)$$

$$\mathbf{S}(\mathbf{X}) = \frac{1}{\nu} \sum_{i=1}^n (\mathbf{x}_i - \bar{\mathbf{x}})(\mathbf{x}_i - \bar{\mathbf{x}})^\top \quad (3.9)$$

$$\mathbf{V}(\mathbf{X}) = \begin{bmatrix} u(\mathbf{x}_1)^2 & u(\mathbf{x}_1, \mathbf{x}_2) & \dots & u(\mathbf{x}_1, \mathbf{x}_n) \\ u(\mathbf{x}_2, \mathbf{x}_1) & u(\mathbf{x}_2)^2 & \dots & u(\mathbf{x}_2, \mathbf{x}_n) \\ \vdots & \vdots & \ddots & \vdots \\ u(\mathbf{x}_n, \mathbf{x}_1) & u(\mathbf{x}_n, \mathbf{x}_2) & \dots & u(\mathbf{x}_n)^2 \end{bmatrix} \quad (3.10)$$

where $\mathbf{V}(\mathbf{X})$ is the covariance matrix, \mathbf{x}_i is a sample from the array of vectors containing input quantity indications and $\bar{\mathbf{x}}$ is the arithmetic mean of that array. For this multivariate case, the minimum value of n will increase linearly with N , such that the standard uncertainty is undefined unless $n > N + 2$.

Comparison of GUM and GUM Supplements approach using example H.2/9.4 Both the GUM and the GUM-S2 provide an identical example which can be used to compare the different standard uncertainties. The example is a simultaneous measurement of resistance and reactance, which uses a measurement model with multiple input quantities and multiple output quantities (measurands). The input quantities are voltage V , current, I , and phase, ϕ , and the measurands are resistance R , reactance, X , and impedance, Z . The measurement model is

defined as:

$$R = \frac{V}{I} \cos \theta, \quad X = \frac{V}{I} \sin \theta, \quad Z = \frac{V}{I} \quad (3.11)$$

Six sets of observations [59] ($n = 6$) of $V; I; \phi$ are obtained independently by measurement. The version of this example given in the GUM uses only $n = 5$ sets, but one additional set of values of $V; I; \phi$ has been added for the GUM-S2 example to allow (3.6) to be defined for $N = 3$ input quantities, a condition which was explained at the end of the previous section. These values, together with their arithmetic means and standard uncertainties as calculated from the two approaches using (3.5) and the matrix form of (3.6) (which is applicable to measurements involving multiple input quantities), are presented in Table 3.1. The ratios of the standard uncertainties from each approach is also included in the table, which are identical for all these input quantities due to their dependence only on n and N , which are also equal for all these input quantities (e.g. when $n = 6$ and $N = 3$, $\sqrt{(\nu/(\nu - 2))} = \sqrt{((n - N)/(n - N - 2))} = \sqrt{3}$). This explains why standard uncertainties evaluated with Category A methods using the minimum number of observations following the GUM-S1/S2 approach are always 1.732 times larger than the standard uncertainties calculated following the GUM approach.

This difference in the input quantity uncertainties calculated from the two approaches propagates through the measurement model and therefore significantly affects the combined standard uncertainties of the measurands. Table 3.2 presents the combined standard uncertainties of the measurands for the described example as evaluated by both approaches, together with a ratio of the uncertainty values. For all three measurands the combined standard uncertainty calculated using the GUM-S1/S2 method is more than double the equivalent values calculated using the GUM method. For other measurement models with higher sensitivities to the input quantities, this difference could be even greater.

Comparison of GUM and GUM Supplements approach using microwave scattering parameters example High-frequency electromagnetic metrology often involves using multiple complex-valued quantities. Common input quantities for this type of measurement, measured using instruments such as vector network analysers (VNA), are scattering parameters (S-parameters), as described in Chapter 2. Because each S-parameter is a complex-valued quantity ($S = (S_{\text{Re}}, S_{\text{Im}})$), there are $2m^2$ input quantities required in a measurement model for the complete response of an m port device. All these quantities are correlated, so a multivariate distribution should be used to represent them. It has been shown previously that for a Category

Value	V/V	I/A	ϕ/rad
x_1	5.007	19.663	1.0456
x_2	4.994	19.639	1.0438
x_3	5.005	19.640	1.0468
x_4	4.990	19.685	1.0428
x_5	4.999	19.678	1.0433
x_6	4.999	19.661	1.0445
\bar{x}	4.9990	19.6610	1.04446
$u(\bar{x})\text{GUM}$	0.0026	0.0077	0.00061
$u(\bar{x})\text{SUPP}$	0.0045	0.0134	0.0011
$\frac{u(\bar{x})\text{GUM}}{u(\bar{x})\text{SUPP}}$	1.732	1.732	1.732

Table 3.1: The indication values from the example “Simultaneous Resistance and Reactance Measurement” and their statistical properties as evaluated by the approaches given in [12, Example H.2] and [23, Example 9.4].

Method	$u(R)/\Omega$	$u(X)/\Omega$	$u(Z)/\Omega$
GUM	0.058	0.241	0.193
GUM-S2	0.130	0.540	0.431
$\frac{\text{GUM-S2}}{\text{GUM}}$	2.241	2.241	2.233

Table 3.2: A comparison of the results obtained for the example “Simultaneous Resistance and Reactance Measurement” using the approaches given in [12, Example H.2] and [23, Example 9.4].

Ports, m	Input quantities, N	Required minimum number of repeat observations, n , for $u(\bar{x})_{SUPP}$ to be defined	$\frac{u(\bar{x})_{GUM}}{u(\bar{x})_{SUPP}}$
1	2	5	1.732
2	8	11	1.732
3	18	21	1.732
4	32	35	1.732
:	:	:	1.732
8	128	131	1.732

Table 3.3: The difference in standard uncertainties obtained using the GUM ($u(\bar{x})_{GUM}$) and the GUM-S1/S2 ($u(\bar{x})_{SUPP}$) approaches to measure a full set of scattering parameters for microwave devices with various numbers of ports, m . Each device has $2m^2$ input quantities, N , and requires a minimum of $N + 3$ repeat observations, n , in order for $u(\bar{x})_{SUPP}$ to be defined.

A evaluation of uncertainty, both the number of repeat observations and the number of input quantities have a significant effect on the difference in uncertainty as calculated from the two approaches presented in the GUM and the GUM-S1/S2. Table 3.3 shows the ratio of uncertainties calculated from both approaches when applied to a measurement using scattering parameters obtained from the minimum number of repeat observations, n , for devices with m ports.

It can be seen that for devices with multiple ports, n can become large in order for 3.6 to be defined and calculate the standard uncertainty. It is often the case that the user will not always have the time or resources available to perform such a quantity of measurements. In microwave measurement environments, connections are typically made by hand using coaxial connectors. A typical measurement may include a Category A evaluation of uncertainty due to connection repeatability. Considering the specific example of a 4-port device, this requirement would result in the need for a minimum of $35 \times 4 = 140$ repeat coaxial connections to be made in order to perform a Category A evaluation of the standard uncertainty using the GUM-S1/S2 approach. By contrast, the classical approach used in the GUM is defined with just 2 repeat observations, which would require only $2 \times 4 = 8$ repeat coaxial connections to be made. Figure 3.5 shows the minimum number of repeat observations required when using the GUM-S1/S2 approach, n , in order to be able to calculate a Category A evaluation of the standard uncertainty of a full

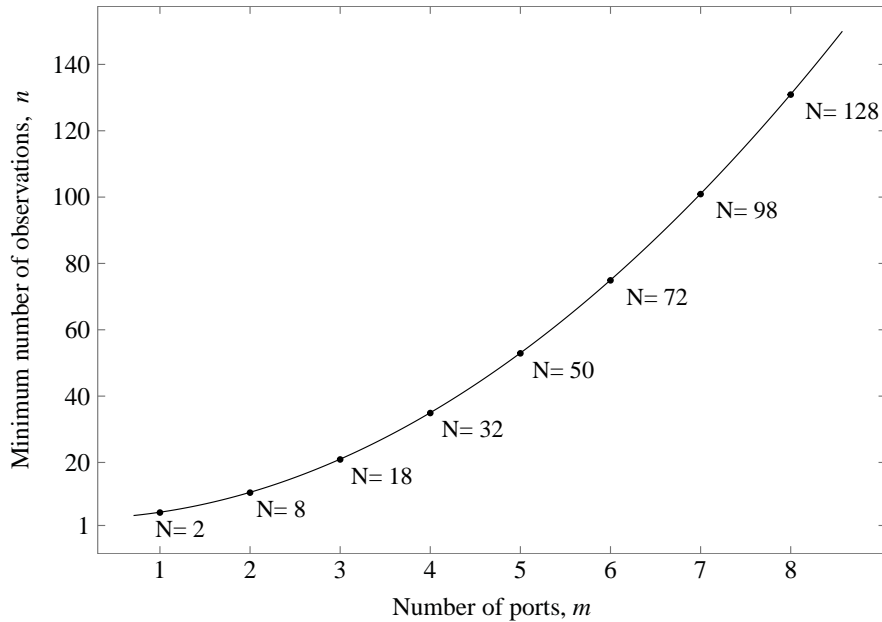


Figure 3.5: The minimum number of observations, n , required to calculate the standard uncertainty of a full set of S-parameters for a microwave device with m ports using the GUM-S2 approach. The number of input quantities, N , for each device is also shown.

set of S-parameters for a microwave device with m ports. In all cases, the standard uncertainty obtained using the GUM-S1/S2 approach is approximately 1.7 times larger than that obtained using the GUM approach.

Discussion The inconsistency of the approaches used in the GUM and its supplements to calculate the standard uncertainty of Category A input quantities of a measurement has two noticeable consequences:

1. There can be a large difference in the standard uncertainties reported by each approach. It is not straightforward to decide which is the correct approach to use, however the GUM approach is likely to be more attractive to commercial laboratories and test engineers since this leads to achieving smaller uncertainties in their results.
2. For situations involving multiple Category A input quantities, the Bayesian approach introduced in the GUM-S1/S2 can require a large number of observations before the standard uncertainty can be defined. Although the standard uncertainty calculated using the GUM approach will become less reliable with fewer observations, it is still possible to obtain

a result with only two observations of any number of input quantities. In a commercial laboratory the additional measurements required by the GUM-S1/S2 approach can be impractical, with many laboratories typically using only two or three measurements per device following the GUM approach. For a single input quantity this would require a potential doubling of the number of observations and therefore the test duration, which would either slow throughput or require more test stations to be added. If implemented, the additional time or financial investment would then produce uncertainties that are significantly larger than those obtained using the GUM approach.

This inconsistency is yet to be resolved, and the draft of an updated GUM which replaced much of the remaining classical approach with Bayesian techniques received many poor reviews when circulated for discussion. Work is now being carried out to find solutions to the issues raised by converting to a fully Bayesian GUM. Specific to the example presented in this Section, an article was recently published which offers a way to use Bayesian statistics to evaluate uncertainty in Category A input quantities with $n \geq 2$ repeat observations, which is the same number required by the classical approach [70].

For the work in this thesis, which is based on multivariate electromagnetic measurement problems, the GUM approach (instead of the Supplement 2 approach) is used. In addition, an existing software framework, introduced later, which is included as part of the complete framework presented in this work, also uses the GUM approach for processing Category A uncertainty components.

3.2.2.2 Category B Evaluation

Category B uncertainty components are those which have not been obtained by repeated measurements. Possible sources include previous measurement data, experience or knowledge of relevant materials and instruments, manufacturer's specifications, data provided by calibration and other certificates and reference data from handbooks.

Values obtained from these sources will typically be an estimate accompanied by either a standard uncertainty or an expanded uncertainty. The latter can be converted to a standard uncertainty, the process of which is described in Section 3.6. Category B uncertainty components are not restricted to Gaussian or t-distributions, and could for example be normal (rectangular), beta, or Cauchy distributions. Unless the combined standard uncertainty is determined via a Monte Carlo method, as explained in the following section, the standard uncertainty must be

known for the value to be used as an input quantity.

3.2.3 Evaluating Combined Standard Uncertainty

In order to determine the standard uncertainty of the measurand (the combined standard uncertainty) the uncertainties of the input quantities must be propagated through the measurement model. The GUM offers several methods to achieve this, which will be described in this section.

3.2.3.1 Monte Carlo Methods

Supplement 1 of the GUM [22] covers the use of a Monte Carlo technique to determine combined standard uncertainty in the measurand. The Monte Carlo technique has three important benefits for the propagation of uncertainty:

1. The measurement model does not need to be known explicitly. In some cases, the algorithm used to obtain a measurement result is proprietary and cannot be made available to the metrologist. Alternatively, the measurement model may be very complicated or involve numerical solutions which cannot be differentiated as required by other propagation methods.
2. Full knowledge of the probability distributions of the input quantities are used and preserved through the uncertainty propagation. Because the input quantity distributions are sampled directly, the complete probability distribution of the measurand can be obtained (see Figure 3.6). This can be very useful when more exotic distributions such as u-shaped distributions are used for input quantities, or if the measurement model is strongly nonlinear, when one cannot make assumptions about the probability distribution of the measurand.
3. The uncertainty propagation preserves nonlinearities in the measurement model. Alternative propagation methods presented in the GUM cause the measurement model to be linearised around the estimate. In most cases where a nonlinear measurement model is used, however, the uncertainty values are sufficiently small that a linear approximation is valid [12, p. 5.1.5]. Often, an initial Monte Carlo propagation is used to validate this assumption.
4. All correlations between input quantities are preserved. For many measurements involving multiple input quantities (especially in electromagnetic measurements), the uncertainties

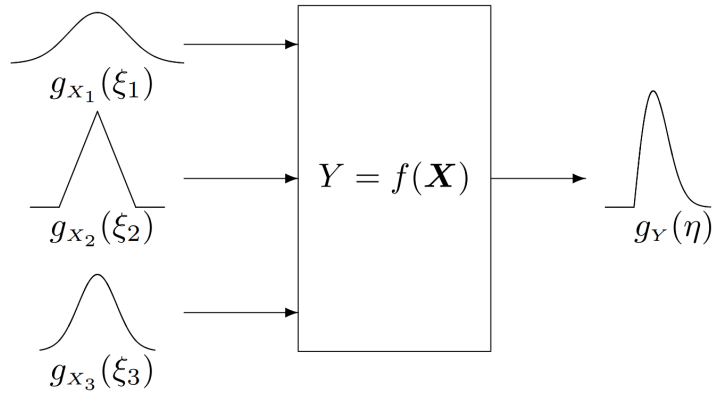


Figure 3.6: An illustration of the propagation of distributions from three input quantities g_{X_1} , g_{X_2} , g_{X_3} , through the measurement model, Y , to the measurand, g_Y [22].

of one or more input quantities may be correlated. This means that when the value of one quantity changes, it affects the values of others. This can both increase or decrease the combined standard uncertainty in the measurand significantly. Chapter 4 will discuss the impact of correlations on VNA measurements.

The primary disadvantage of Monte Carlo methods is the time required to process them. For an accurate evaluation of uncertainty, the number of samples must be sufficiently large. Generally, the GUM recommends 10⁶ samples for a 95% coverage interval accurate to one or two significant digits [22, p. 7.2.1]. The number of samples increases with the size of the desired coverage interval of similar accuracy. For many measurements today, the processing power of modern computers is sufficient for the duration of uncertainty propagations using Monte Carlo methods to be acceptable. However, in situations where the measurement model is very time-consuming to process, or where the uncertainty evaluation must be very fast, linear propagation techniques may be preferred. A detailed explanation of the steps involved in performing a Monte Carlo propagation can be found in Section 7 of [22].

3.2.3.2 Law of Propagation of Uncertainty

The primary propagation method presented in the GUM is the Law of Propagation of Uncertainty (LPU). This method uses first-order derivatives of the measurement model, together with the variances (and co-variances) of the input quantities, to determine a value for the combined standard uncertainty. The use of first-order derivatives means that the measurement model is

linearised, which in many applications can be a valid assumption. The LPU provides different equations for combining independent (uncorrelated) and correlated input quantities. For independent input quantities,

$$u_c^2(\bar{y}) = \sum_{i=1}^N \left(\frac{\partial f}{\partial x_i} \right)^2 u^2(\bar{x}_i), \quad (3.12)$$

where $u_c^2(\bar{y})$, the combined variance, is the square of the combined standard uncertainty, f is the function describing the measurement model, and x_i is an input quantity with variance $u^2(\bar{x}_i)$. For correlated input quantities (whose covariances always form a symmetric and positive semi-definite matrix),

$$u_c^2(\bar{y}) = \sum_{i=1}^N \sum_{j=1}^N \frac{\partial f}{\partial x_i} \frac{\partial f}{\partial x_j} u(\bar{x}_i, \bar{x}_j) = \sum_{i=1}^N \left(\frac{\partial f}{\partial x_i} \right)^2 u^2(\bar{x}_i) + 2 \sum_{i=1}^{N-1} \sum_{j=i+1}^N \frac{\partial f}{\partial x_i} \frac{\partial f}{\partial x_j} u(\bar{x}_i, \bar{x}_j). \quad (3.13)$$

Supplement 2 to the GUM offers a matrix formulation of (3.13) [23, p. 6.2.1.3], which handles the multivariate case where multiple measurands are encountered. If the covariance matrix of dimension $N \times N$ associated with \bar{x} is

$$\mathbf{U}(\bar{x}) = \begin{bmatrix} u(\bar{x}_1, \bar{x}_1) & \dots & u(\bar{x}_1, \bar{x}_n) \\ \vdots & \ddots & \vdots \\ u(\bar{x}_n, \bar{x}_1) & \dots & u(\bar{x}_n, \bar{x}_n) \end{bmatrix} \quad (3.14)$$

the covariance matrix of dimension $m \times m$ associated with \bar{y} is

$$\mathbf{U}(\bar{y}) = \begin{bmatrix} u(\bar{y}_1, \bar{y}_1) & \dots & u(\bar{y}_1, \bar{y}_n) \\ \vdots & \ddots & \vdots \\ u(\bar{y}_n, \bar{y}_1) & \dots & u(\bar{y}_n, \bar{y}_n) \end{bmatrix} \quad (3.15)$$

and the sensitivity matrix $\mathbf{C}_{\bar{x}}$ of dimension $m \times N$ containing the first-order partial derivatives of the measurement model to each input quantity (the Jacobian of the measurement model) is given by evaluating

$$\mathbf{C}_{\bar{x}} = \begin{bmatrix} \frac{\partial f_1}{\partial X_1} & \dots & \frac{\partial f_1}{\partial X_N} \\ \vdots & \ddots & \vdots \\ \frac{\partial f_m}{\partial X_1} & \dots & \frac{\partial f_m}{\partial X_N} \end{bmatrix} \quad (3.16)$$

at $\mathbf{X} = \bar{\mathbf{x}}$, then $\mathbf{U}_{\bar{y}}$ is given by

$$\mathbf{U}_{\bar{y}} = \mathbf{C}_{\bar{\mathbf{x}}} \mathbf{U}_{\bar{\mathbf{x}}} \mathbf{C}_{\bar{\mathbf{x}}}^\top \quad (3.17)$$

The LPU does not provide any information about the shape of the probability distribution of $\mathbf{U}_{\bar{y}}$ or its components. The results of the measurement are obtained from the estimates and the combined standard uncertainties – the positive square roots of the diagonal terms of the covariance matrix.

3.2.3.3 Finite Difference Methods

Included in the definition of the LPU is an alternative method of determining the sensitivity coefficients in (3.16), without the need to know the measurement model, f , explicitly. This technique can be described as a finite difference method and involves measuring the change in Y while varying a particular X_i and holding all other input quantities constant. This is often used when there may not be a model available for a particular process but a rudimentary uncertainty analysis is required, or if the computational power is available to recompute the finite differences when the estimates change. Typically, the sum of the estimate and the standard uncertainty of each input quantity $\bar{x}_i + u(\bar{x}_i)$ is used, although a more rigorous version also includes the standard uncertainty subtracted from the estimate $\bar{x}_i - u(\bar{x}_i)$ to check for asymmetry. Because only two points are used to solve for each sensitivity coefficient (the estimate and the estimate plus standard uncertainty), this uncertainty propagation also linearises the measurement model.

If all of the input quantities are considered independent and the standard uncertainty was chosen as the value with which to perturb the input quantities, then by subtracting the estimate of the measurand from each sample and adding the results in quadrature, the combined standard uncertainty in the measurand can be obtained:

$$u_c(\bar{y}) = \sqrt{\sum_{i=1}^N \left[\frac{1}{2} \{f[x_1, \dots, \bar{x}_i + u(\bar{x}_i), \dots, x_N] - f[x_1, \dots, \bar{x}_i - u(\bar{x}_i), \dots, x_N]\} \right]^2} \quad (3.18)$$

3.2.4 Expanded Uncertainty and Coverage Intervals

Although it is recommended to express a result with combined standard uncertainty $u_c(\bar{y})$, it is often required, especially in safety critical applications, for the uncertainty to encompass a larger fraction of the distribution of values that could reasonably be attributed to the measurand.

An expanded uncertainty, U , is instead used and is related to the combined uncertainty by $U = ku_c(\bar{y})$ [12, p. 6.2.1]. The multiplying factor, k , is termed the coverage factor and is typically in the range 2 to 3, often either of those two integer values and is defined by specifications or standards relating to the application. Using expanded uncertainties, the result can be expressed as $\bar{y} \pm U$, which is a popular format for datasheets and specifications.

To obtain a coverage factor that states a probability (e.g. 95%) that the true value of a measurand is within the associated interval is not straightforward, and depends on the probability distribution of the measurand. If all input quantities are Category A uncertainty components and the measurement model is linear, then the measurand distribution can be assumed to be Gaussian. In this case, the coverage interval is known as a confidence interval and can be given as a percentage by $\text{erf}(z/\sqrt{2}) \times 100$, where $\text{erf}(x)$ is the Gauss error function of x .

In situations where the above conditions cannot be met, a level of confidence can be obtained by calculating the effective degrees of freedom ν_{eff} of the distribution of the measurand. This process is explained in Annex G of [5]. For Monte Carlo propagations with sufficient samples, the confidence interval can be found by analysing the distribution of the measurand and obtaining the deviation from the estimated value which encompasses the desired percentage of samples (e.g. 95%).

3.3 Sensitivity Analysis

A benefit of propagating uncertainties through the measurement model is that an analysis of the sensitivity of the measurands to each input quantity can be performed. The sensitivity coefficients obtained from the measurement model can either be compared directly or multiplied by the standard uncertainty of the respective input quantity, in order to obtain an uncertainty figure for the measurand which can be compared with those calculated for other input quantities. This method is similar to the finite difference propagation technique described in 3.2.3.3, which can also be used to perform a sensitivity analysis. Because the input quantities are perturbed from their estimate sequentially (while all others are held at their estimate), this form of sensitivity analysis is termed “sequential perturbation”.

The results of the sensitivity analysis can be very useful to the metrologist. Not only can the relative impact of different input quantity uncertainties be reviewed, but also complicated behaviour in the combined standard uncertainty may be better understood; Figure 3.7 shows an example. Sensitivity analyses are also an efficient approach to reducing combined standard

uncertainty. Once input quantities with dominant contributions have been identified they can be targeted for improvement – or in some cases an alternative measurement model can be used which avoids them.

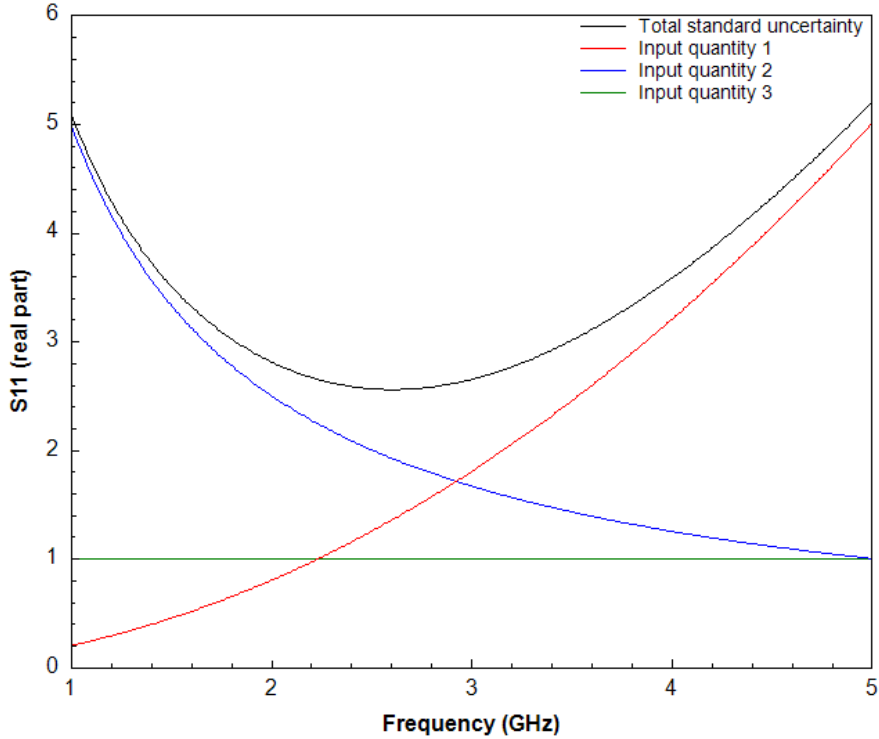


Figure 3.7: An example of results from a sensitivity analysis which reveal the origins of the complicated behaviour of the combined standard uncertainty with respect to a variable (in this case frequency).

3.4 Conclusions

This chapter presented how measurements underpin modern life, supporting trade and commerce and facilitating new discoveries in science and engineering. Through traceability and the unit system, the evaluation and management of uncertainty in measurements generates confidence and trust. In an attempt to standardise the definition and representation of measurement uncertainties, an internationally-used guidance document, the GUM, offers rigorous methods to evaluate these uncertainties. However, the GUM continues to be developed, and recently an inconsistency was created in the evaluation of Category A uncertainty components. This chapter

has reviewed the inconsistency from the objective of electromagnetic measurements, an area of metrology where the effects have been shown to be potentially significant.

Three methods for propagating uncertainty through a measurement model to determine the combined standard uncertainty of the measurands were described. Although the Monte Carlo method preserves the most information about both the uncertainties of the input quantities and the measurement model, the higher computational effort can be prohibitive in some cases. Instead, the LPU provides two linear alternatives, which are often much more efficient but require validation to ensure that the measurement model can be treated as linear.

The idea of expanded uncertainty and coverage intervals was introduced, these being met frequently in Category B uncertainty components defined from datasheets and specifications. A confidence interval is straightforward to calculate if the measurement involves only Category A uncertainty components and has a linear measurement model, or if a Monte Carlo propagation is used and the probability distribution of the measurand can be attributed to a standard type. In other cases, a coverage interval can be calculated using knowledge of the input quantities and further guidance from the GUM.

Finally, this chapter described sensitivity analysis, which can be carried out using results from the LPU procedure. The framework presented in this thesis utilises a sensitivity analysis to allow the user to examine and attempt to minimise significant sources of uncertainty, which is especially important in sensitive electromagnetic measurements such as those made on-wafer.

4 Evaluating Uncertainty in Vector Network Analyser Measurements

4.1 Introduction

The dramatic growth of radio-based devices and applications over the last 50 years has led to the VNA becoming a critical instrument in most RF and microwave laboratories. Many of these applications required both accurate and reliable measurements from these VNAs, particularly so in areas such as manufacturing, modelling and design. This is often driven by requirements given in international Quality Management documents such as the ISO 9000 series of standards [71] (for manufacturing and process control) and the ISO 17025 standard [72] (for calibration and testing).

The requirements given in these international standards are for measurements that can be demonstrated as fit-for-purpose (in terms of the achievable level of accuracy, etc) and made traceable to the international system of units [73], [74]. These requirements were not trivial for a VNA due to the complicated nature of the VNA's operating principles, for example the calibration mathematics. Combined with the available computing power and cost at that time, a full or rigorous evaluation of uncertainty for VNA measurements, per for example the ISO GUM document, was difficult and time-consuming. This led to much work by experts in this field to develop easier methods that addressed these needs in ways that were suitable for use by end-users in the manufacturing, calibration and testing communities. Much of this work was undertaken by the ANAMET Technology Group (www.npl.co.uk/anamet) during the 1990s. This resulted in a series of reports [75]–[77] describing the development of a guidance document that gave a procedure for assessing the performance of calibrated VNAs. The resulting guidance document [10] was published by the European co-operation for Accreditation (EA, www.european-accreditation.org)

so that laboratories operating to the ISO 17025 standard and/or ISO 9000 series of standards could implement the method for their own purposes. Ownership of this EA document was later transferred to the European Association of National Metrology Institutes (EURAMET) and re-published [11] as part of their Calibration Guides series of documents. This document, along with the recent updated version, is available as a free download from the EURAMET web-site: www.euramet.org.

In addition to the EURAMET guide, VNA manufacturers have also produced their own advice for users to estimate the combined standard uncertainty in their measurements [78] and provided software tools in some cases [79]–[81]. Often this advice is based on the same methods presented in the EURAMET guide.

In more recent years rigorous evaluations of VNA uncertainty have become possible, through the efforts of NMIs, industry, and their access to greater computing resources. The difference between the previous approaches (which we will call “residual error” evaluations) and rigorous evaluations concerns the way in which uncertainty contributed by the VNA calibration is estimated and included in the measurement model. The two methods will be discussed later in this Chapter. Figure 4.1 illustrates the general structure of VNA uncertainty sources and evaluation, from which each component will now be explained.

4.2 VNA Measurement Model Input Quantities

4.2.1 Calibration Standards

In order to perform the calibration, or error correction, of a VNA as described in Chapter 2, we must compare measurements of impedance standards to definitions of their true values in order to obtain error coefficients. It is interesting that although sources of error in the calibration cover both systematic and random types, when the calibration is performed and these quantities are measured, any random errors are “frozen” in the evaluated combined uncertainty, their contribution becoming purely systematic.

4.2.1.1 Definitions

Because the definitions of impedance standards are based on prior measurements, and all measurements include uncertainty, they are also included as a source of uncertainty in the VNA measurement model. We will now look at how uncertainty can be included in the three types of

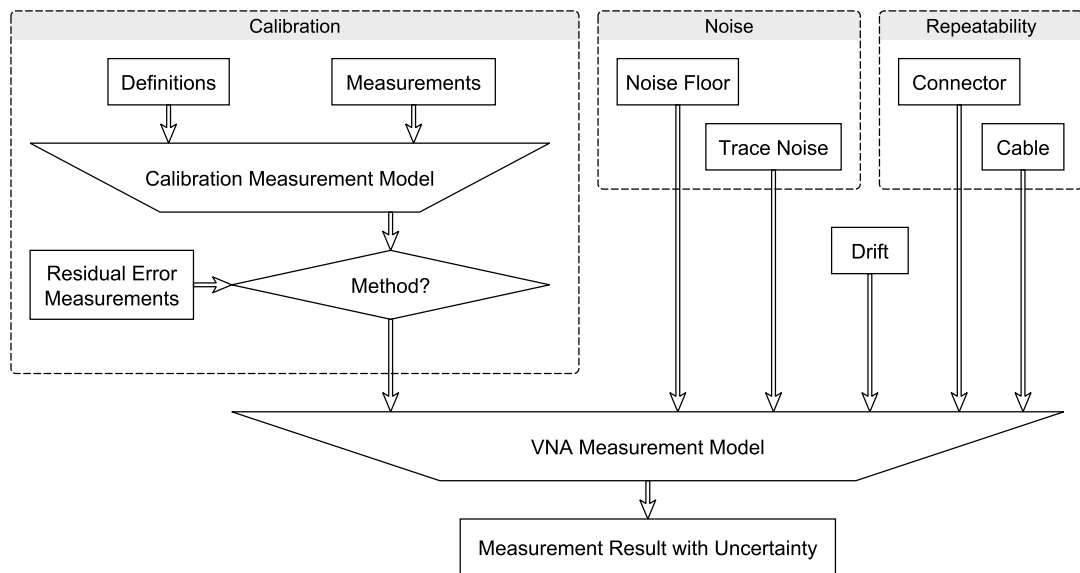


Figure 4.1: Structure of VNA uncertainty evaluation. Input quantities are shown at the top of the diagram, grouped where applicable. Uncertainties from the calibration are either evaluated directly (rigorous/full evaluation) or are estimated after the calibration has been performed (“residual error” evaluation). Typically the calibration measurement model is processed as part of the VNA measurement model, but it is shown separately here to distinguish the difference between VNA uncertainty evaluation methods.

standard definition commonly used in VNA calibration routines.

Databased Definitions The simplest definition of an impedance standard is the databased definition, which consists of a table of S-parameter values. The standard is characterised by measurement on a VNA which has been calibrated to a suitable accuracy, i.e. using standards which are at an appropriate position in the traceability chain (closer to the primary standard). The combined standard uncertainty of the characterisation is then provided with the estimates as the definition of the standard.

It is important to characterise the standard across a suitable frequency range, usually the entire range for which it can be applied. In addition to the combined standard uncertainty, the covariances between the real and imaginary components of the measured S-parameters can also be included in the standard definition for more accurate uncertainty evaluations in measurements using the standard [82]. If the standard will be used to calibrate VNAs producing results to be used in time-domain studies or multi-harmonic studies (i.e. nonlinear work), then ideally covariances between S-parameters for each frequency should be included. Because this is something which would consume a lot of data storage, the saving of this information is not supported by VNAs at this time, although external software can be used to include this [17].

Polynomial Model Definitions In order to reduce the amount of data required to accompany the standard, one-port models are often defined as coefficients of a polynomial fit between reflection coefficient and frequency. This characterisation is performed by the manufacturer and the coefficients are available in the user manual or specification sheet for the impedance standards. Similar to the databased definition, care must be taken to ensure the characterised polynomial fit is valid across a suitable frequency range.

An example of a short-circuit polynomial fit, as defined in [83], is

$$L_S = L_0 + L_1 f + L_2 f^2 + L_3 f^3, \quad (4.1)$$

$$Z_S = j2\pi f L_S, \quad (4.2)$$

$$\Gamma_S = \frac{Z_S - Z_r}{Z_S + Z_r}, \quad (4.3)$$

where L_S and Z_S are the respective inductance and impedance of the short-circuit, L_n are coefficients provided by the definition of the standard, Z_r is the reference impedance and Γ_S is the reflection coefficient of the short-circuit at frequency f . A similar model is used for open-circuits, with the inductive component replaced with a capacitive one.

Although no manufacturers are yet providing uncertainties with the polynomial coefficients supplied in their standard definitions, some have included the ability for future incorporation in the data file structure. In addition to uncertainty originating from the measurement of the standard, there will also be uncertainties relating to the error of the polynomial fit. Because of this, the polynomial definition is typically the least accurate type of standard definition, however it is popular due to the portability of the small number of coefficients which can be defined for the entire set of manufactured models.

As an alternative fitting technique, artificial neural networks have also been investigated as a way of storing information about standards [84]. However, the ability to evaluate the uncertainty introduced by the training of the neural network is not as straightforward as for the fitting of the polynomial model.

Physical Definitions Typically understood as the most accurate, physically defined standards use robust geometric models to calculate their impedances from dimensional measurements with excellent traceability. Models are available in coaxial transmission line for short-circuits, open-circuits and arbitrary line lengths. Good examples of these models and their derivations can be found in [83], [85, Appendix C]. Matched loads are more difficult to accurately model and so they are typically included as a databased standard, even if the other standards are physically defined. In order to avoid this issue, the TRL calibration can be used, which requires standards that can all be physically defined. This combination of calibration model and standard definition is commonly used by NMIs when performing traceable characterisations of other standards (i.e. databased definitions).

To obtain uncertainties in the reflection coefficients of physically defined standards, which are the measurands which we would then like to use as input quantities to the VNA uncertainty evaluation, an additional uncertainty evaluation must be performed. This takes the estimates and uncertainties of the dimensional measurements of the standards and propagates them through the measurement model (the geometric model relating dimension and frequency to reflection coefficient) to obtain the reflection coefficients with uncertainties required.

Dimensional measurements of the standards are usually supplied by the manufacturer for TRL calibration kits, but like the other definition types can be supplanted by recent measurements performed by NMIs or calibration providers. Another benefit of physically defined impedance standards is that their definition is valid over their entire valid frequency range, removing the risk associated with databased and polynomial definitions.

Covariance information between each parameter is not required to be supplied by the definition because the dimensional measurements should be uncorrelated (they are separately manufactured parts). During the uncertainty evaluation to obtain the reflection coefficients of the standards, covariances between both the complex impedance components and those at different frequencies are calculated. Therefore physical definitions are well suited to both portability, accuracy and use with time-domain or nonlinear measurements.

4.2.1.2 Measurements

During the calibration procedure the impedance standards are measured. Although the VNA is not yet calibrated, it is still performing a measurement (with reference to an arbitrary impedance) and so all of the sources of uncertainty additional to those from the calibration will be included. Sources such as noise are therefore counted several times during a VNA measurement due to their inclusion in the prior calibration measurements. Because of this, it is important to include correlations where possible for these sources as they will have a greater impact on the combined standard uncertainty of the result.

4.2.2 Noise

Noise plays an important role in RF and microwave engineering and a lot of effort and technology is used to minimise its impact. It is a random effect which is unavoidable and cannot be corrected for, both in communication systems and instrumentation. Wireless transmission systems and receivers must be designed to handle signals with a considerable amount of noise and receive weak signals with a very low signal-to-noise ratio. Likewise, VNA transmission measurements of devices with high isolation or reflection measurements of devices with low insertion loss also exhibit a low signal-to-noise ratio. To obtain accurate results, it is important for VNA manufacturers to provide instruments with low noise sources and receivers. To ensure that measurements which are more susceptible to noise are accurate, it is important to quantify the noise affecting the measurements so that it can be included as a contribution to their combined standard uncertainties.

The amount of electrical noise in VNA measurements is a sum of thermal noise and contributions from the VNA components. Thermal noise, caused by the random motion of free electrons in a conducting material by heat, is specified as $4 \times 10^{21} \text{ W/Hz}$ (-174 dBm/Hz) [78]. The intermediate frequency bandwidth (IFBW) setting on the VNA controls the frequency range of

signals being measured at each discrete point in the sweep, and can typically be set from 1 Hz to more than 10 kHz. It is this figure which multiplies the thermal noise to provide a theoretical minimum noise floor if we were to assume the VNA did not contribute any noise itself. The disadvantage of a very low IFBW is that the VNA takes longer to perform the measurement, so there is a compromise between speed and accuracy. This provides a good example of where uncertainty evaluation can have a direct benefit to measurement accuracy - if the IFBW is reduced the uncertainty due to noise should also reduce. By quantifying the uncertainty the engineer can make an informed decision as to what value to set the IFBW, which could have time implications, especially important in a manufacturing environment.

In addition to the thermal noise, the VNA contributes noise from the source, receiver and other test set components (i.e. local oscillator phase noise). Setting attenuators to lower values will improve noise as resistors add additional thermal noise to the measurement. The noise figure (NF) of a VNA is typically quoted in the specifications, and can be used with the thermal noise to calculate the theoretical noise level L_N of the VNA measurement [78]:

$$L_N = -174\text{dBm} + NF + 10 \log(S_F)\text{dB} + 10 \log\left(\frac{\text{IFBW}}{\text{Hz}}\right)\text{dB} \quad (4.4)$$

where S_F is the IF filter shape factor, relative to an ideal rectangular filter. For the purposes of uncertainty evaluation, VNA noise level is measured on the instrument itself and is typically included in the measurement model as two input quantities, noise floor and trace noise. It is important that the VNA settings (IFBW, test port power, averaging) are the same as will be used for the DUT measurements, and that no calibration is applied.

Noise floor describes the noise present in the measurement with no external signal present. It can be measured with a matched load connected directly to the test port and should not include any noise contribution from the VNA source. Alternatively it can be measured from the transmission measurements of a 2-port VNA while short-circuits or open-circuits are connected for the trace noise measurement described below. Many measurements are made ([11] suggests a few hundred) and the standard deviation is calculated for each frequency point.

Trace noise includes noise contributions from the VNA source and is a function of the measured power at the receiver. It is measured with a short-circuit or open-circuit connected directly to the test port.

4.2.3 Repeatability

Both the connections to the DUT and movement of the VNA port extension cables contribute uncertainty to the repeatability of VNA measurements. These errors will vary when a different device is mechanically connected to the test setup, and are included for both the DUT measurement and the measurements of the impedance standards during calibration.

4.2.3.1 Connections

Connector repeatability is a fundamental quality of precision RF and microwave connectors. It can have a significant impact on DUT measurements if the response of the connector varies between multiple connections, and this perturbs the reference impedance of the calibrated VNA away from $50\text{-}\Omega$ if this occurs between connecting calibration standards.

In order to measure connector repeatability uncertainty, a short-circuit can be connected to a calibrated VNA and the reflection coefficient measured. Measurements are then repeated, reconnecting the short at a different azimuthal rotation each time. This should be done at least three times with rotations of 120° , although some guidance recommends up to 16 times [11].

4.2.3.2 Cable Stability

When test port cables are flexed, their physical dimensions are perturbed, which in turn affects their S-parameter response. Specialist VNA test port extension cables are provided to mitigate the effects of cable flexure, although they do not remove them. It is therefore advisable to restrict the movement of these cables using clamps and supports, and also to wait a suitable time (typically 30 seconds or more) for stresses in the internal dielectric to settle.

Cable stability can be characterised in different ways depending on the VNA measurement model used. The general method is to perform repeated measurements while moving the cable between a range of positions which cover the maximum extent the cable will move during measurements of the calibration standards and DUTs. Specifically, some methods connect a short-circuit to each test port cable [11], and others perform the measurements in-situ by repeating DUT measurements between moving the cables [17].

4.2.4 Drift

Drift does not strictly fit into the random or systematic error category, because it can vary over the course of measurements but is not random in nature. The dominant cause of drift is

environmental conditions, especially temperature variations. Temperature affects the physical dimensions and S-parameters of RF components in the test setup and also the behaviour of the electronic devices inside the source and receiver - both of which perturb the result of the measurement.

Drift is an important source of uncertainty to include for measurements occurring over a long period of time after calibration, especially those in a test environment or in standards labs while performing a large number of repeat measurements. In order to minimise the effects of drift, the laboratory which the VNA is located in should have good temperature control and all the equipment should have been powered on for at least 24 hours for their internal temperatures to settle.

In order to measure uncertainty due to drift, many repeat measurements are performed over a long period (24 hours or more). This procedure can be automated so that an operator is not required for the entire period. An alternative method of including uncertainty due to drift can be achieved by performing calibration measurements of standards both before and after the DUT measurements. The calibrations can be averaged and a crude standard deviation obtained.

4.2.4.1 VNA Linearity

One source of VNA measurement uncertainty which is still included in some evaluations is that from the nonlinearity of the receivers. However, in modern VNAs automatic level control corrections are sufficiently accurate to allow this error to be neglected [86], [87].

4.3 Simplified Residual Model for VNA Uncertainty Evaluation

4.3.1 Method

The EURAMET Guide [11] presents a process for evaluating the uncertainty of measurements performed on a calibrated VNA, allowing users to verify that values measured using the instrument are of acceptable accuracy. This process involves measuring a selection of dominant contributions to measurement uncertainty and combining them appropriately. Contributions include both systematic errors, which remain constant over the period of measurements, and random errors, which do not. The error model for voltage reflection coefficient (Γ) measurements performed with a VNA is represented in [11] by the following equations for one-port (4.5)

and two-port (4.6) measurements:

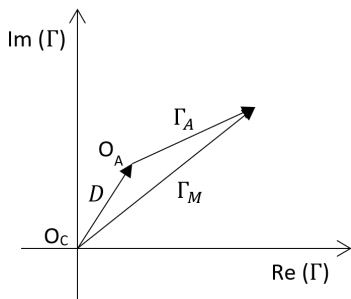
$$U_\Gamma = D + TT + M\Gamma^2 + R_\Gamma \quad (4.5)$$

$$U_\Gamma = D + TT + M\Gamma^2 + R_\Gamma + S_{21}^2\Gamma_L \quad (4.6)$$

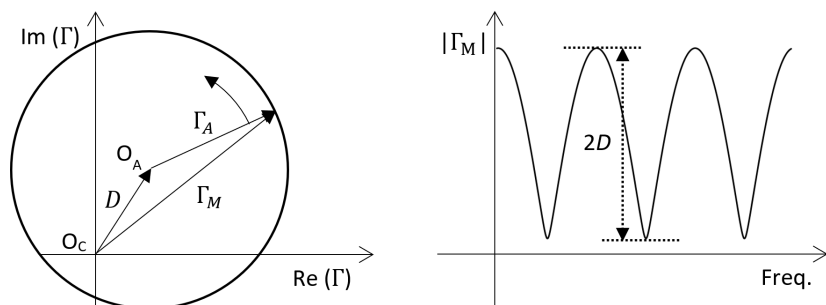
where U_Γ is the combined uncertainty in the measurement, D is the residual directivity, T represents the effect of tracking and nonlinearity, M is the residual test port match (TPM), Γ is the measured voltage reflection coefficient, R_Γ is the sum of all the random contributions, S_{21} is the nominal attenuation of the device-under-test (DUT), and Γ_L is the residual load match. The most significant systematic error contributors to the measurement uncertainty are, in most cases, the directivity and TPM.

To measure Γ , the VNA must separate reflected and incident voltage waves and then sample them using complex receivers. However, various components in the signal path may cause a portion of the incident wave to leak into the reflected wave receiver without having reached the DUT. This directivity error should be removed by applying correction terms extracted during the VNA calibration. However, as no calibration will be perfect, some residual directivity error will remain (referred to as effective directivity in [11]). To measure the residual directivity, a matched load can be connected to the test port being assessed. This should theoretically reflect none of the incident wave and the only voltage present at the reflected wave receiver should be due to the residual directivity. In practise, the match of the load will never be perfect, so it is likely that using this method the residual directivity will typically be either over- or underestimated. An improved method, used in [11] and widely accepted for use with coaxial measurements, is called the ‘ripple extraction technique’. This uses a similar principle to measure the residual directivity, but significantly improves the accuracy of the residual error evaluation. An illustration of its method is provided in Figure 4.2.

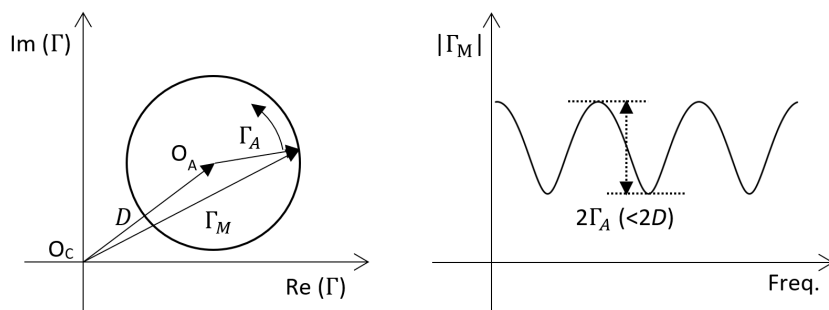
To perform the ripple extraction technique, a short length of line is connected to the test port, to the end of which is added a near-matched load covering the frequency range under test. The critical dimensions of the line section (length and radii) should be traceable to national standards and have a characteristic impedance identical to that of the VNA setup. For these reasons a beadless airline is suggested in [11]. The load can be either the same as that used for calibration or another with $0.1 \geq |\Gamma| \geq 0.2$ (in linear units) to ensure that $|\Gamma| \geq |D|$. If $|\Gamma| < |D|$, then the measured residual directivity will be underestimated as explained by Figure 4.2. If the calibration matched load is used for the measurement, the small reflection from a second connection and any loss in the airline will cause Γ to be greater than the residual directivity



(a) When measured on the calibrated VNA, a perfect matched load would reveal the actual origin (O_A) on a polar plot of Γ as offset from the calibrated origin (O_C) by the residual directivity (D). If a realistic matched load offset by a line section is instead measured, Γ as measured by the VNA (Γ_M) will be the sum of the residual directivity D and the actual Γ (Γ_A).



(b) As Γ_M is measured across a swept frequency range, the phase change in the line increases causing the phase of Γ_A to sweep also. This rotates Γ_A , resulting in ripples in the plot of $|\Gamma_M|$ against frequency. The magnitude of the ripples is equal to $2D$.



(c) However, if $\Gamma_A < D$, then the ripple magnitude is now $2\Gamma_A$ instead of $2D$ and the residual directivity as evaluated using the ripple extraction technique would be underestimated.

Figure 4.2: A graphical representation of the ripple extraction technique, including a possible failure mechanism.

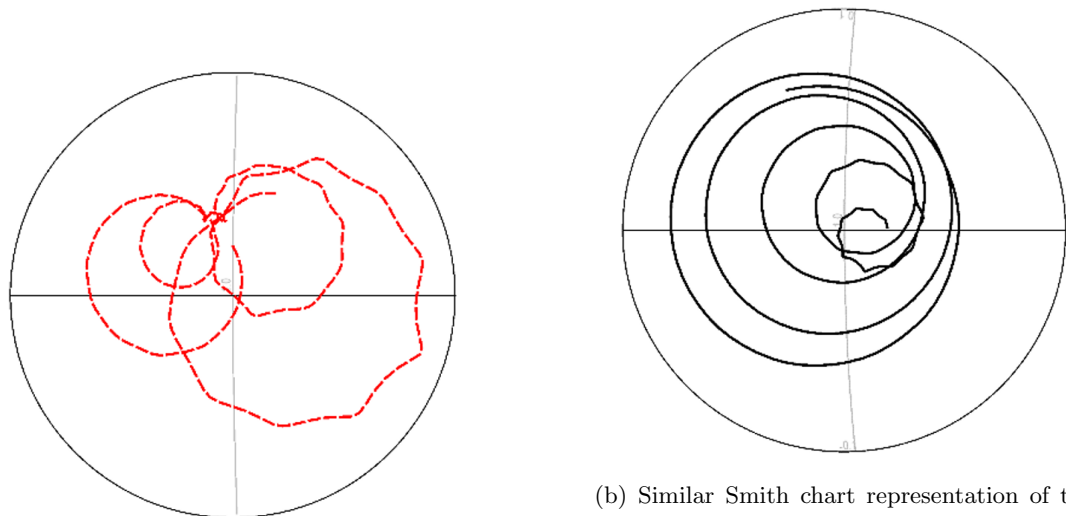
from the original measurement of the load. Alternatively, because $|\Gamma| < 0.1$ for the matched load used for calibration, using another load with a known higher $|\Gamma|$ ensures that there is no underestimate. Once the instrument has been configured, Γ is measured and the magnitude plotted against frequency using a linear scale. A ripple will then be visible on the trace, from which the residual directivity can be calculated from:

$$D = \frac{\text{MRA}_{\text{matched-load}}}{2} \quad (4.7)$$

where MRA is the maximum ripple amplitude. For coaxial measurements as specified in [11], there is a high probability that the condition required to avoid underestimation of $|D|$ is met. However, in order to assess the suitability of the technique in waveguide a method of assessing this condition has been used. By examining either a complex plot (polar or Smith chart) or a phase plot, the geometric symptom shown in Figure 4.2 can be identified. When using a complex plot, the origin should lie within the circumference of the reflection coefficient trace for a valid determination of the residual error to be achieved. For any frequency range where it does not, the ripple technique provides an underestimation of the residual error. When using a phase plot, there will be regular wrapping of the reflection coefficient phase for frequency ranges where the residual error is correctly measured, whereas when underestimation occurs the phase will vary by $< 180^\circ$ per period. An example of both plots are shown in Figure 4.3, where the result from the different load indicates an accurate residual directivity estimate across the entire measured spectrum, but the result from the calibration load shows an underestimate of the residual directivity is likely between 16 and 22 GHz. Either of these methods can be used to identify when a calibration and the ripple extraction technique needs to be repeated. If the repeat measurements still fail the test, then the choice of loads may need to be altered.

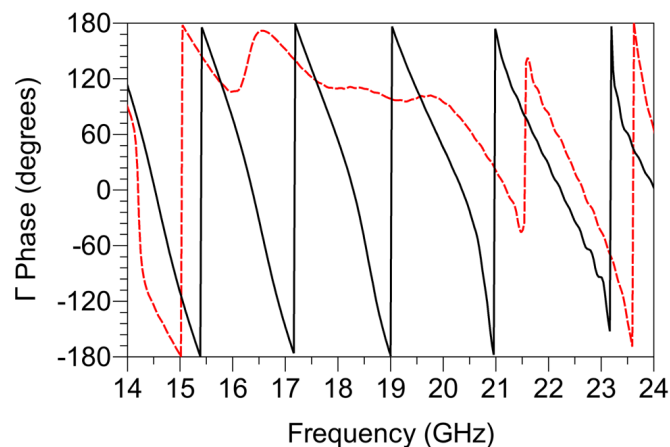
TPM is caused by imperfections in the impedance match between components in the VNA setup. This causes delayed reflections that interfere with the DUT measurement and can provide false values. Calibration also corrects for TPM, but as with directivity some residual error will remain. To measure residual TPM, a short circuit is connected to the test port being assessed. This should reflect the entire incident signal and therefore maximise any reflections in the VNA setup. If residual TPM error is present then the measured Γ will be < 1 . However, the short circuit may not provide a perfect reflection and so the ripple extraction technique is favoured for this measurement also.

To measure residual TPM using the ripple extraction technique, the same procedure as for residual directivity is followed but the matched load at the end of the line is replaced by a short



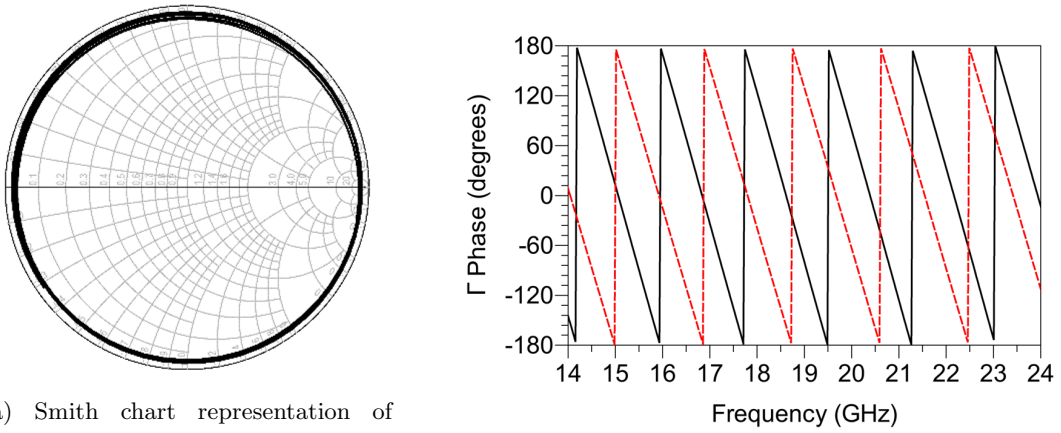
(a) A Smith chart representation, magnified about the origin, of the calibration load result.

(b) Similar Smith chart representation of the different load result. The intersection of the two grid lines on the Smith charts represents the origin of the plot ($|\Gamma| = 0$), and both are scaled separately for clarity.



(c) Phase plot of both results, with the calibration load represented by the red dotted trace and the different load by the black solid trace.

Figure 4.3: Measurements of residual directivity plotted over the frequency range of 14–24 GHz performed in coaxial transmission line using both the load used for calibration and a load from a different calibration kit. The magnitude of the reflection coefficient in both cases is around 10 milliunits.



(a) Smith chart representation of the result when using the calibration short-circuit. The result when using a short-circuit from a different calibration kit appears almost identical.

(b) Phase plot of the results when using the calibration short-circuit (dotted red trace) and the different short-circuit (solid black trace).

Figure 4.4: Measurements of residual TPM plotted over the frequency range of 14–24 GHz performed in coaxial transmission line.

circuit. A similar plot is acquired and the residual TPM is given by:

$$M = \frac{\text{MRA}_{\text{short-circuit}}}{2} \quad (4.8)$$

Since the reflection coefficient for this measurement should be close to 1, there is no risk that this value will be greater than the true residual TPM and cause an underestimate as can be the case for residual directivity. This is shown in Figure 4.4, where the origin of the Smith chart is clearly inside the circular trace (Figure 4.4a) and the phase consistently wraps across the entire measured spectrum (Figure 4.4b).

To perform the technique for both described residual error sources requires just three components: A short circuit, matched load, and a short section of line. These components are realizable in both coaxial and rectangular waveguide, so the technique should be physically possible to perform in waveguide setups. The technique can be applied to any type of calibration – for example three-known-loads and thru-reflect-line (TRL). In coaxial, the short-open-load-thru (SOLT) variant of the former is used. However, in waveguide an open circuit is not straightforward to realise or widely adopted, so a common variant of SOLT calibration which uses an offset short (SOSLT) will be used instead.

4.3.2 Application to Waveguide VNAs

Although both the EURAMET guide and VNAs using rectangular metal waveguide test ports have both existed for many years, there was no published evidence that the methods employed in the guide (the ripple technique) could be successfully applied to those measurements. The author undertook an investigation into this during the degree where they compared residual error measurements in coaxial line to those in waveguides at frequencies ranging from 8.2 GHz to 750 GHz (submillimetre-wave). This section presents the results of the subsequent papers [24], [88].

4.3.2.1 Coaxial Transmission Line and Microwave Waveguide

The ripple extraction technique was first performed on coaxial line in accordance with the EURAMET Guide [11] instruction as described in the previous section. The guide itself provides a range of typical values for both residual directivity and TPM ripple measurements with which our results can be compared to ensure that the process was followed correctly. All measurements presented in this investigation were acquired using a Keysight 5247A PNA-X instrument fitted with 1.85 mm ports attached to flexible port extender cables with rugged connectors. The coaxial measurement setup used a 75-mm beadless airline and the calibration kit matched load and short circuit. Figure 4.5 shows the ripple trace obtained by plotting $|\Gamma|$ against frequency for residual directivity and TPM measurements using an SOLT calibration. Apart from the dominant ripple, other variations in $|\Gamma|$ are due to the imperfect response of the matched load and the beadless line. The results of the measurements, along with the expected ranges provided in [11], are presented in Table 4.1. It can be seen that the measured values for the coaxial line setup fall within the typical ranges specified by [11].

The same method was applied to two types of centimetre band waveguide, WR-90 and WR-42. These waveguides have usable frequency ranges of 8.2–12.4 GHz and 18.0–26.5 GHz respectively. To avoid the effects of non-propagating (evanescent) modes created by the waveguide to coaxial adapter, an appropriate length of straight waveguide was attached to each adapter where possible and the measurement planes defined at the end of the lines. The results of the ripple extraction technique for the two waveguide sizes are shown in Table 4.2:

4.3.2.2 Millimetre-wave Waveguides

To perform measurements at frequencies above 50 GHz, a range of external frequency extender heads were attached to the VNA. These extender heads included a line section attached to each

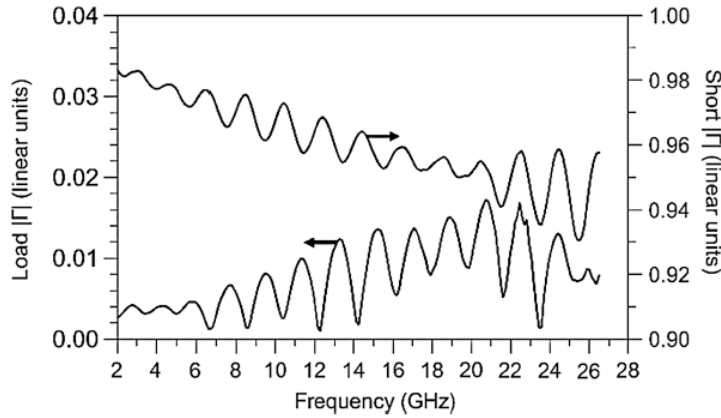


Figure 4.5: Magnitude of the reflection measurement of a matched load and a short-circuit offset by a length of coaxial line. The VNA was calibrated using the SOLT method.

Table 4.1: Residual directivity and TPM values obtained for 3.5 mm coaxial line VNA calibrations as measured by the ripple extraction method. Both SOLT and TRL calibration techniques were assessed. The range of representative residual error values from [11] has also been included for comparison.

Cal. type	Residual directivity		Residual TPM	
	Port 1	Port 2	Port 1	Port 2
SOLT	0.008	0.009	0.014	0.010
TRL	0.008	0.007	0.002	0.002
EURAMET guide [11]	0.002–0.02	0.002–0.02	0.005–0.02	0.005–0.02

Table 4.2: Residual directivity and TPM values of WR-15 and WR-05 waveguide VNA calibrations as measured by the ripple extraction method. Both SOSLT and TRL techniques were used to calibrate the VNA.

Frequency, GHz	Waveguide size	Cal. type	Residual Directivity		Residual TPM	
			Port 1	Port 2	Port 1	Port 2
8.2–12.4	WR-90	SOSLT	0.005	0.004	0.007	0.006
		TRL	0.003	0.006	0.002	0.002
18–26.5	WR-42	SOSLT	0.003	0.004	0.010	0.005
		TRL	0.002	0.002	0.002	0.001

Table 4.3: Residual directivity and TPM values of WG25 and WG30 waveguide VNA calibrations as measured by the ripple extraction method. Both SOSLT and TRL calibration techniques were measured.

Frequency, GHz	Waveguide size	Cal. type	Residual directivity		Residual TPM	
			Port 1	Port 2	Port 1	Port 2
50–75	WR-15	SOSLT	0.002	0.002	0.018	0.017
		TRL	0.002	0.002	0.009	0.007
140–220	WR-05	SOSLT	0.008	0.009	0.019	0.024
		TRL	0.007	0.008	0.021	0.015

test port of suitable length to avoid effects caused by evanescent modes that may exist close to the test port. To study the performance of the ripple extraction technique at millimetre wavelengths, WR-15 and WR-05 waveguides were chosen. These waveguides have operating frequency ranges of 50–75 GHz and 140–220 GHz respectively. The results of the ripple extraction are shown in Table 4.3:

4.3.2.3 Submillimetre-wave Waveguides

The final stage of the investigation studied the ripple extraction technique when applied to submillimetre wavelength VNA setups. The waveguide chosen for these measurements was in the 500–750 GHz band (WR-1.5) for which only one frequency extender head was available. Owing to the requirement for a through standard when using the TRL calibration method, only a three-known-loads calibration was performed, which was the one-port version of SOSLT (SOSL). The line section used was ~ 25.4 mm in length and was part of a calibration and verification kit manufactured by Virginia Diodes, Inc. All waveguide flanges, apart from the short-circuit, used precision alignment dowels located above and below the aperture. Figure 4.6 shows the setup used during the measurement of residual directivity, with a line and match connected to the frequency extender head.

It can be seen that the residual directivity is significantly smaller than the residual TPM. By assessing the phase wrapping of the ripple trace obtained for evaluating residual directivity, as shown in Figure 4.7, the ripple extraction technique appears to be subject to the failure mechanism described in the previous Section 4.3.1 and illustrated in Figure 4.2c. The lack of phase wrapping across the entire operating bandwidth shows that the ripple extraction technique

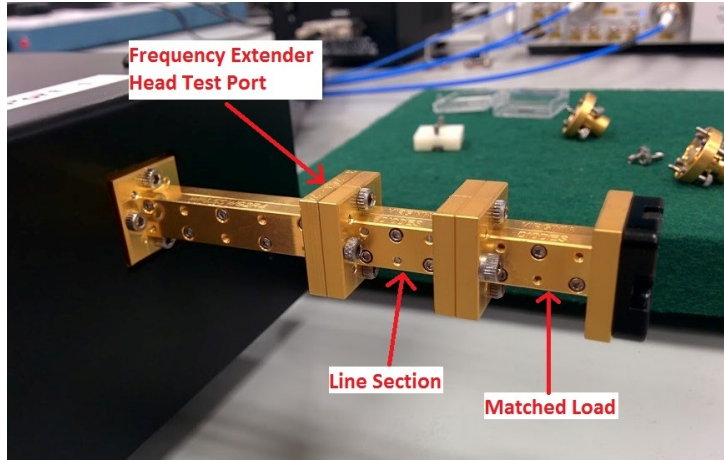


Figure 4.6: Test port setup used for residual directivity measurements in WR-1.5 waveguide.

Frequency, GHz	Waveguide size	Cal. type	Residual directivity	Residual TPM
500–750	WR-1.5	SOSLT Cal. 1	0.021	0.142
		SOSLT Cal. 2	0.025	0.065

Table 4.4: Residual directivity and TPM values of two WR-1.5 waveguide VNA calibrations as measured by the ripple extraction method. Two similar types of calibration were performed using different standards from the same kit.

was not operating within the required assumptions necessary for the technique to be valid, and therefore provided an underestimate of the residual directivity. The calibration kit used for this experiment included two full sets of standards, so the matched load was swapped and the ripple extraction technique was repeated. The issue was not resolved by this change, so the calibration was repeated, this time using the other matched load. The ripple extraction technique was then performed with the matched load used for the original calibration. However, no combination of these components provided a valid residual directivity value as assessed by the phase wrapping method. A likely cause of this effect is the poor connection repeatability inherent in this waveguide size, using typical precision UG-387 flanges. If the waveguide apertures have a greater misalignment during calibration than when the ripple extraction technique is performed, the effect of the discontinuities can cause the calibration matched load to appear to have a higher $|\Gamma|$ than the one used for the ripple extraction technique (even if the opposite were in fact true). These conditions cause the residual directivity to be underestimated as explained in Section 4.3.1.

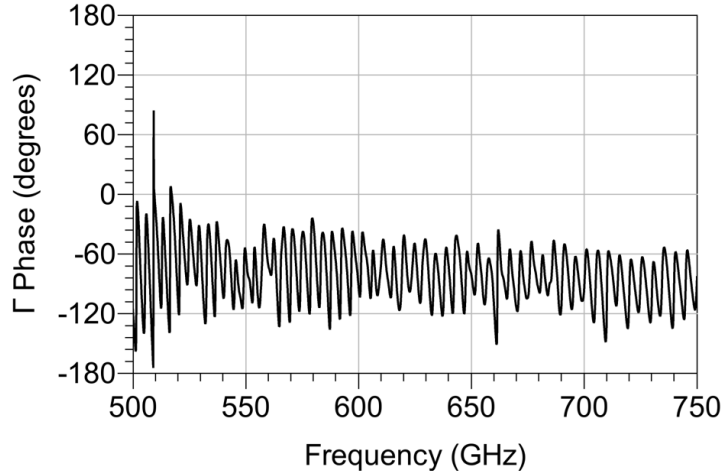


Figure 4.7: Phase plot for a residual directivity evaluation performed in WR-1.5 waveguide using an SOSLT calibration.

4.3.2.4 Waveguide Discontinuities

When a discontinuity is present between two sections of rectangular waveguide, an increased reflection will be seen at the location of the join. There are three types of discontinuity possible in rectangular waveguide: E-plane and H-plane lateral displacements, angular displacement, and corner rounding. A report produced by Bannister *et al.* [89] presented the effects of these discontinuities at centimetre and millimetre wavelengths. Subsequent work by Kerr extended this using simulations [90], [91].

The error in Γ contributed to by the effect of such discontinuities is proportional to wavelength, and therefore also the aperture size of the waveguide. At submillimetre wavelengths, the error has been shown to be considerable [92], [93]. Recently, efforts have been made to improve the connection repeatability for waveguide at these wavelengths, and a new IEEE standard [94] presents three new connector types which significantly improves the alignment. Another potential improvement attempts to reduce misalignment errors during calibration by replacing the waveguide offset short with a radiating open, and new calibration algorithms have been developed to accompany this [95]. The open standard must be very well characterised, and the technique has not yet seen widespread uptake.

4.3.2.5 Discussion

In centimetre-wave waveguides (WR-90, WR-42), the ripple extraction technique provided values of residual directivity and TPM similar to those obtained in coaxial line. This is not surprising as providing a good quality match is used for calibration and the connections are well made and aligned, both errors should not have significant contributions outside of the VNA itself. When extended to millimetre-wave waveguide, the residual errors were found to be larger, but still within the recommended values for coaxial lines. At submillimetre wavelengths, the two calibrations that were performed resulted in significant differences in the residual errors. A likely cause for these differences is the effect of discontinuities in the waveguide components (due to poor connection repeatability and demanding mechanical tolerances) used during the calibration, especially the matched load and offset short. Additionally, by studying the phase of the measured Γ , it was shown that the ripple extraction technique was not operating within required assumptions necessary for the technique to be valid and was therefore underestimating the true value of the residual directivity. The cause of this may also be related to the poor repeatability of the waveguide connection, causing the Γ of the matched load used for the ripple extraction to be lower than that used for the calibration. Some effort were made to resolve this issue, but were unsuccessful. New improvements to submillimetre-wave waveguide flanges could significantly reduce this problem and allow the ripple technique to work more consistently with these very small waveguides [94].

A useful assessment method to test the validity of the ripple extraction technique was presented earlier in this paper, and should be performed whenever the technique is used. This assessment method views Γ measured during the ripple extraction technique on either a phase plot, a polar plot or a Smith chart. When using a phase plot, this assessment has passed if the phase is seen to be wrapping across the operating bandwidth. When using a polar plot or Smith chart, this assessment has passed if the origin of the chart lies within the circumference of the trace. If the technique is deemed to have failed based on this assessment, the VNA should be recalibrated and the ripple extraction technique should be repeated. If this does not affect the assessment result, then the near-matched load or short-circuit used during the technique should be swapped with another (preferably known to have a higher Γ) and the ripple extraction technique repeated again. Only when this assessment has passed can the results from the ripple extraction technique be considered reliable.

4.3.2.6 Conclusion

This investigation studied the effectiveness of the ripple extraction technique when applied to rectangular waveguide measurements at centimetre, millimetre and submillimetre wavelengths. Typical values of residual directivity and TPM in these three ranges have been provided. For centimetre- and millimetre-wave waveguides the ripple extraction technique works as expected. Since the standards used in this investigation are commercially available and the calibration techniques are available on nearly all VNAs, the values of residual error given in this paper are considered representative and suitable for use as reference values by other users of similar types of measurement system, to compare their own values against. This is because the performance of these systems is usually dominated by the quality of the standards and the type of calibration technique that is used. However, this investigation has also shown that the ripple extraction technique may not currently be a reliable way of measuring residual error in submillimetre wavelength systems. The effect of discontinuities at submillimetre-wave waveguide interconnections has been considered as a cause of this issue.

4.4 Rigorous Models for VNA Uncertainty Evaluation

4.4.1 Method

A rigorous evaluation of VNA uncertainty can be applied by using a measurement model which includes explicit relationships of the measurands to all input quantities. This is opposed to the residual model where the combined uncertainty from a collection of input quantities (relating to the calibration) is approximated. By including explicit relationships for all input quantities, the uncertainty evaluation can be directly traceable to primary standards.

There are several formulations of rigorous VNA measurement models in use, and most of them have been written into a software framework due to their complexity. The differences between the models are due to optimising the same mathematical relationships for different methods of processing. This section will now describe three popular VNA uncertainty frameworks.

4.4.2 Keysight PNA-X Dynamic S-parameter Uncertainty

The Keysight PNA-X Dynamic S-parameter Uncertainty option is an extension to the software provided on Keysight PNA-X VNAs. This software extension uses a separate graphical window

to allow the user to manage sources of uncertainty (input quantities), which are then referenced by the VNA software to evaluate the combined standard uncertainty in the S-parameter measurements it produces.

Uncertainties for input quantities are provided in the form of calibration kits, cables and test ports. Mechanical standards in calibration kits can be characterised with uncertainty information by either measuring them on another PNA-X with the uncertainty software option, or supplied with that information from the manufacturer if they are Keysight products. Likewise, electronic calibration units from Keysight also include uncertainty characterisations in their definition files and can be loaded directly into the PNA-X software. Cable stability can be measured in a guided process through the uncertainty software and assigned to that cable identity for future use. Likewise, the test-port is used as an identity to store measurements of noise floor and trace noise, which are again measured through a guided process.

A calibration using uncertainty information is then performed, after which the VNA will perform measurements as normal. However, with the calibration applied it is possible to also view uncertainty information in real-time (i.e. calculated after every sweep) on the display. This can be in the form of error bars and lines showing standard deviations for scalar measurands like magnitude and phase, and also uncertainty ellipses showing standard deviations of complex values on polar plots or Smith charts.

The measurement model used within the PNA-X Dynamic Uncertainty Option is not fully disclosed, but it is based on a multi-port formulation developed by Garelli and Ferrero [96]. This model rearranges the traditional calibration mathematics and creates new parameters which are very efficient for solving n -port calibration problems. This is a desirable property for commercial applications of VNAs where some communications products may require more than 24 ports to fully characterise their S-parameters.

Uncertainty information is stored in several file formats. The “.unp” format, similar to the “.snp” format, contains S-parameter data for an n -port device along with uncertainties in their respective scalar components (either real/imaginary or magnitude/phase). The Databased Standard Definition “.dsd” format contains characterisations of calibration standards, which in addition to uncertainty data from the “.unp” format includes information about the type of calibration standard which is used by the software to ensure calibrations are performed correctly. Finally, the “.sdatecv” file format can also be read from and written to, which is native to the VNA Tools II software explained shortly. A more detailed overview of the methods used in the software can be found in the product Application Note [97].

4.4.3 METAS VNA Tools II

VNA Tools II is a piece of standalone software developed by the Swiss NMI, the Federal Institute of Metrology (METAS) [14]. Based on an uncertainty propagation library called UncLib [98], also by METAS, the software is not attached to a particular VNA but can instead drive instruments from several popular manufacturers, or post-process existing measurements.

The underlying uncertainty propagation library, UncLib, specialises in linear propagation of uncertainty according the method described in the GUM document introduced in Chapter 3. Monte Carlo propagation is also included in the library, but is not as well supported. VNA Tools II defines a rigorous VNA measurement model using mathematics functions from UncLib, to which it provides measurement data and processes the uncertainty evaluation [99].

In addition to the uncertainty evaluation, VNA Tools II allows users to store collections of characterised cables and calibration standards, as well as record all measurements in a journal for both short-term reference and archiving evidence of traceability.

To store uncertainty information for S-parameter measurements, a new file format was invented for VNA Tools II, which uses the “.sdatcv” filename extension. This file format stores S-parameter data with covariances between the real and imaginary components for each parameter at a particular frequency. Covariance data of parameters between frequency points is not saved as this can create very large files for typical VNA frequency sweeps, and is not useful when evaluating measurement uncertainty in the frequency domain for devices operating linearly. As mentioned earlier, this file format is also supported by the Keysight PNA-X Dynamic S-parameter Uncertainty option, allowing standards to be used between the two different software frameworks.

4.4.4 NIST Microwave Uncertainty Framework

The Microwave Uncertainty Framework (MUF) published by the US National Institute of Standards and Technology (NIST) is another software framework for evaluating uncertainty from an NMI [17], [100], [101]. Similar to VNA Tools II, the software does not need to be used with a specific brand of VNA because it can read existing measurement files (e.g. S-parameters) and perform calibrations during post-processing. The facility is available, however, to control Keysight VNA instruments remotely which can automate long measurement tasks for metrology studies.

Because the MUF was written to support general RF and microwave metrology research at

NIST, many measurement models are included in the framework, of which VNA measurement models are just a few. The framework is provided as a collection of individual applications: **Post-Processor** contains a library of measurement models which can be evaluated using either Monte Carlo or finite difference (including sensitivity analysis) propagation techniques. **Model** allows two-port components to be defined, which can be cascaded together using **Cascade** and have their numerical parameters (e.g. length, resistance) assigned with statistical distributions using **Parameter**. One-port devices such as impedance standards are modelled as two one-port devices back-to-back. **Combine** takes a series of repeated measurements as an input and produces an estimate with associated uncertainty, according to classical probability methods. Finally, the **VNA Uncertainty Calculator** is a customised version of **Post-Processor** which includes a graphical layout to simplify loading of the many input quantities required for the VNA measurement models. Separate models are included for VNAs with up to eight ports, and six calibration types are available [102].

The MUF does not propagate uncertainty using covariance information stored in conventional matrices. Instead, at first chance it converts uncertainty information into a set of Monte Carlo samples. The order of these samples is carefully preserved throughout subsequent calculations, which has the effect of propagating covariance information throughout the uncertainty evaluation. For example, when a physically-defined impedance standard is modelled with parameters assigned statistical distributions, the MUF will sample from each distribution, evaluate the model and produce a sample to be used as an observation of an input quantity. This sample-based preservation of covariance information is very useful for input quantities with strong correlations - for example the real and imaginary components of a complex S-parameter measurement. Rather than statistically averaging a set of repeat measurements to assign a single covariance value, as outlined in the GUM document, the repeat measurements are preserved so that the distribution of covariance information is also used during the uncertainty evaluation. For most types of uncertainty source in the MUF this benefit is not realised because Monte Carlo samples are synthesised from statistical definitions (e.g. models, parameters), but for large numbers of repeat samples the functionality is available. The side-effect of this benefit is that keeping all of the measurement data, or synthesised Monte Carlo samples, can consume a lot of memory. However, modern computing resources mean that the space requirement is no longer a difficulty.

One of the most flexible features of the MUF is that any user can define their own models and post-processors (both are measurement models). This allows the MUF to provide uncertainty evaluations for new methods of electromagnetic wave metrology and communication systems

research [103], [104].

4.5 NVNA Uncertainty Evaluation

It was explained in Chapter 2 that in order to measure nonlinear devices using a VNA, the absolute power and phase of the waves at all test ports must be known. For a VNA to obtain this information, it must undergo additional calibration steps involving a phase reference and power meter. In addition, for mixer-based VNAs (the type used throughout this work), a stable phase reference must be connected to another port of the VNA and measured alongside any DUT measurements. Each of these additional requirements add input quantities to the NVNA measurement model when compared to that of the VNA, and these will now be discussed.

4.5.1 Phase Reference

The phase reference used during calibration contributes both systematic and random error sources. Because it is used as a calibration standard, systematic error due to inaccuracies of the characterisation is a primary concern. This is especially true for the phase calibration, where the error coefficients calculated using measurements of the characterised reference have a direct relationship with the calibrated DUT waves. This is different to the relative calibration of the VNA, where at least some of the coefficients are the result of information from several different impedance standards, therefore reducing the impact of a single inaccuracy in the characterisation or measurement of a single standard. In addition, for measurements of nonlinear microwave (and millimetre-wave) devices, harmonics of interest can be well above 10 GHz, where the wavelength in a transmission line is short and connector and cable repeatability errors (i.e. random errors) can have a large effect on the accuracy of the phase calibration.

The second phase reference used during measurements with a mixer-based NVNA recovers the true phases of measured waves after the local oscillator frequency changes. This phase reference does not contribute systematic error because the absolute phase values are mathematically cancelled during calibration (when measuring the first phase reference) and therefore they do not need to be known. Random errors due to connector and cable repeatability are also insignificant when measuring this device because their contributions are also cancelled during calibration and the device is never reconnected or moved afterwards. Instead, for this phase reference the dominant uncertainty contribution is drift, because to quantify the varying local oscillator phase and correct the DUT measurements, the reference phase must be constant. For this reason

commercially available phase references will typically use temperature-controlled electronics to minimise the drift of the produced harmonic tones, which improves the issue [105]. Because this phase reference is driven by another source (usually from within the NVNA, e.g. a 10 MHz reference clock), the phase noise and amplitude of this source will also have a significant effect on the uncertainty contribution. Blockley *et al.* provide an excellent review of this source of uncertainty and its impact on NVNA measurements [106]. The key finding of this review is that for measurements using an IFBW of 100 Hz or below, the uncertainty contribution of random errors originating from the phase reference is negligible for typical DUT measurements. Although for VNA measurements IFBW settings above 100 Hz can be common for wideband frequency sweeps, the harmonic nature of NVNA measurements means that the IFBW is typically 30 Hz or below, which satisfies the recommendation from [106]

To provide a suitably accurate characterisation of the phase reference a sampling oscilloscope can be used to measure the output of the device [107]. This oscilloscope can be calibrated using electro-optic techniques traceable to primary standards [108], [109]. This service is provided by NIST for Keysight phase references and includes information on the uncertainty in both the amplitude and phase of each measured harmonic [110]. The covariances between these components, and between those at different frequencies, are not included. This can significantly affect the combined uncertainty of some nonlinear DUT measurements, including those involving cross-frequency terms such as behavioural models described later in Chapter 5.

For this research two phase references were taken to NIST and re-characterised. The results of this characterisation included covariance information between the tone measurements at different harmonics and therefore can be used in a rigorous evaluation of uncertainty for nonlinear behavioural models. Results of the characterisation are shown in Figures 4.8 and 4.9, which show excellent agreement between the estimates at each frequency and Fourier-transformed time step. Due to the considerable effort required to perform a characterisation using an electro-optically calibrated sampling oscilloscope, a new technique was trialled to characterise our phase references using an NVNA. The instrument was calibrated using a phase reference which already had a traceable characterisation including covariance information, from which the our phase references were then measured. This will produce a characterisation with larger uncertainties because an additional measurement has been included in the traceability chain. The results show uncertainties of around 0.5 degrees across the spectrum, with a considerable ripple in measured phase occurring above 35 GHz. The origin of this ripple was not found during the characterisation, but it occurred during de-embedding steps.

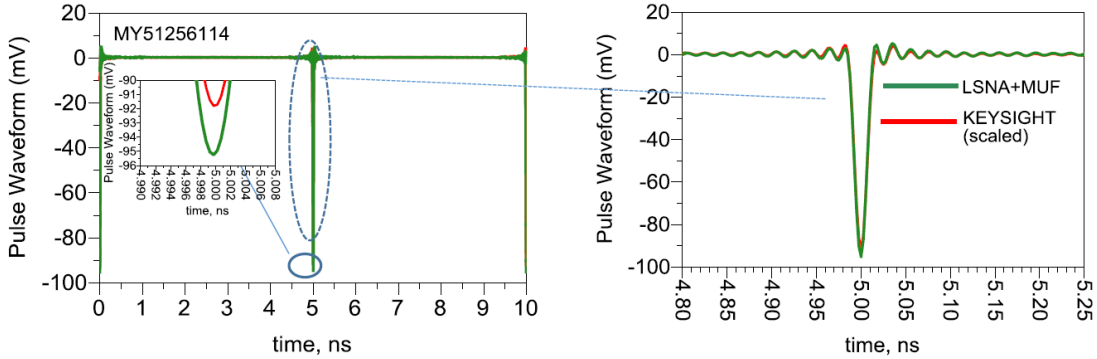


Figure 4.8: Time domain representation of the pulse train which creates the harmonic comb in the frequency domain. The pulses repeat every 5 ns when the generator is driven with a 10 MHz stimulus. This figure is used with permission from a report produced by Gustavo Avolio¹, who performed the measurements at NIST using the Microwave Uncertainty Framework (MUF). The results show good agreement when compared with the Keysight characterisation stored on the device memory.

4.5.2 Power Meter

Power measurement is a well-established field of electromagnetic wave metrology and is widely applied to measurements in industry as well as academia. Because of this, manufacturers have produced application notes and software to help users evaluate the uncertainty in their power meter measurements [110], [111]. The uncertainty evaluation presented in this project is based on the power meter measurement model used by Keysight and described in [110], due to the use of Keysight power meters and the fact that this model is already included in the MUF software.

The distribution of uncertainty contributions are shown in Figure 4.10. The impedance mismatch between the source to be measured and the power sensor is the dominant source of uncertainty, which is not surprising as it has a direct effect on the amount of power that reaches the sensing element.

The measurement model for the power meter can be written as

$$P = \frac{M_u(P_m - t)}{K_b m}, \quad (4.9)$$

where P is the power incident to the sensor (the measurand), M_u is the gain due to mismatch of the power sensor, P_m is the value given by the power meter, t is the sum of offset errors including

¹Gustavo Avolio is a nonlinear device measurement specialist, who was also on invited secondment to NIST from KU Leuven, and is now working for Anteverta-mw, a Maury Microwave company.

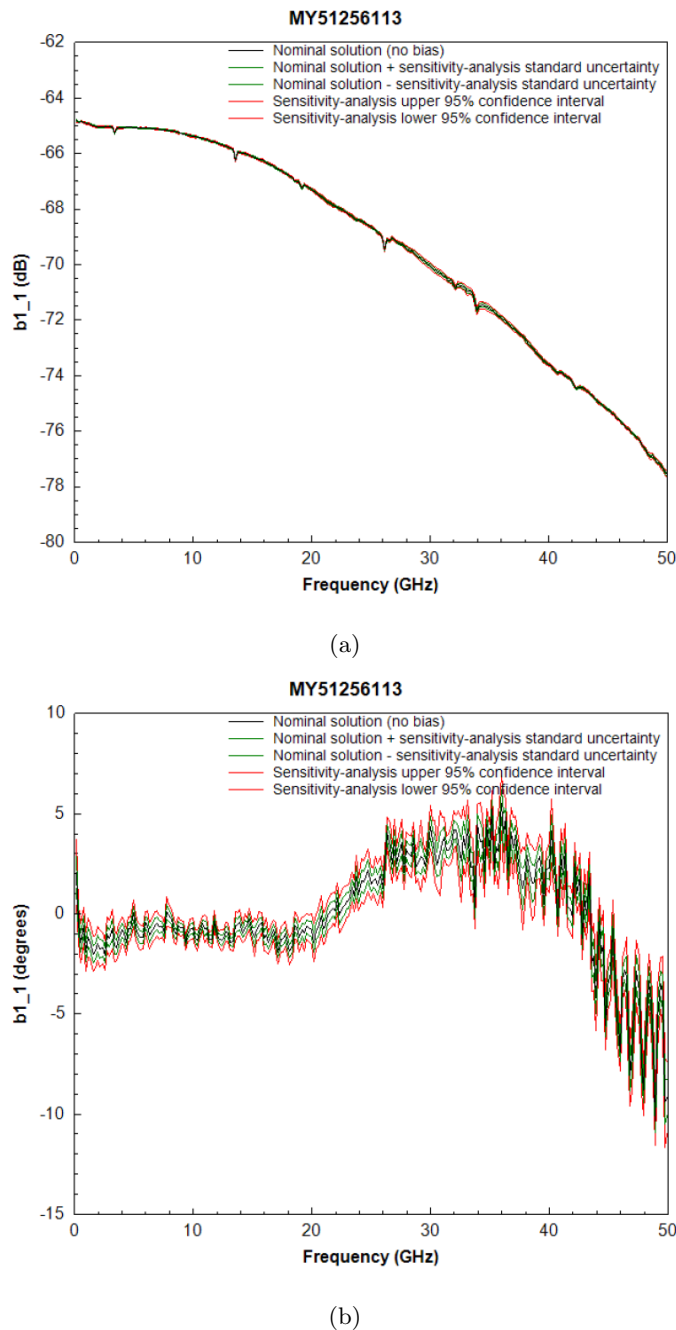


Figure 4.9: Results of the phase reference characterisation performed at NIST for unit MY51256113 displayed using the MUF measurement viewer software. The device was connected to port one of the NVNA performing the measurement, so the amplitude (a) and phase (b) of the b wave for the fundamental harmonic at port one (b_{1-1}) is shown.

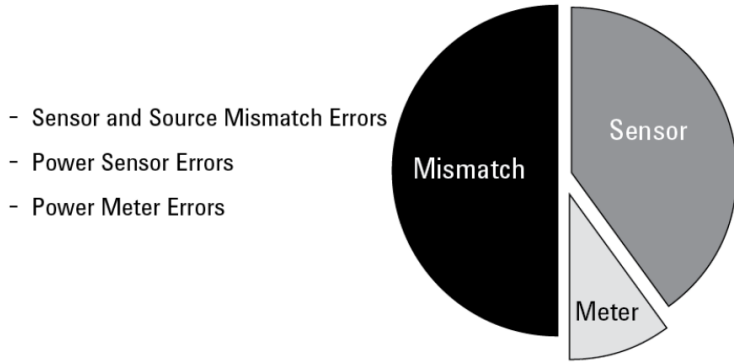


Figure 4.10: This chart shows a typical distribution of uncertainty values for its three largest causes: mismatch, sensor and meter specifications. It reveals why low mismatch specifications for the power sensor and source is so crucial [110].

noise and zeroing errors, K_b is the calibration factor of the power sensor, and m is the sum of multiplicative errors including sensor calibration and instrumentation errors.

For an ideal measurement, M_u and m are all equal to one and t is equal to zero. When the model is used with a simple evaluation of uncertainty, the worst-case values for each error can be inserted or the root-sum-of-squares (RSS) calculated to provide a range of values which the result could take. This is the propagation technique suggested in the [110]. The MUF implementation instead sets all the input quantities to their nominal values (e.g. one or zero for the pure error terms) and instead assigns distributions to each of them. The uncertainty propagation then samples each input quantity from their distribution and obtains a sample for the measurand. A sensitivity analysis can also be performed for this model, and an example result is shown in Figure 4.11.

4.5.3 Propagation of Uncertainties

Although there are many guides and software frameworks available for propagating uncertainty through VNA measurements, there are only two published options currently available for NVNA measurements [16], [17].

4.5.3.1 Analytical Covariance-Based Propagation

Lin and Zhang published a covariance-based analytical method for linear propagation of uncertainty which allows a GUM-based technique to be applied to NVNA uncertainties [16]. Partial

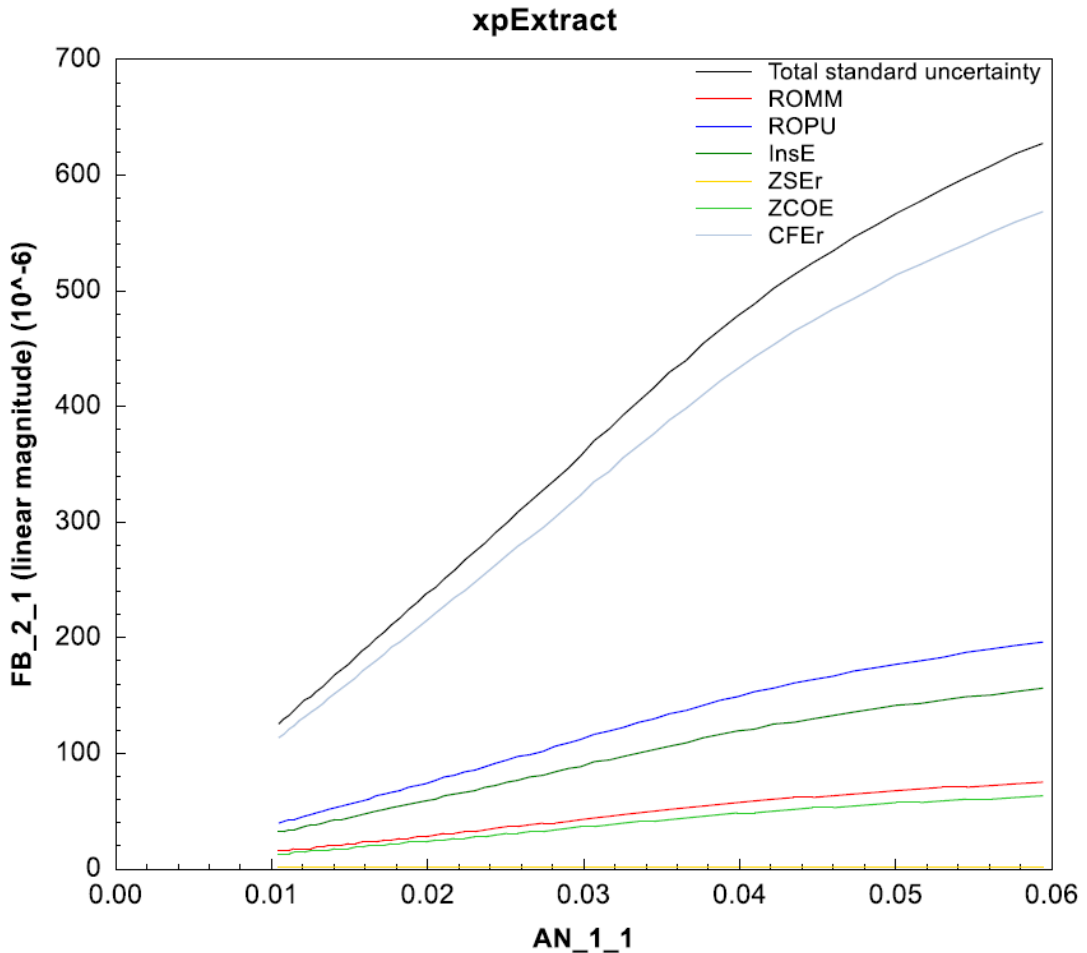


Figure 4.11: An example sensitivity analysis showing the effect of power meter uncertainties on an X-parameter measurement. The plot shows the amplitude of the X-parameter representing the large-signal output of the amplifier into a matched load versus a swept input power. The values are in units of square-root Watts. The input quantities Reference Oscillator Mismatch (ROMM), Reference Oscillator Power Uncertainty (ROPU) and Instrument Error (InsE) all contribute to m , Zero Set Error (ZSEr) and Zero Carryover Error (ZCOE) contribute to t , and Calibration Factor Error (CFEr) represents the error in K_b . Mismatch error is not included in the power meter model but is modelled as a cascaded adapter attached to the power sensor instead.

derivatives with respect to all input quantities have been derived for the NVNA measurement model, which is shown graphically in Figure 4.12. These include the use of Cauchy-Riemann derivatives in order to accommodate ratios of the complex components used to calculate magnitude and phase values for the respective parts of the absolute calibrations.

4.5.3.2 Numerical Propagation

The MUF includes both S-parameter and wave-parameter measurement models for a VNA. The wave-parameter model was extended at NIST and used to create an NVNA measurement model which can be used to propagate uncertainty for nonlinear device measurements using the numerical methods included in the MUF - namely Monte Carlo and sequential perturbation. This was the approach chosen for the work in this project because there were already published results from this framework and it was actively supported [18]. In addition, the MUF includes preserves information about correlations between frequencies in the form of indexed Monte Carlo samples. This is an alternative to the very large covariance matrices required to otherwise store this information at each step of the propagation (although there have been recent efforts to improve this burden using principal component compression [112]). This ability is significant when using the results of the measurement to produce time-domain or cross-frequency information as required by nonlinear behavioural models, where without these correlations included the combined uncertainty may be considerably perturbed.

Figure 4.13 shows a screenshot of the MUF software VNA Uncertainty Calculator with the LSNA tab open. This part of the software allows a user to enter models for the power meter and adapters, and measurements for the power and phase calibrations. The phase reference does not use a model, but instead a characterisation file including covariances as described earlier in this section.

4.6 Conclusion

This chapter has studied the application of uncertainty evaluation to measurements performed on both VNA and NVNA instruments. After a brief introduction to typical sources of uncertainty encountered in these measurements, two versions of VNA measurement models were explained. The residual error model provides a less computationally-intensive propagation of uncertainty, which was noticeably beneficial in the years when it was developed, but this concern is now less relevant. It was shown that the residual error model can also suffer from problems during

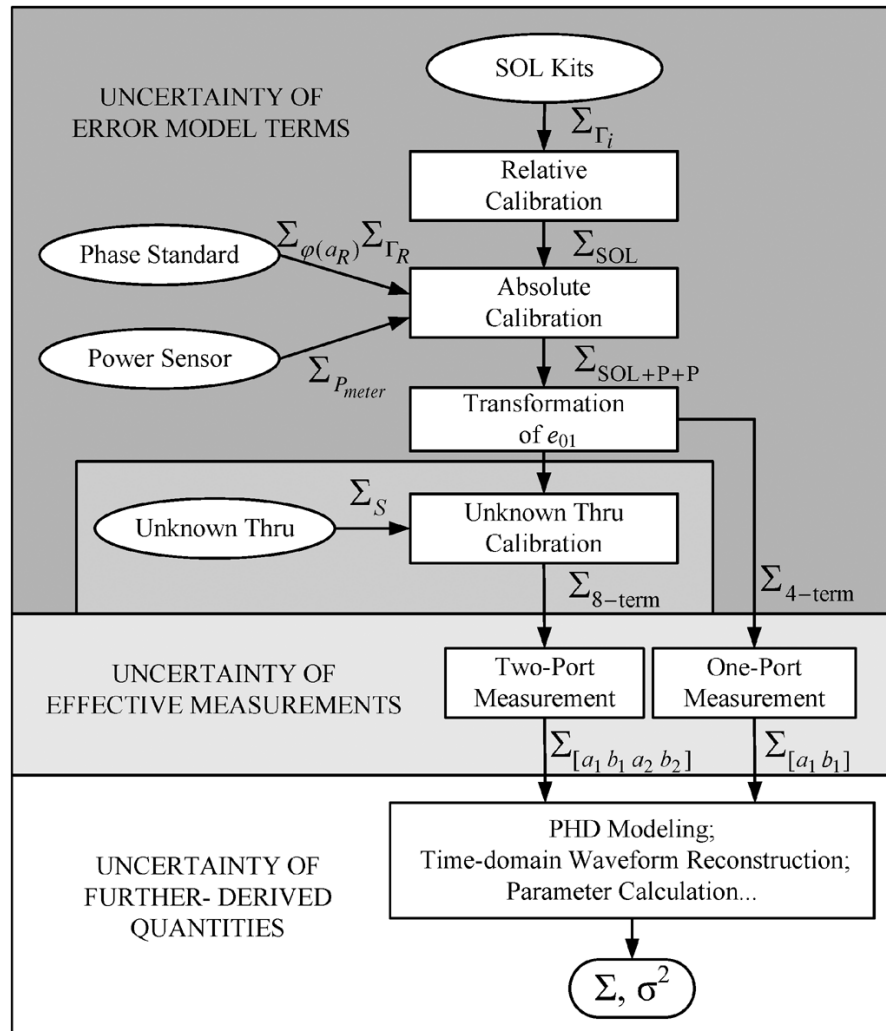


Figure 4.12: The NVNA measurement model used in [16]. Here, Polyharmonic Distortion (PHD) Modeling can be substituted for X-parameters or alternative nonlinear behavioural models.

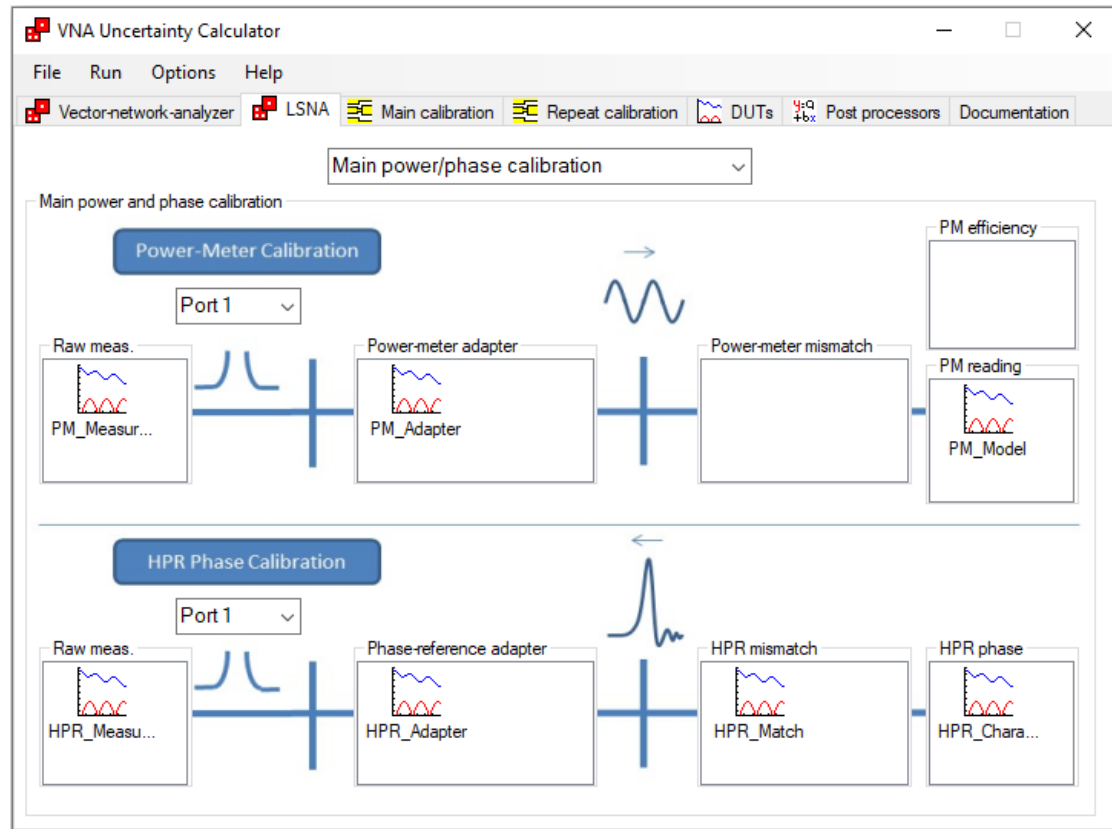


Figure 4.13: The LSNA calibration tab of the MUF VNA Uncertainty Calculator application. Each file icon represents a “.meas” file, which contains an index of Monte Carlo samples generated from a statistical analysis of repeated measurements for each quantity. It is by this method that the MUF propagates distribution information and preserves covariance information. The power meter mismatch and efficiency input boxes are empty as they are included in the model which generated the processed power meter reading file (“PM_Model”).

the ripple measurement method used to characterise some of the input quantities, and is also not reliable when used in submillimetre-wave rectangular metallic waveguide. In contrast, the rigorous VNA measurement model provides more accurate values for combined uncertainties, especially as it correctly preserves correlations through the propagation. This can be achieved either via linear propagation methods as defined in the GUM document, or via Monte Carlo techniques as defined in the GUM supplement, both of which were explained in Chapter 3.

The extension of VNA uncertainty to NVNA measurements was also discussed, where there is a requirement to add the absolute power and phase calibrations to the VNA measurement model. Due to NVNA uncertainty evaluation being relatively new in the field of microwave metrology, there are only two available frameworks to provide such evaluations. The single software solution, the MUF, provides multiple propagation methods and includes a sensitivity analysis feature. It can propagate cross-frequency correlations which are important for use in nonlinear behavioural models. For these reasons, the MUF was selected for use in this project as the framework to use to propagate measurement uncertainty into nonlinear behavioural models.

5 Propagating Measurement Uncertainty into Nonlinear Behavioural Models

5.1 Introduction

The advantages of behavioural models for nonlinear microwave devices was introduced in Chapter 1, where it was shown they can provide an intellectual-property-friendly black-box method to predict device performance.

The core aim of a behavioural model is to fit mathematical functions to terminal-based measurement data without the need for an understanding of the detailed physics within the device. Nonlinear behavioural models have developed over time and there are several different formulations in use today, of which the most common will be described in this Chapter. The reason there is no single optimal model is a question of application. Models which are most efficient and fit functions to more data dimensions may not be accurate for all device behaviours, whereas other models are more versatile but less data-efficient.

Before this research, no prior published work propagated a rigorous evaluation of measurement uncertainty through measurement data into an extracted nonlinear behavioural model. This information is of great use to both the modelling engineer, who can evaluate the sensitivities of their behavioural model to different sources of error in the measurement and extraction procedures, and the design engineer, who can quantify and compare the combined uncertainty in performance characteristics of circuits simulated using the extracted model. Both of these benefits will be presented in this chapter.

5.2 Nonlinear Behavioural Models

I shall first introduce a generic frequency-domain model of the nonlinear device, illustrated in Figure 5.1, which defines the various quantities required to understand the following behavioural models. The power waves A and B at port n can be written as:

$$A_n = \frac{V_n + I_n Z_n}{2\sqrt{\Re(Z_n)}} \quad (5.1)$$

$$B_n = \frac{V_n - I_n Z_n^*}{2\sqrt{\Re(Z_n)}}, \quad (5.2)$$

where V and I are voltages and currents, respectively, and Z is the port impedance - typically $50\text{-}\Omega$.

5.2.1 The Volterra “VIOMAP” Model

One of the first examples of a nonlinear behavioural model for microwave amplifiers was the Volterra input-output map, or “VIOMAP” [113]. This model was developed in the early nineties by Verbeyst and Vanden Bossche of the Hewlett Packard Network Measurement and Description Group (NMDG¹) at Vrije University in Brussels. In an effort to find an S-parameter equivalent for nonlinear devices, VIOMAP replaces the parameters themselves with a sum of Volterra kernel components at each harmonic frequency [114], [115].

Although the VIOMAP model was shown to be cascadable [113], applicable across the Smith chart for efficient load-pull measurements [116], and useful for characterising predistortion [117], it had two major shortcomings. Firstly, it could only be used to model weakly nonlinear devices.

¹now owned by National Instruments

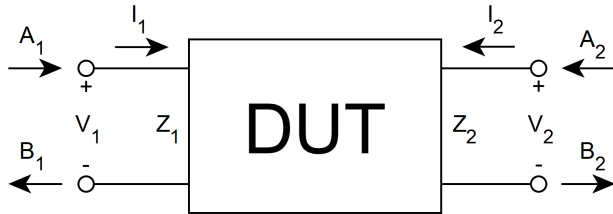


Figure 5.1: A representation of the different quantities described in nonlinear behavioural models, shown for a typical two-port device-under-test (DUT).

This issue was tackled by introducing orthogonal polynomials on which to base the Volterra kernel [118], although the choice of these polynomials was not clear to users and required a lot of computation, thus they were not widely adopted. Secondly, the measurement procedure was customised to suit different applications, which appeared to increase the barrier for entry to new users who could not confidently buy standard equipment to perform the measurements.

5.2.2 Scattering Functions

Scattering functions, originally termed describing functions from their nonlinear analysis origin, were introduced by Verspecht and reduced the computational overhead for modelling strong nonlinearities when compared to the VIOMAP model [119]. They are expressed as a function mapping N complex numbers representing the input signal A into the k^{th} spectral component of the output signal B :

$$B_k = F_k(A_1, A_2, \dots, A_N), \quad (5.3)$$

where F_k is the scattering function for k . The VIOMAP model can be shown to be a subset of the scattering function approach, where the functions are constrained to a limited set of polynomials.

It should be mentioned here that all models described in this section require the device to be time-invariant, meaning that a time delay (or phase shift) in the input signal causes an equivalent time delay (or phase shift) in the output signal. This is typically the case for amplifiers, but more integrated communications components which include, for example, internal oscillators, cannot be modelled using the approaches described in this chapter.

Similar to the VIOMAP model, scattering functions are also complicated to apply and were not popular as a nonlinear modelling paradigm.

5.2.3 Hot S-parameters

Hot S-parameters were developed as a nonlinear behavioural model to extend S-parameters and allow stability and distortion characterisation of amplifiers [120], [121]. The model has several variations depending on the behaviour of interest, and there also exists an enhanced hot S-parameter model which incorporates additional information (in anticipation of the polyharmonic distortion model and the X-parameter model derived from it, which is described later).

Fundamentally, the hot S-parameter model, when used to characterise the distortion of amplifiers, provides a set of S-parameter measurements which are indexed against both frequency f (like standard S-parameters) and also the amplitude of the incident tone $|a_1|$:

$$\begin{bmatrix} B_1(f) \\ B_2(f) \end{bmatrix} = \begin{bmatrix} \text{hot}S_{11}(f, |A_1|) & \text{hot}S_{12}(f, |A_1|) \\ \text{hot}S_{21}(f, |A_1|) & \text{hot}S_{22}(f, |A_1|) \end{bmatrix} \begin{bmatrix} A_1(f) \\ A_2(f) \end{bmatrix} \quad (5.4)$$

The enhanced version of the model includes two additional parameters which describe more completely the nonlinear output matching characteristic ($\text{hot}S_{22}$):

$$\begin{bmatrix} B_1(f) \\ B_2(f) \end{bmatrix} = \begin{bmatrix} \text{hot}S_{11}(f, |A_1|) & \text{hot}S_{12}(f, |A_1|) \\ \text{hot}S_{21}(f, |A_1|) & \text{hot}S_{22}(f, |A_1|) \end{bmatrix} \begin{bmatrix} A_1(f) \\ A_2(f) \end{bmatrix} + \begin{bmatrix} T_{12}(f, |A_1|) \\ T_{22}(f, |A_1|) \end{bmatrix} e^{j\phi(A_1(f))} A_2^*(f) \quad (5.5)$$

where $e^{j\phi(A_1(f))}$ normalises the phase of A_2 relative to A_1 , A_2^* is the conjugate of A_2 and T_{ij} are the two new parameters in the enhanced model.

For an amplifier operating in the nonlinear regime, both the magnitude and phase of reflections at the output, due to matching, can have a significant impact on the device performance [2, Figure 12.13]. Figure 5.2 illustrates versions of the hot S-parameter model with different $\text{hot}S_{22}$ definitions.

The amplifier stability form of hot S-parameters will not be discussed here, but an overview is available in [121].

5.2.4 X-Parameters

X-parameters [41], from Keysight, are the commercial realisation of the poly-harmonic distortion model [122], which itself is an application of scattering functions with particular constraints. The most significant constraint is that any output of device which the model is applied to behaves linearly with respect to incident tones at harmonics of the fundamental, which is illustrated in Figure 5.3.

The X-parameter formulation can be developed from the scattering function origin. Firstly, the output $B_{p,k}$, at port p and harmonic k , is defined as:

$$B_{p,k} = \sum_{q,l} S_{p,k;q,l}(|A_{1,1}|) P^{k-l} A_{q,l} + \sum_{q,l} T_{p,k;q,l}(|A_{1,1}|) P^{k+l} A_{q,l}^*, \quad (5.6)$$

where $A_{q,l}$ is the input at port q and harmonic index l , and P is a phase normalisation coefficient such that $P = e^{j\phi(A_{1,1})}$, similar to (5.5). This equation contains two scattering functions which are sensitive to the large-signal input at the fundamental, $A_{1,1}$. The second function, $T_{p,k;q,l}$, is identical to $S_{p,k;q,l}$ except that it is a coefficient of the conjugate of the input wave, $A_{q,l}^*$. As with the enhanced Hot S-parameters, this is a more generalised way to

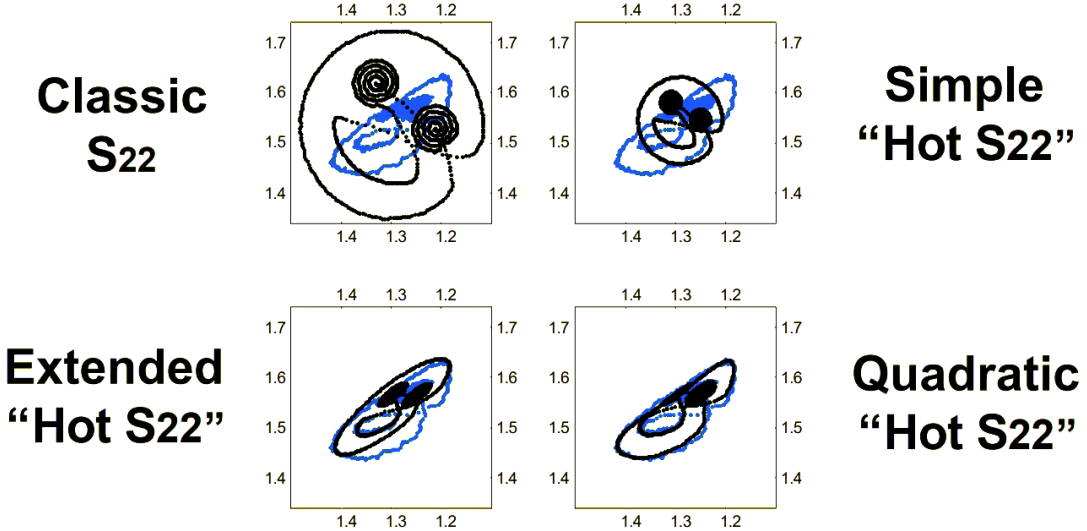


Figure 5.2: Performance of hot S-parameter models with different *hotS22* definitions, showing in polar form the measured (blue) and predicted (black) b_2 wave for a modulated large-signal a_1 wave, with values in Volts. Classic S_{22} means no dependence of S_{22} on $|a_1|$, simple “Hot S_{22} ” means a linear dependence of S_{22} on $|a_1|$, extended “Hot S_{22} ” includes dependence of S_{22} on $|a_1|$ and a_2 , and quadratic “Hot S_{22} ” includes a second order dependence of S_{22} on a_2 [120].

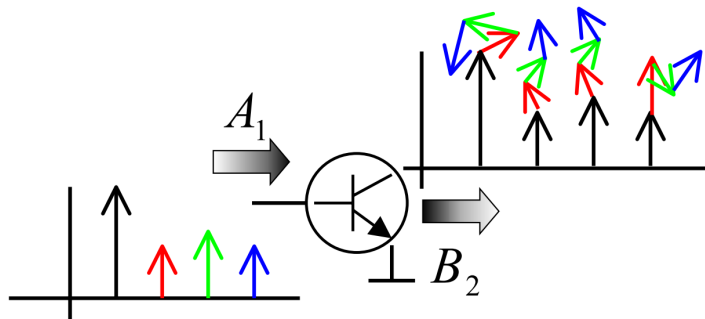


Figure 5.3: The harmonic superposition principle. If the input at port one (A_1) contains several small-signal harmonics, the output at port two (B_2) will comprise of the large-signal response plus the sum of responses due to each small-signal input harmonic, at each frequency [122]. The plots show complex phasors of increasing harmonic index along the horizontal axis, where the colour of the output phasors relate to the contribution from the respective input phasor.

incorporate the sensitivity of the model to the phase of input signals at harmonics on any port. Mathematically, the requirement of these two functions is a result of the non-analyticity of the complex-valued scattering functions. It is possible to instead define the functions in terms of real and imaginary components, but the normal and conjugate definition is standard for X-parameters and so will be taken forward here.

Because the phase is normalised with respect to that of $A_{1,1}$, we can also define $T_{p,k;1,1} = 0$ as the entire device response for this port and harmonic combination will be captured in $S_{p,k;1,1}$, which also represents the response to the large-signal input at port one at the fundamental tone. If we assume that the harmonic superposition principle is valid for our model, we can then simplify it by extracting the large-signal response as a separate term and treat the remaining functions as linear, with the restriction that they do not apply when $q,l = 1,1$. A good overview of this linearisation process of scattering functions is provided in [123].

We can now write our model as:

$$B_{p,k} = X_{p,k}^F(|A_{1,1}|)P^k + \sum_{q,l \neq (1,1)} [X_{p,k;q,l}^S(|A_{1,1}|)A_{q,l}P^{k-l} + X_{p,k;q,l}^T(|A_{1,1}|)A_{q,l}^*P^{k+l}], \quad (5.7)$$

where X^F (the large-signal term), X^S and X^T (the small-signal terms) are called X-parameters.

Two informative comparisons between the performance of scattering functions and X-parameters in modelling nonlinear device behaviour can be found in [124], [125].

The X-parameter model is heavily marketed by Keysight to be a complete solution for modelling nonlinear device behaviour. Additions to the model include mixer characterisation using multi-tone stimuli [126], the inclusion of memory effects [127], the prediction of load-pull performance from a single X-parameter measurement at $50\text{-}\Omega$ [128], and recently the inclusion of electro-thermal effects [129]. The X-parameters themselves are closely related to elements of the Jacobian matrix used within harmonic balance simulations. This feature means that X-parameters can be extracted in a straightforward way from circuit simulations, and existing X-parameter models based on measurements can be included in simulations. At least two circuit simulators support X-parameter models at the time of writing, including Keysight Advanced Design System (ADS) [130] and National Instruments AWR Microwave Office [131].

5.2.5 The Cardiff Model

Although X-parameters are sufficient to characterise the nonlinear behaviour of many amplifiers, the standard model² only includes third-order mixing products (via the $P^{(\cdot)}$ terms in (5.7)). While the harmonic superposition principle holds, which is the case for weak-to-moderate nonlinear devices with well-matched ports, this is not always true for strongly nonlinear devices such as amplifiers driven in class F modes, or devices with port impedances far from 50Ω . In order to avoid this X-parameters can be extracted as a function of both $|A_{1,1}|$ and $A_{2,1}$, but this can increase the model size significantly, especially for load-pull applications with phase and magnitude sweeps of $A_{2,1}$ [132]. An alternative approach, The Cardiff model, named after it's origin at Cardiff University, UK, incorporates n^{th} -order mixing products (typically truncated to seventh-order terms) and reduces the model dependence for fundamental load-pull to $|A_{1,1}|$ and $|A_{2,1}|$ only [133], [134].

The formulation of the Cardiff model is represented differently to that of X-parameters, however, they are a natural extension of that model and are equivalent when used with third-order mixing products. The measurement and extraction process is usually performed with a sampler-based NVNA featuring a real-time sampling oscilloscope and consists of a load-pull measurement [135].

For this project, X-parameters were chosen as the nonlinear behavioural model for which to focus on developing an uncertainty propagation, due to their current popularity. The framework which has been developed can be extended to include other behavioural models, but does not currently support them.

5.3 X-Parameter Extraction Procedure

X-parameters can be extracted from either measured or simulated data. A least-squares estimation can be used for both cases, however it is often more efficient to extract X-parameters directly from harmonic balance internal variables when simulating data. This section will describe the process involved for the least squares estimation of X-parameters from measured data, and two implementations developed during this project.

²It is possible to extend the X-parameter model to include higher order mixing products, however this is not supported by commercial measurement or simulation solutions.

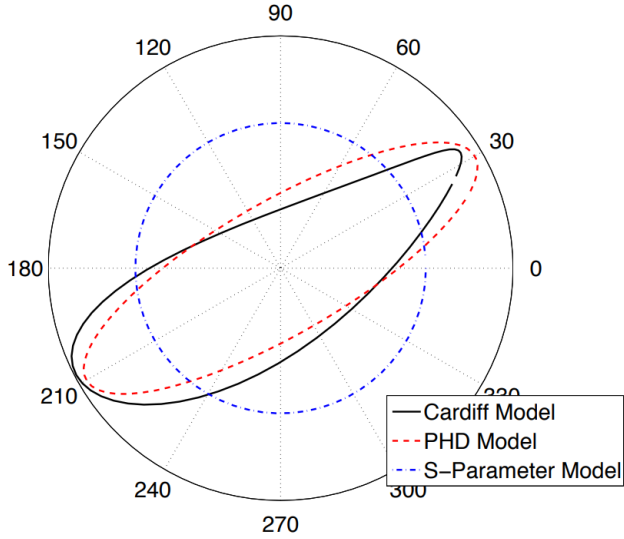


Figure 5.4: The relationship of device output $b_{p,k}$ against varying input wave phase $\angle a_{q,l}$ ($q, l \neq 1, 1$) for different nonlinear behavioural models, showing the effect that higher order mixing products have on the accuracy of the model [136]. The PHD model is equivalent to X-parameters in this case.

5.3.1 Method

To perform device measurements from which X-parameters can be extracted, an NVNA setup as shown in Chapter 2 must be prepared, with the additional requirement of a second signal source which can be applied at either of two ports. All measurements taken during this project used the following Keysight equipment: an N5247A PNA-X NVNA, N1913A EPM Series Power Meter and two U9391G Comb Generators as phase references. Variables used in this section are in reference to (5.7).

The large-signal X-parameter, X_F , is simple to measure as it captures to the response of the device to a single large-signal drive tone at the fundamental frequency on port one ($A_{1,1}$). It is indexed against $|A_{1,1}|$, so this power is swept and measurements at each port p and harmonic k are made. The drive tone amplitude $|A_{1,1}|$ is said to define a large-signal operating point (LSOP) against which all of the X-parameters are indexed.

The small-signal X-parameters, X_S and X_T , model the interactions between small-signals incident to the device and $A_{1,1}$. To capture this behaviour, measurements are made with a second tone (“extraction” or “tickler” tone) applied to each port and harmonic in turn. If we

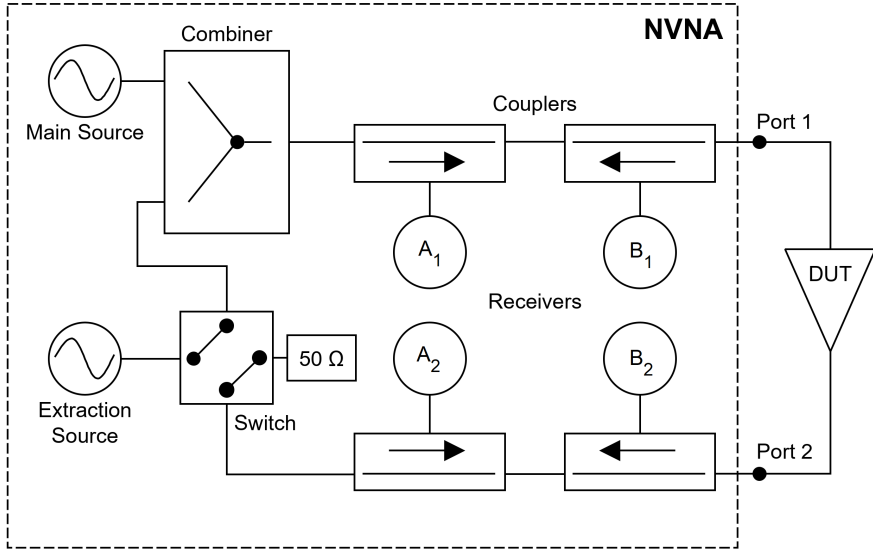


Figure 5.5: The NVNA setup required for X-parameter measurements. The switch terminates the unused port to a 50-Ohm load. The phase reference is connected to a spare receiver but not shown.

ignore the conjugate term X-parameter X_T (which is similar to the simple “Hot S22” model in Figure 5.2), these measurements are all that is required to extract X-parameters. This equates to $N + N \times Q \times L$ stimulus conditions, where N is the number of LSOPs, Q is the number of ports and L is the number of harmonics. For each stimulus condition, the NVNA measures the device output on all ports at each harmonic. A diagram of the NVNA setup required for these measurements is shown in Figure 5.5.

However, to extract the full X-parameter model we must make additional measurements to characterise the phase-dependence of the mixing products between the extraction tones and the LSOP. This is the behaviour captured by the X_T parameters. Two measurement methods were developed to perform this task: offset-frequency and offset-phase. The offset-frequency method is not supported by the current version of the PNA-X firmware and appears to have fallen out of use, so the offset phase method alone will be explained. Further information can be found in [41].

Instead of a single extraction tone applied at each port and harmonic, a second measurement must be performed at an orthogonal phase ($\theta + 90^\circ$) to the initial extraction tone. An illustration of these measurements using phasors is given in Figure 5.6. After subtracting the large-signal only measurement from these two new measurements, we obtain two small-signal contributions

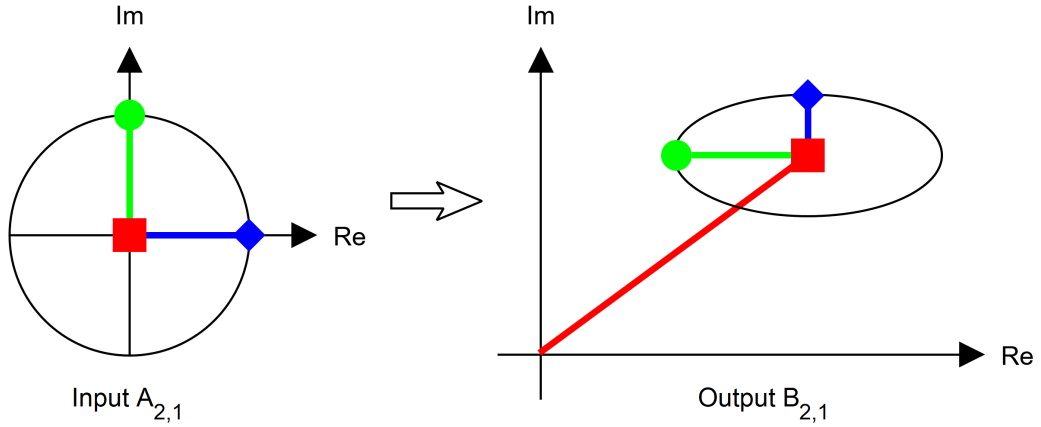


Figure 5.6: An example of the offset-phase method for measuring device response for X-parameter extraction. The red square stimulus is with no extraction tone, and the blue diamond and green circle stimuli are with extraction tones applied at 0° and 90° , respectively. Although $A_{2,1}$ and $B_{2,1}$ are specified, this effect occurs for all tones other than the fundamental on port one [122].

which can be used to solve the following equations:

$$B_{p,k}^{SS1} = X_{p,k,q,l}^S A_{q,l}^{SS1} + X_{p,k,q,l}^T (A_{q,l}^{SS1})^*, \quad (5.8)$$

$$B_{p,k}^{SS2} = X_{p,k,q,l}^S A_{q,l}^{SS2} + X_{p,k,q,l}^T (A_{q,l}^{SS2})^*. \quad (5.9)$$

To improve noise errors it is advisable to make more than two measurements of different extraction tone phases (typically four) and solve for X_S and X_T using a least-squares estimation. The extraction tone amplitude should be as low as possible to ensure that the device is responding linearly to the added tone (it is effectively performing a perturbation analysis described in Chapter 3), and Keysight suggests that it should be 16 dB below the largest LSOP signal. The extraction process can in fact be simplified further by using a matrix least-squares arrangement to solve for the entire X-parameter model, which removes the need to subtract the large-signal response from all the extraction tone measurements. If we define a matrix \mathbf{A} such that each row contains the NVNA measurements for a single extraction tone stimulus (from 1 to QL , with 0 being no extraction tone):

$$\mathbf{A} = \begin{bmatrix} 1 & 0 & A_{(2,1)_0} & A_{(2,1)_0}^* & A_{(1,2)_0} & A_{(1,2)_0}^* & A_{(2,2)_0} & A_{(2,2)_0}^* & \dots \\ 1 & A_{(1,1)_1} - A_{(1,1)_0} & A_{(2,1)_1} & A_{(2,1)_1}^* & A_{(1,2)_1} & A_{(1,2)_1}^* & A_{(2,2)_1} & A_{(2,2)_1}^* & \dots \\ 1 & A_{(1,1)_2} - A_{(1,1)_0} & A_{(2,1)_2} & A_{(2,1)_2}^* & A_{(1,2)_2} & A_{(1,2)_2}^* & A_{(2,2)_2} & A_{(2,2)_2}^* & \dots \\ \vdots & \dots \\ 1 & A_{(1,1)_{QL}} - A_{(1,1)_0} & A_{(2,1)_{QL}} & A_{(2,1)_{QL}}^* & A_{(1,2)_{QL}} & A_{(1,2)_{QL}}^* & A_{(2,2)_{QL}} & A_{(2,2)_{QL}}^* & \dots \end{bmatrix} \quad (5.10)$$

and a vector $\mathbf{b}_{p,k}$ of length QL is defined to contain the respective measurements of a single output wave $b_{p,k}$:

$$\mathbf{b}_{p,k} = \begin{bmatrix} B_{(p,k)_0} \\ B_{(p,k)_1} \\ \vdots \\ B_{(p,k)_{QL}} \end{bmatrix}, \quad (5.11)$$

then the X-parameters can be solved for using the following least-squares estimation:

$$\hat{\mathbf{X}}_{p,k} = (\mathbf{A}^\top \mathbf{A})^{-1} \mathbf{A}^\top \mathbf{b}_{p,k} \quad (5.12)$$

with the vector $\hat{\mathbf{X}}_{p,k}$ containing X-parameters:

$$\hat{\mathbf{X}}_{p,k} = \begin{bmatrix} X_{p,k}^F \\ X_{p,k,1,1}^S \\ X_{p,k,2,1}^S \\ X_{p,k,2,1}^T \\ X_{p,k,1,2}^S \\ X_{p,k,1,2}^T \\ X_{p,k,2,2}^S \\ X_{p,k,2,2}^T \\ \vdots \end{bmatrix}. \quad (5.13)$$

The parameter $X_{p,k,1,1}^T$ will always equal zero for conventional measured X-parameters because the phase normalisation (time shift) which occurs during measurement means that any extraction tone applied to port one at the fundamental will always have the same phase value. Therefore, effectively $X_{p,k,1,1}^S$ from measured X-parameters equals $X_{p,k,1,1}^S + X_{p,k,1,1}^T$ from simulated X-parameters extracted from harmonic balance simulations, where this stage of phase

normalisation is not performed. For the latter, the response is correctly separated between the two X-parameters, which means that this phase-dependence information is captured correctly.

5.3.2 Implementation

The PNA-X NVNA contains a specific firmware for nonlinear measurements and a software option to allow X-parameter measurements to be performed and the model extracted on the NVNA itself. This is adequate for typical user requirements and the processing time is relatively fast (up to a few seconds) compared with the duration of measurements (hours for dense LSOP sweeps with several harmonics). However, to propagate uncertainty into X-parameters using this extraction method with numerical techniques supported by the MUF is very time-consuming, and practically restricts the number of Monte Carlo samples which can be used to perform the uncertainty propagation. For the experiments performed in this project, over 300 sources of error are included from the nonlinear measurements (of which an extract are listed in Appendix B). This means that at least 300 X-parameter extractions must be computed for the sequential perturbation and sensitivity analysis alone. For these reasons, only 1000 Monte Carlo samples were used, which was deemed appropriate by resampling using bootstrap methods [137].

Once X-parameter measurements have been performed and the parameters themselves automatically extracted, it is possible to save not only the X-parameters (as a “.xnp” file), but also the X-parameter measurements (as a “.xmeas” file), which contain tables of power wave measurements relating to all sweeps, including those of extraction tone stimuli. This file is then loaded into the MUF as a DUT measurement to be propagated through the calibration measurement model, as described in Chapter 3. The addition of X-parameter measurement file support to the MUF was included as part of this project, with support from the developers at NIST. During this work, several further additions and improvements were made to the software, including file access changes which reduced the processing time of all MUF uncertainty evaluations by a factor of at least 100. Once the X-parameter measurements have been perturbed as part of the uncertainty propagation, they are then sent back to the NVNA for X-parameter extraction, which is detailed in the following section.

The NVNA does not need to be calibrated before the X-parameter measurements are performed because the power waves will be instead corrected during the MUF calibration step. However, it does not affect the result if a preliminary calibration is performed, and it can be useful to verify that the calibration standards are in good order and the DUT is behaving as expected.

To address the issue of slow extraction for large numbers of perturbed measurements, an alternative X-parameter extractor was implemented from scratch as a MUF post-processor (code listing in Appendix A). This would allow the samples to be run on more powerful hardware than the NVNA onboard computer, and even scale across multiple servers in a compute cluster. The processing flow for both approaches is illustrated in Figure 5.7. Both extraction implementations will now be explained.

5.3.2.1 PNA-X Extraction

The PNA-X X-parameter measurement software is designed to guide the user through all steps of the process: calibration, device measurements and model extraction. Because the model extents (number of ports, harmonics, etc) are defined before measurement, the software will normally perform the X-parameter extraction immediately after the measurements have finished. This is desirable as it presents the user with visible plots of the parameters on the NVNA screen similar to traditional VNA measurements. There is no supported way to provide X-parameter measurements from a file and perform a stand-alone extraction. This is regrettable as it is the only way perturbed samples from the MUF uncertainty propagation can be processed into X-parameters and hence propagate the uncertainty further.

Fortunately, the software includes a somewhat esoteric feature which can be utilised to remove this limitation. Because the PNA-X hardware is limited on the amount of memory it can fit on a physically compact embedded computer, very large sweeps of measurements (as required for X-parameters extracted from load-pull experiments) can require more memory than is present. Therefore, because the X-parameters are extracted from the entire dataset, the software provides the ability to save “intermediate files” which are just subsets of the X-parameter measurements in “.xmeas” format. The intention is that once the measurements are complete, the user immediately clicks on the option to “Extract X-parameters from intermediate files” and they are presented with the same end results as normal. Because the intermediate files are ASCII-encoded and not binary, it is possible to perform a dummy measurement (which initialises the file location), replace the intermediate file with a perturbed X-parameter measurement file processed by the MUF, and run the command to extract X-parameters. Through experimentation it has been found that the extraction routine only examines the supplied file, so the measurement setup used for the dummy measurement is not important and is chosen to minimise delay (i.e. sweeps containing a single point).

All of these steps can be performed remotely using the DCOM automation interface for the

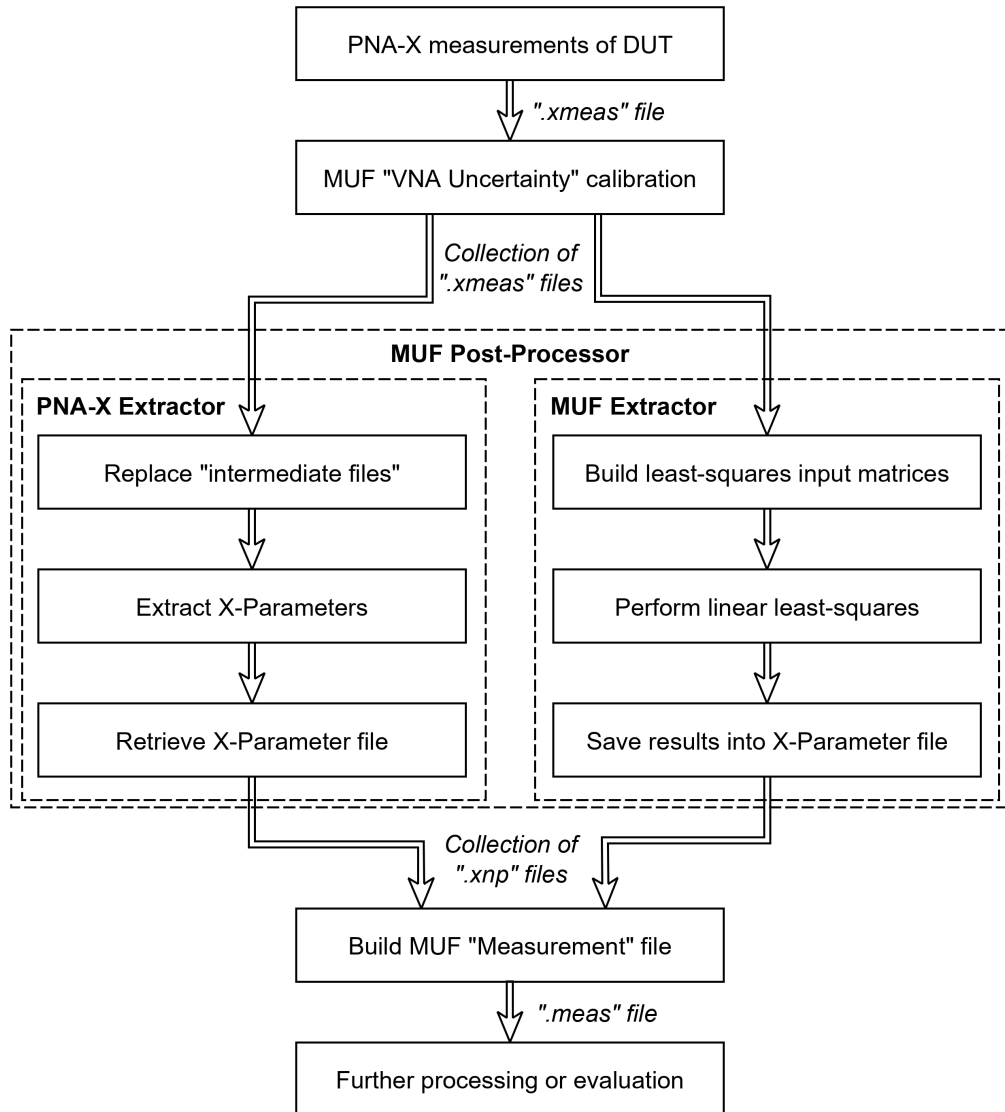


Figure 5.7: Processing flow showing X-parameter extraction methods that are compatible with propagating uncertainty via numerical methods (i.e. Monte Carlo and sequential perturbation). Both the PNA-X and MUF extraction routines are called from a MUF post-processor which allows the user to select the desired approach. Both routines take X-parameter measurement files of the DUT as their input, and return X-parameter files.

PNA-X [138]. The MUF Post-Processor software accepts a programming function as a measurement model and evaluates it against each numerical sample contained in input files produced by previous MUF processes. Therefore, the automated PNA-X extraction was implemented as a MUF post-processor which would transfer a sample to the PNA-X, request an extraction be performed, and retrieve the X-parameter results. The Post-Processor software then automatically builds a MUF Measurement file, which indexes all the propagated perturbed samples for future use or statistical evaluation. This connection to the PNA-X is done via computer network, which allows instruments in remote labs to be used for the extraction. This could be of use in manufacturing where production lines can be spread globally. During the secondment to NIST this was tested between Colorado, USA and Surrey, UK with no significant delay when compared with local networks.

5.3.2.2 MUF Custom Post-Processor

The alternative X-parameter extractor, which is ultimately incorporated into the same MUF post-processor as the PNA-X automation code as a different option, is based on the least-squares estimation presented earlier in this section. It should be noted that the PNA-X algorithms may differ from that method, as they are intellectual property of Keysight and not openly available.

The implemented extractor was compared with the output from the PNA-X and mostly showed excellent agreement. There were some discrepancies with terms involving extraction tones applied at the fundamental frequency on port one, but these are expected as it is not known how the Keysight algorithm generates the LSOP value which is subtracted from these measurements. Keysight have also made it known that there is additional pre-processing of the measurements before X-parameter extraction in their algorithm. However, the few differences between extraction algorithms which occur are small enough (e.g. 1 dB at -50 dBm) that it is at least suitable for academic use in this project. With that being said, due to time constraints the MUF X-parameter extractor was only completed shortly before the end of this project, therefore all of the uncertainty propagation used in publications and this dissertation was performed with the PNA-X extractor. The potential for processing Monte Carlo and other propagation samples much faster, by deploying the extractor on faster processors or compute clusters, means that this work may be of great use in future research.

5.4 Evaluation of the Combined Standard Uncertainty of X-Parameters Extracted from Measurement Data

The uncertainty propagation described in the previous section was successfully applied to both a connectorised microwave amplifier (Mini-Circuits ZX60-14012L+ [139]) and a surface-mount millimetre-wave amplifier mounted on an evaluation board with coaxial launches (Analog Devices HMC342LC4 [140]). Due to millimetre-wave amplifiers being a current research focus because of 5G infrastructure development, this amplifier was chosen as the example for a publication presenting the results of this project [26]. Parts of this publication will be included in the remaining sections of this chapter. The experiment will now be described.

The MUF was used to perform the calibration of electromagnetic wave parameters measured using a Keysight 67 GHz N5247A PNA-X NVNA. The DUT [140] has a typical gain of 19 dB and a 1-dB compression point at approximately 9 dBm output power at 25 GHz. To obtain results showing both the linear and nonlinear regimes of operation, the source power was swept between -22 dBm and -2 dBm in 0.25 dB steps. The fundamental frequency was set at 25 GHz, with a harmonic at 50 GHz also measured. The evaluation board was connected via adapters to cables with 2.4 mm precision connectors. The calibration plane was located between the cables and the adapters (i.e. the adapters were included as part of the DUT), and the measurement setup had a nominal impedance of $50\text{-}\Omega$. The intermediate frequency bandwidth (IFBW) was set to 10 Hz. The built-in X-parameter measurement routine was used and configured to extract cross-frequency terms between both harmonics using measurements at 4 extraction tone phases (this is the default setting). A photograph of the setup is shown in Figure 5.8.

Uncertainties are propagated through all steps of the calibration by the MUF. Sources of uncertainty that were included covered the definitions and measurements of the passive calibration standards, the power meter calibration and measurement, the phase reference characterization and measurement, cable flexure, and connection repeatability of all calibration steps. Uncertainty due to random noise in the high-dynamic range receivers was omitted as it has been shown to be negligible with respect to that arising from other error sources in LSNA measurements [106]. A partial list of the names of included uncertainty sources is provided in Appendix B.

The MUF supports several calibration algorithms, and for this measurement the multiline TRL calibration algorithm [47], [48] was chosen to allow direct dimensional traceability to national measurement standards. The calibration standards used were from a 1.85 mm precision

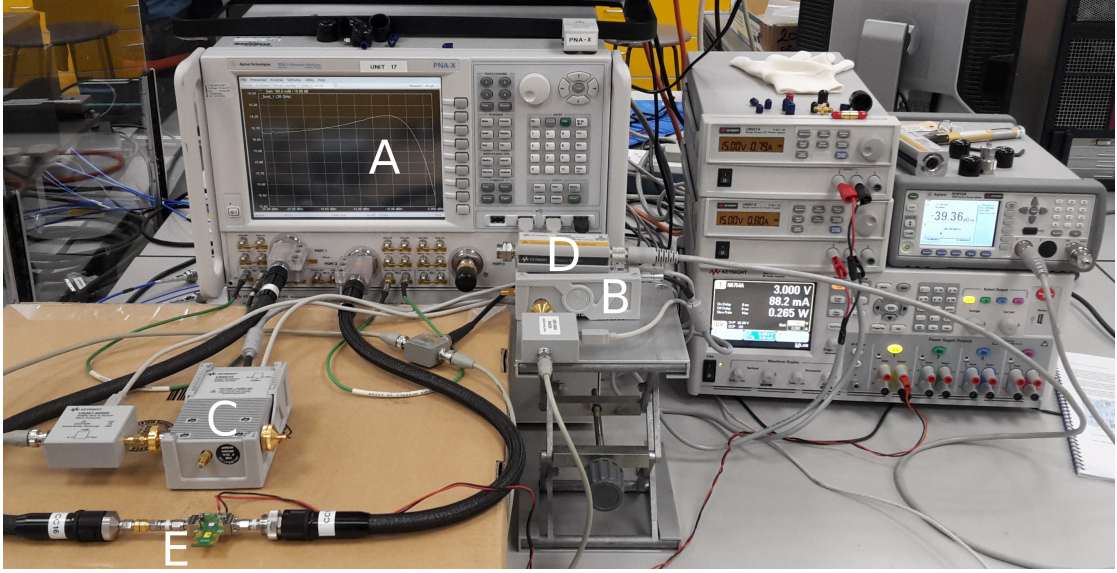


Figure 5.8: The measurement setup used for extracting X-parameters from the DUT. Shown is the PNA-X LSNA (A), the phase reference comb generator (B), the phase calibration comb generator (C), the power meter (D), and the connected DUT (E).

Table 5.1: Nominal values and standard uncertainties for the TRL coaxial line standards.

Dimension	Line 1 value (mm)	Line 2 value (mm)
Line length	13.004 ± 0.003	14.913 ± 0.003
Line inside dia.	0.803 ± 0.001	0.803 ± 0.008
Line outside dia.	1.850 ± 0.005	1.850 ± 0.005

coaxial calibration kit (Rosenberger RPC-1.85 LRL). Table 5.1 gives the dimensions of the line standards used for the calibration. To include the effect of connector repeatability on the passive calibration, each standard was measured three times with the connector rotated 120°. These measurements were passed to the MUF program Combine which produces a mean value with an associated uncertainty.

The calibration model for the power meter itself is defined in [110] and includes the reference oscillator mismatch, the reference oscillator power uncertainty, the zero-set error, the zero carry-over error, the instrumentation error, and error in the power sensor calibration factor. The estimates and uncertainties used for these parameters in the calibration are shown in Table 5.2 and are derived from specifications supplied by the manufacturer. The mismatch of the power

Table 5.2: Standard uncertainties for power meter uncertainty contributions derived in [110]

Contribution	Standard uncertainty
Reference oscillator mismatch	0.2%
Reference oscillator power uncertainty	0.6%
Zero-set error	0.5% meter full scale
Zero carry-over error	0.2% meter full scale
Instrumentation error	0.5% meter full scale
Calibration factor error	0.024

Table 5.3: Nominal phase and standard uncertainty for harmonic phase reference at calibration frequencies

Frequency (GHz)	Characterized phase (deg.)	Measured phase (deg.)
25	181.5 ± 0.4	-16.8 ± 1.5
50	170.8 ± 1.0	61.0 ± 2.5

sensor was also measured using a calibrated VNA and included in the absolute calibration. Connector repeatability was assessed for this measurement in the same way as for the passive standards.

The two phase references used for both calibration and synchronisation of the mixer-based NVNA were Keysight 67 GHz comb generators [141]. The phase uncertainties for the calibration phase reference are given in Table 5.3 and were obtained through characterization with a sampling oscilloscope at NIST, which is traceable to national measurement standards via electro-optic calibration [107], [109] as described in Chapter 4.

5.4.1 X-Parameter Uncertainties

In this example we used a Monte Carlo method with 1000 samples to propagate uncertainty to the X-parameters of the DUT. This required 8 hours of processing for the calibration and a further 8 hours of processing for the X-parameter extraction. A histogram is provided in Figure 5.9 showing good agreement between the Monte Carlo results and sensitivity analysis. This level of agreement is typical for all of the extracted X-parameters.

The estimated values and standard uncertainties from the Monte Carlo analysis for the magnitude and phase of a sample of X-parameter terms are shown in Figure 5.10. It can be seen in all

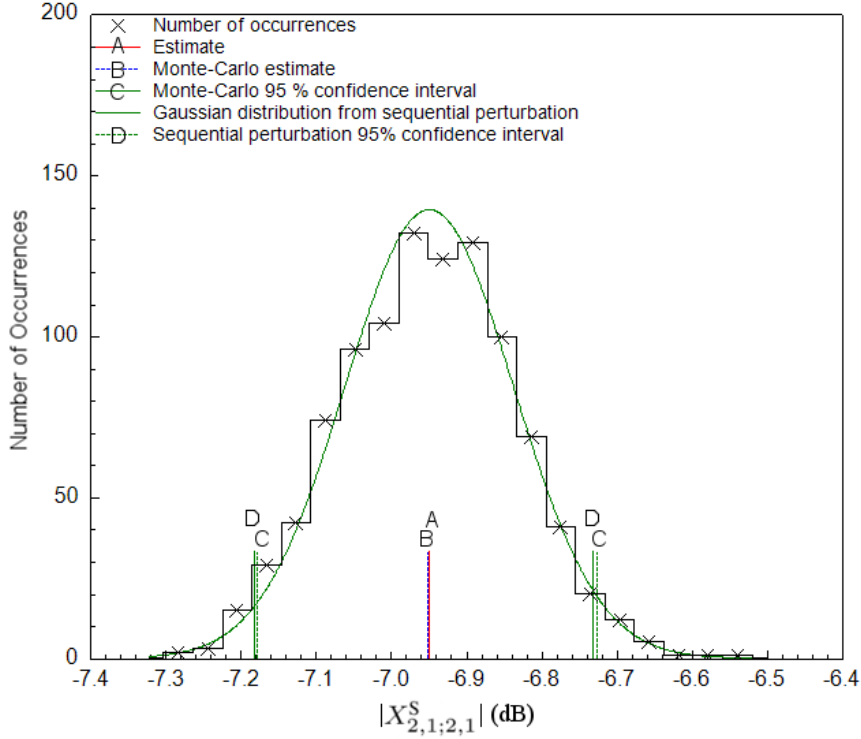


Figure 5.9: Histogram comparing the Monte Carlo and sequential perturbation uncertainty results for $X_{2,1;2,1}^S$ (25 GHz) of the DUT at -2.4 dBm source power. The vertical line in the center of the plot (A) shows the nominal value (estimate), (B) shows the Monte Carlo average, and (C, D) show the Monte Carlo and sequential perturbation 95% confidence intervals, respectively.

plots that there is a clear change in uncertainty for several X-parameters as the DUT transitions between the linear and nonlinear regimes.

The phase noise seen at lower powers in the estimate of $X_{2,1;2,2}^T$ is not accompanied by an increase in measurement uncertainty. This suggests that it arises from the extraction routine, which contributes another source of uncertainty not studied in this project. By design, the X^T parameters are negligible in the linear regime, and so this effect will have little contribution when the model is used.

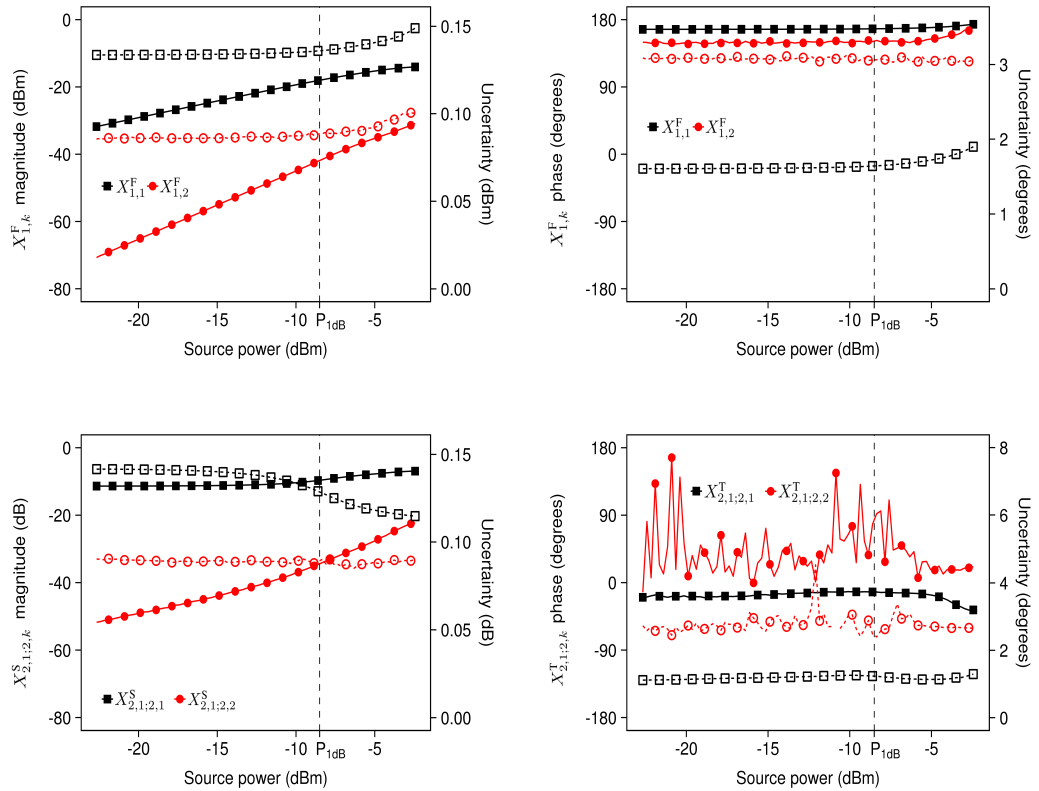


Figure 5.10: Estimates (solid line and shapes, left scale) and standard uncertainties (dashed line and hollow shapes, right scale) for the magnitude and phase of a sample of the extracted X-parameters. Harmonic indices 1 and 2 relate to measurement frequencies of 25 and 50 GHz, respectively. Uncertainties are a linear variation of the scale value.

5.4.2 Sensitivity Analysis for X-parameter Uncertainties

Figure 5.11 shows a sample of the sensitivity analysis results for the X-parameter uncertainty obtained using sequential perturbation. Because over 300 sources of uncertainty were included in the analysis they have been grouped for clarity.

It can be seen in Figure 5.11 that the power calibration has a dominant contribution to the uncertainty in the magnitude of X_{12}^F . This is to be expected because the X^F terms represent the absolute electromagnetic waves output from the DUT, and the uncertainties from the power meter in the LSNA calibration (i.e. in the corrected wave measurements) are significantly larger than those from the TRL standards.

The TRL calibration uncertainty is also a dominant contribution to the uncertainty in the magnitude of most of the small-signal X^S and X^T terms. Because these terms are similar to S-parameters, in that they represent a ratio between electromagnetic waves, any correlated error components are cancelled. Both the power and phase calibration errors are correlated for terms concerning a single frequency, but only power calibration errors appear to be correlated for cross-frequency terms. This can be seen from the lack of uncertainty contribution from the phase calibration to the $X_{2,1;2,1}^T$ term.

For these example measurements, it can also be seen that the uncertainty contribution from cable flexure (and reconnection) was significant in all results. This is a well-known issue for electromagnetic measurements at millimeter-wave frequencies and above. This uncertainty contribution could be reduced by further limiting cable movement using mechanical fixturing.

5.5 Propagation of Uncertainty from X-Parameters into Circuit Simulations

Once the behavioural model has been extracted from measurements, it can be used in circuit simulators to predict the performance of circuit designs. Because the uncertainty information is stored as a collection of samples, it can be propagated through the circuit simulator by sweeping the sample index and running the simulation for each value. From this array of results, a statistical analysis can be performed to determine the standard uncertainty of the performance metric in question. The sensitivity analysis can be propagated in a similar way, as there is a sample in the model file for the perturbation of each input quantity. It is also possible to evaluate uncertainty in circuit simulations containing multiple DUTs processed using the MUF,

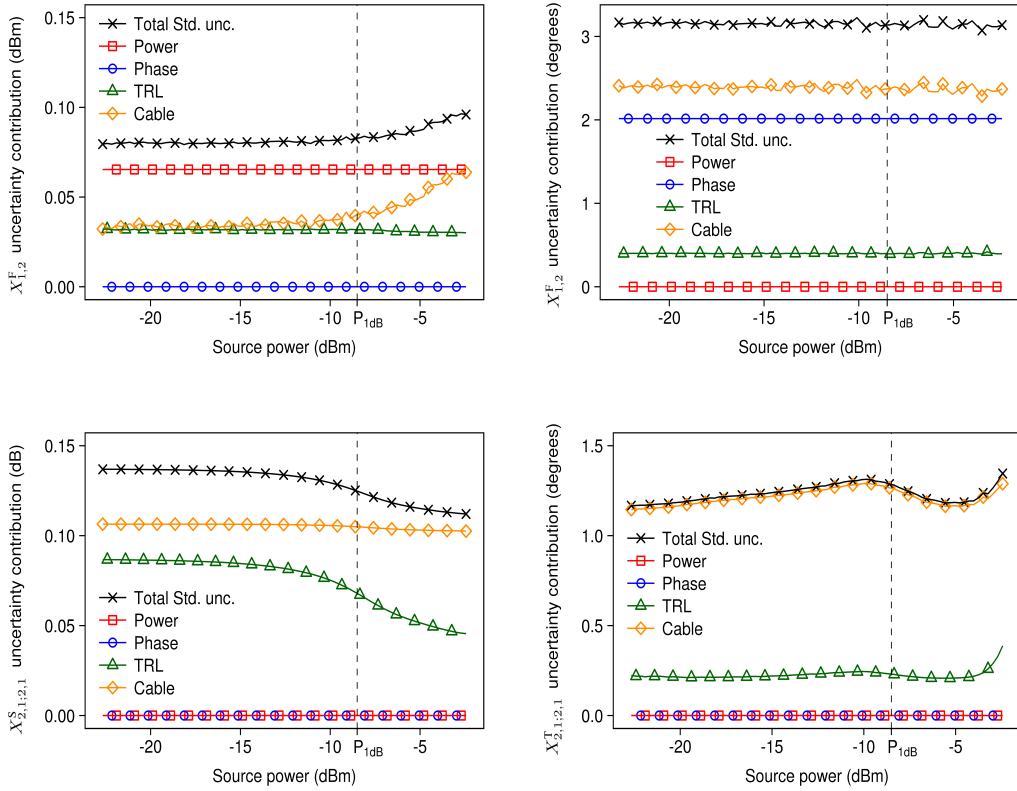


Figure 5.11: Sensitivity analysis results for a sample of the extracted X-parameters. Harmonic indices 1 and 2 relate to measurement frequencies of 25 and 50 GHz, respectively. Because the uncertainty is expressed as a linear variation of a decibel value, a non-zero horizontal line represents a linear relationship with source power.

for example in a two-stage, balanced, or Doherty amplifier configuration. If the same variable is used to sweep the sample index for all DUTs, then any uncertainty correlations will be preserved. An example would be if multiple DUTs in the circuit were measured on an LSNA using the same calibration. The measurement uncertainties which were captured into the X-parameter behavioral model can now be propagated to typical circuit metrics such as forward gain, input or output match, power-added efficiency (PAE), error vector magnitude (EVM) and adjacent channel power ratio (ACPR).

To demonstrate this, an example simulation has been created in Advanced Design System (ADS). The DUT is represented as an X-parameter model, and the simulator sweeps both the Monte Carlo sample index and the source power using the results from the MUF uncertainty evaluation. For this example the X-parameter file from the previous section was used. The schematic of the design is shown in Figure 5.12, and typical design plots of gain and PAE are provided in Figure 5.13. It can be seen that although the uncertainties of both parameters increase significantly with source power, the 95% expanded uncertainties are below 0.2 dB and 0.4% for gain and PAE, respectively. It should be noted that the PAE result only includes uncertainty from the RF component and that the DC values were provided from a single observation.

5.6 Conclusions

This chapter has presented an overview of the main nonlinear behavioural models used to characterise microwave amplifiers for use in the design process. It is possible to see how over time the models have progressed from general but complicated Volterra and scattering function origins, through to more portable but simpler models such as X-parameters to promote industry usage, and finally the return to more capable solutions via the Cardiff model and X-parameter extensions.

A rigorous evaluation of uncertainty in nonlinear behaviour models of microwave and millimetre-wave amplifiers was presented, using a new framework based on the MUF through Monte Carlo and linear sensitivity analysis approaches. Both approaches preserve correlations between errors and provide a rigorous uncertainty evaluation. This has been demonstrated by extracting X-parameters with uncertainties from a typical millimeter-wave amplifier. The resulting model has been incorporated into circuit simulations to obtain gain and PAE results incorporating measurement uncertainty. The extracted amplifier model exhibited 95% expanded uncertainties of less than 0.2 dB gain and less than 0.4% PAE.

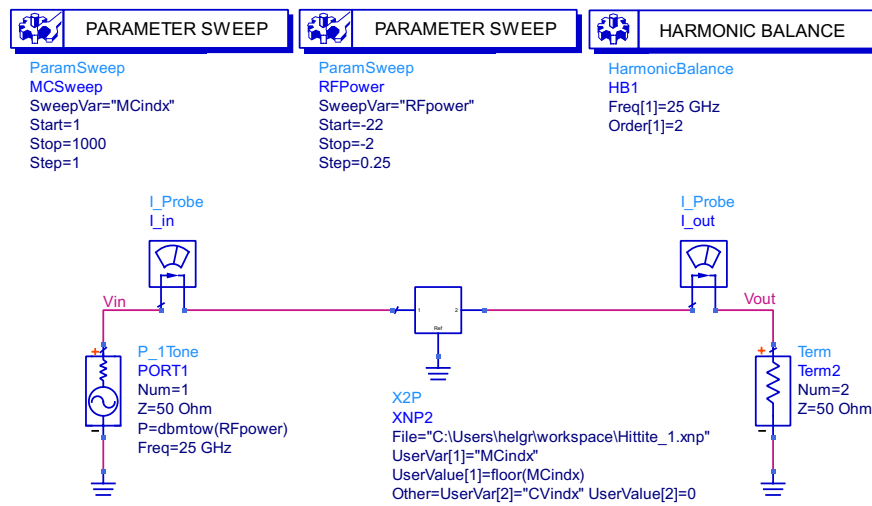


Figure 5.12: An example circuit simulation schematic using an X-parameter model in ADS. The source power and X-parameter Monte Carlo sample index is swept by the Parameter Sweep components, and a harmonic balance simulation is carried out for each value of those sweeps.

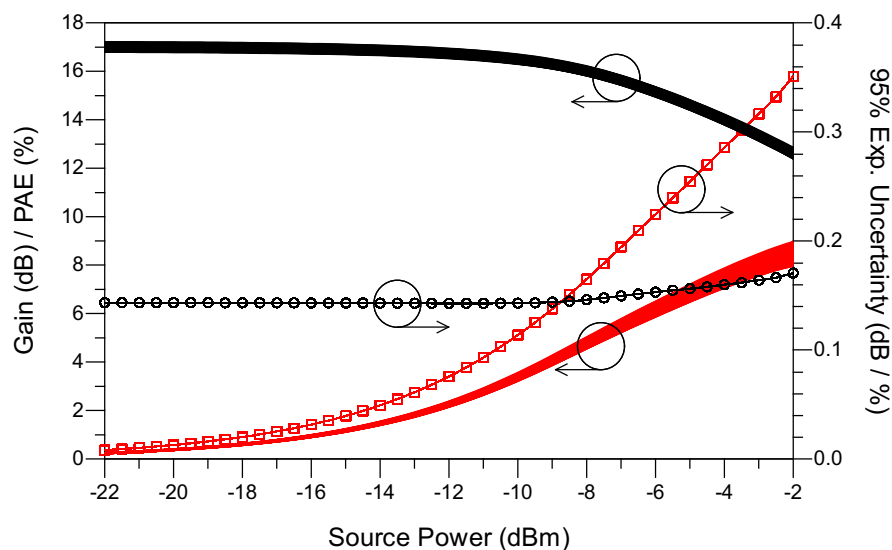


Figure 5.13: Results from the ADS circuit simulation. The higher black trace shows the Monte Carlo samples for the gain of the circuit, whereas the lower red trace shows the PAE. The black trace with circles and red trace with squares show the 95% expanded uncertainties for gain and PAE, respectively.

To improve confidence in the design process of systems involving nonlinear devices, the uncertainty in both compact and behavioral models is required. This work has produced, for the first time, an evaluation of measurement uncertainty in a popular behavioral model, by developing a framework which can be easily adapted to support alternative models. In addition, the produced portable device model can be used in existing circuit simulators, allowing access to this information for statistical design techniques and to help achieve first pass design success for complicated nonlinear systems.

6 Conclusion

This dissertation has investigated several aspects of metrology for 5G applications. Due to the demanding performance requirements of the hardware used to implement this vision, it is crucial to underpin its development with accurate, confident measurements.

At the beginning of this dissertation (Section 1.3) three main objectives were declared, which supported research and development towards future wireless technologies, including 5G communications and radar. To conclude, the achievements towards each objective will now be summarised.

During initial research into metrological best practice for RF measurements, it was discovered that a key international guidance document [1] contained ambiguous instructions which could have a large effect on the uncertainties of RF measurements. Because of the popularity of this document, a review article was published [2] to highlight this ambiguity in anticipation of an update to [1]. Although for many types of measurement this ambiguity has little effect, for RF measurements, especially those involving S-parameters, the impact is significant. In new hardware implementations for future communications networks, massive numbers of antennas mean that measurements involving large numbers of s-parameters for a single device will become more common. For these measurements some of the guidance becomes unfeasible for typical manufacturer test processes, and even research applications. In addition, the resulting uncertainties obtained from the two options offered by the ambiguity differ by a factor up to 1.7, which is a significant difference.

Investigation into metrology at millimetre-wave and higher frequencies found that there were areas of core calibration and uncertainty analysis methodology which were missing when compared with similar measurements at lower frequencies. The validity of the “ripple technique”, widely used to perform basic uncertainty evaluations in coaxial transmission line according to guidance such as [3], had not previously been tested in waveguide at these high frequencies (or at any frequency). Future wireless communications are planned to use increasingly higher fre-

quencies such as E-band (60–90 GHz), and frequencies around 300 GHz are being investigated for ultra-high bandwidth data transfer and streaming. To efficiently route these signals inside transceiver front-ends, waveguide is a common choice of transmission medium. The results of the investigation into the ripple technique in waveguide found that it was valid in waveguides up to 220 GHz, but mechanical alignment repeatability in waveguide at frequencies above this (WR-1.5) could cause the technique to fail [4], [5]. New developments in waveguide standards at this frequency should improve this repeatability and hopefully allow the ripple technique to provide uncertainty evaluations for measurements performed at these frequencies.

The main contribution of this work, however, was the first propagation of measurement uncertainty from nonlinear device measurements into a behavioural model, specifically X-parameters [6]. This model is widely used in the amplifier design industry to allow engineers to simulate nonlinear device performance. The increasingly difficult design specifications required by 5G and other developing communications standards, combined with the commercial drive for first-pass design success, puts pressure on engineers to extract model parameters with accuracy and confidence. Until now, that confidence, quantified by measurement uncertainty, has not previously been rigorously evaluated. The evaluation presented in this dissertation used the NIST Microwave Uncertainty Framework as an established and proven base from which to extend NVNA power wave uncertainties into a behavioural model. An invited secondment to NIST was used to improve this framework and extend it to work with the X-parameter nonlinear behavioural model. X-parameters were chosen as the model to implement for this work due to their popularity and compatibility with major vendors of both instrumentation and design simulation software, however it is possible to use the same framework to implement alternative behavioural models. In fact, the main challenge with this project was reverse-engineering the implementation of the X-parameter extraction in order to propagate measurement uncertainties. Alternative models may provide freely-available implementations and mathematical formulations for their extraction.

Finally, the uncertainty evaluation was demonstrated for a millimetre-wave amplifier. Over 300 sources of uncertainty were included, and all calibrations used traceable standards. The extracted model was subsequently used in an industry-standard circuit simulator as part of an amplifier design. The uncertainties were propagated through the simulations, using only built-in features, to allow impact of the measurement uncertainty in the extracted model to be seen in the final amplifier performance predictions. This new ability allows designers to review the quality of their model choices and develop confidence in their measurement instrumentation and processes.

6.1 Future Work

Two of the three objectives of this dissertation have clear opportunities for future research.

The waveguide VNA uncertainty evaluation work presented in Chapter 4 highlighted issues with the repeatability of the mechanical alignment of the UG-387 flanges used on WR-1.5 waveguide. Since that investigation was completed, a new IEEE Standard has been published (and reviewed [7]) which details new flange designs to increase the alignment repeatability. Therefore, it would be useful to repeat the evaluation of the uncertainty evaluation in WR-1.5 submillimetre-wave waveguide to investigate if the new flange designs make it valid.

The nonlinear behavioural model uncertainty evaluation would benefit greatly from the addition of another type of model. The Cardiff model [8] is a good candidate for this, as it is also commercially available and currently used in industry. With two models implemented in the framework, it would be possible to compare the sensitivities of the performance metrics of amplifiers simulated with them, which may provide new insights into their accuracy. This work could also review measurements of other nonlinear devices compatible with the behavioural models, such as mixers. On-wafer DUTs can also be included, using both calibration de-embedding techniques or the on-wafer absolute calibration standards under development [9].

Similar comparisons would be valuable between the different architectures of NVNA used to extract the models. The implementation developed in this work uses a mixer-based architecture, but measurement uncertainty propagated into behavioural models from sampler-based NFNAs should also be evaluated.

The reproducibility of behavioural model extraction, comparing the uncertainties in model parameters extracted from the same DUT at different labs using the same equipment is another opportunity for research using this new framework. Reproducibility studies are commonly used by both NMIs and industry to measure the variation in measurements across laboratories, which, combined with knowledge of the uncertainty tolerances of the application, can inform them where to focus on improving metrology [10].

Finally, an evaluation of behavioural model uncertainty using analytical propagation should be possible to develop, which can provide further verification against the numerical method presented here. This requires the derivation of Jacobian matrices relating the raw measured power waves to the model parameters. For mixer-based NFNAs, Jacobian matrices for calibrated power waves have already been published in [11]. Once those for the behavioural model have been derived, they can be cascaded to provide a complete analytical propagation of uncertainty.

References

- [1] The Ericsson Mobility Report, Ericsson, [Online]. Available: <https://www.ericsson.com/en/mobility-report> (visited on 09/11/2019).
- [2] S. C. Cripps, *RF Power Amplifiers for Wireless Communications*, 2nd Edition. Norwood, MA, USA: Artech House, Inc., 2006.
- [3] N. Kosaka, S. Fujiwara, A. Okamura, K. Chomei, Y. Sasaki, K. Horiguchi, H. Katayama, and A. Inoue, “A high-efficiency and high-gain, plastic packaged GaN HEMT for 3.5-GHz-band LTE base stations,” in *IEEE Int. Symp. Radio-Freq. Integr. Technol. (RFIT)*, Taipei, Taiwan, Aug. 2016, pp. 1–3.
- [4] S. Bhardwaj and J. Kitchen, “Broadband parallel Doherty power amplifier in GaN for 5G applications,” in *IEEE Topical Conf. RF/Microw. Power Amplifiers Radio Wireless Appl. (PAWR)*, Orlando, FL, USA, Jan. 2019, pp. 1–3.
- [5] V. Camarchia, M. Pirola, R. Quaglia, S. Jee, Y. Cho, and B. Kim, “The doherty power amplifier: Review of recent solutions and trends,” *IEEE Trans. Microw. Theory Techn.*, vol. 63, no. 2, pp. 559–571, Jan. 2015.
- [6] P. Aaen, J. A. Plá, and J. Wood, *Modeling and Characterization of RF and Microwave Power FETs*, ser. The Cambridge RF and Microwave Engineering Series. Cambridge University Press, 2007.
- [7] NXP MRFX1K80H 65 V wideband RF power LDMOS transistor, [Online]. Available: <https://www.avnet.com/wps/portal/ebv/products/new-products/npi/2017/nxp-mrfx1k80h> (visited on 09/19/2019).
- [8] D. F. Williams, R. A. Chamberlin, W. Zhao, J. Cheron, and M. E. Urteaga, “The role of measurement uncertainty in achieving first-pass design success,” in *IEEE Compound Semicond. Integr. Circuit Symp. (CSICS)*, Austin, TX, USA, Oct. 2016, pp. 1–4.

- [9] J. Cheron, D. F. Williams, K. Lukasik, R. A. Chamberlin, B. F. Jamroz, E. N. Grossman, W. Wiatr, and D. Schreurs, “Propagation of compact-modeling measurement uncertainty to 220 GHz power-amplifier designs,” in *Asia-Pacific Microw. Conf. (APMC)*, Kyoto, Japan, Nov. 2018, pp. 744–746.
- [10] European co-operation for Accreditation, “EA guidelines on the evaluation of vector network analysers (VNA),” Tech. Rep. EA-10/12, May 2000.
- [11] European Association of National Metrology Institutes (EURAMET), “Guidelines on the evaluation of vector network analysers (VNA), version 2,” Tech. Rep. cg-12, Mar. 2011.
- [12] BIPM, IEC, IFCC, ILAC, ISO, IUPAC, IUPAP and OIML, *Guide to the Expression of Uncertainty in Measurement JCGM 100:2008 (GUM 1995 with minor corrections)*, 2008. [Online]. Available: <http://www.bipm.org/utils/common/documents/jcgm/JCGM%20100%202008%20E.pdf>.
- [13] J. P. Hoffmann, P. Leuchtmann, J. Schaub, and R. Vahldieck, “Computing uncertainties of s-parameters by means of Monte Carlo simulation,” in *69th ARFTG Microw. Meas. Conf.*, Honolulu, HI, USA, Jun. 2007, pp. 1–7.
- [14] METAS. VNA tools II, [Online]. Available: <https://www.metas.ch/metas/en/home/fabe/hochfrequenz/vna-tools.html> (visited on 07/16/2019).
- [15] A. Lewandowski, D. F. Williams, P. D. Hale, J. C. M. Wang, and A. Dienstfrey, “Covariance-based vector-network-analyzer uncertainty analysis for time- and frequency-domain measurements,” *IEEE Trans. Microw. Theory Techn.*, vol. 58, no. 7, pp. 1877–1886, Jul. 2010.
- [16] M. Lin and Y. Zhang, “Covariance-matrix-based uncertainty analysis for NVNA measurements,” *IEEE Trans. Microw. Theory Techn.*, vol. 61, no. 1, pp. 93–102, Jan. 2012.
- [17] National Institute of Science and Technology. On-wafer calibration software, [Online]. Available: <https://www.nist.gov/services-resources/software/wafer-calibration-software> (visited on 07/16/2019).
- [18] G. Avolio, A. Raffo, J. Jargon, P. D. Hale, D. M. M.-P. Schreurs, and D. F. Williams, “Evaluation of uncertainty in temporal waveforms of microwave transistors,” *IEEE Trans. Microw. Theory Techn.*, vol. 63, no. 7, pp. 2353–2363, Jul. 2015.
- [19] D. F. Williams, R. A. Chamberlin, W. Zhao, J. Cheron, and M. E. Urteaga, “Transistor model verification including measurement uncertainty,” *IEEE Trans. Microw. Theory Techn.*, vol. 64, no. 11, pp. 3927–3933, Nov. 2016.

- [20] E. Dahlman, G. Mildh, S. Parkvall, J. Peisa, J. Sachs, Y. Selén, and J. Sköld, “5G wireless access: Requirements and realization,” *IEEE Commun. Mag.*, vol. 52, no. 12, pp. 42–47, Dec. 2014.
- [21] L. T. Stant, P. H. Aaen, and N. M. Ridler, “Comparing methods for evaluating measurement uncertainty given in the JCGM ‘evaluation of measurement data’ documents,” *Measurement*, vol. 94, pp. 847–851, Dec. 2016.
- [22] BIPM, IEC, IFCC, ILAC, ISO, IUPAC, IUPAP and OIML, *Supplement 1 to the “Guide to the Expression of Uncertainty in Measurement” - Propagation of distributions using a Monte Carlo method JCGM 101:2008*, 2008. [Online]. Available: <http://www.bipm.org/utils/common/documents/jcgm/JCGM%20101%202008%20E.pdf>.
- [23] ——, *Supplement 2 to the “Guide to the Expression of Uncertainty in Measurement” - Extension to any number of output quantities JCGM 102:2011*, 2011. [Online]. Available: <http://www.bipm.org/utils/common/documents/jcgm/JCGM%20102%202011%20E.pdf>.
- [24] L. T. Stant, P. H. Aaen, and N. M. Ridler, “Evaluating residual errors in waveguide VNAs from microwave to submillimetre-wave frequencies,” *IET Microw. Antennas Propag.*, vol. 11, no. 3, pp. 324–329, Feb. 2017.
- [25] H. Song, H. Hamada, and M. Yaita, “Prototype of kiosk data downloading system at 300 ghz: Design, technical feasibility, and results,” *IEEE Communications Magazine*, vol. 56, no. 6, pp. 130–136, Jun. 2018.
- [26] L. T. Stant, M. J. Salter, N. M. Ridler, D. F. Williams, and P. H. Aaen, “Propagating measurement uncertainty to microwave amplifier nonlinear behavioural models,” *IEEE Trans. Microw. Theory Techn.*, vol. 67, no. 2, pp. 815–821, Nov. 2018.
- [27] Dylan williams ieee xplore author details, [Online]. Available: <https://ieeexplore.ieee.org/author/37085349096> (visited on 09/21/2019).
- [28] D. Williams, “Traveling waves and power waves: Building a solid foundation for microwave circuit theory,” *IEEE Microw. Mag.*, vol. 14, no. 7, pp. 38–45, Nov. 2013.
- [29] N. Marcuvitz, *Waveguide Handbook*, ser. Electromagnetics and Radar Series. McGraw-Hill, 1951.
- [30] R. Marks and D. F. Williams, “A general waveguide circuit theory,” in *J. Res. Natl. Inst. Stan.*, vol. 97, Oct. 1992.

- [31] K. Kurokawa, “Power waves and the scattering matrix,” *IEEE Trans. Microw. Theory Techn.*, vol. 13, no. 2, pp. 194–202, Mar. 1965.
- [32] D. F. Williams and B. K. Alpert, “Causality and waveguide circuit theory,” *IEEE Trans. Microw. Theory Techn.*, vol. 49, no. 4, pp. 615–623, Apr. 2001.
- [33] D. Williams and R. Marks, “The interpretation and use of s-parameters in lossy lines,” in *36th ARFTG Microw. Meas. Conf. Dig.*, vol. 18, Monterey, CA, USA, Nov. 1990, pp. 84–90.
- [34] P. H. Smith, “Transmission line calculator,” *Electronics*, vol. 12, no. 1, pp. 29–31, Jan. 1939.
- [35] D. M. Pozar, *Microwave Engineering*. Wiley, 2004.
- [36] V. Teppati, A. Ferrero, and M. Sayed, Eds., *Modern RF and Microwave Measurement Techniques*, ser. The Cambridge RF and Microwave Engineering Series. Cambridge University Press, 2013.
- [37] J. P. Dunsmore, *Handbook of Microwave Component Measurements: with Advanced VNA Techniques*. Wiley, 2012.
- [38] D. Rytting, “ARFTG 50 year network analyzer history,” in *IEEE MTT-S Int. Microw. Symp. Dig.*, Atlanta, GA, USA, Jun. 2008, pp. 11–18.
- [39] B. Parzen and A. Yalow, “Theory and design of the reflectometer,” *Elec. Commun.*, vol. 24, no. 1, pp. 94–100, Mar. 1947.
- [40] Rohde & Schwarz. (Mar. 14, 2014). Vector network analysis with up to 48 ports, Microwave Journal, [Online]. Available: <http://www.microwavejournal.com/articles/21785-vector-network-analysis-with-up-to-48-ports> (visited on 08/18/2019).
- [41] D. E. Root, J. Verspecht, J. Horn, and M. Marcu, *X-Parameters: Characterization, Modeling, and Design of Nonlinear RF and Microwave Components*. Cambridge University Press, 2013.
- [42] R. J. Collier and A. D. Skinner, Eds., *Microwave Measurements*, ser. IET Electrical Measurement Series. Institution of Engineering and Technology, 2007.
- [43] D. Rytting, “Network analyzer error models and calibration methods,” *ARFTG Short Course on Meas. and Metrology for RF Telecommun.*, Nov. 2000.
- [44] S. Rehnmark, “On the calibration process of automatic network analyzer systems,” *IEEE Trans. Microw. Theory Techn.*, vol. 22, no. 4, pp. 457–458, Apr. 1974.

- [45] J. V. Butler, D. K. Rytting, M. F. Iskander, R. D. Pollard, and M. Vanden Bossche, “16-term error model and calibration procedure for on-wafer network analysis measurements,” *IEEE Trans. Microw. Theory Techn.*, vol. 39, no. 12, pp. 2211–2217, Dec. 1991.
- [46] W. Egan, *Practical RF System Design*. Wiley, 2004.
- [47] G. F. Engen and C. A. Hoer, “Thru-reflect-line: An improved technique for calibrating the dual six-port automatic network analyzer,” *IEEE Trans. Microw. Theory Techn.*, vol. 27, no. 12, pp. 987–993, Dec. 1979.
- [48] R. B. Marks, “A multiline method of network analyzer calibration,” *IEEE Trans. Microw. Theory Techn.*, vol. 39, no. 7, pp. 1205–1215, Jul. 1991.
- [49] M. Sipila, K. Lehtinen, and V. Porra, “High-frequency periodic time-domain waveform measurement system,” *IEEE Trans. Microw. Theory Techn.*, vol. 36, no. 10, pp. 1397–1405, Oct. 1988.
- [50] T. Van den Broeck and J. Verspecht, “Calibrated vectorial nonlinear-network analyzers,” in *IEEE MTT-S Int. Microw. Symp. Dig.*, vol. 2, San Diego, CA, USA, May 1994, pp. 1069–1072.
- [51] J. B. Scott, J. Verspecht, B. Behnia, M. Vanden Bossche, A. Cognata, F. Verbeyst, M. L. Thorn, and D. R. Scherrer, “Enhanced on-wafer time-domain waveform measurement through removal of interconnect dispersion and measurement instrument jitter,” *IEEE Trans. Microw. Theory Techn.*, vol. 50, no. 12, pp. 3022–3028, Dec. 2002.
- [52] W. Van Moer and Y. Rolain, “A large-signal network analyzer: Why is it needed?” *IEEE Microw. Mag.*, vol. 7, no. 6, pp. 46–62, Nov. 2006.
- [53] U. Lott, “Measurement of magnitude and phase of harmonics generated in nonlinear microwave two-ports,” *IEEE Trans. Microw. Theory Techn.*, vol. 37, no. 10, pp. 1506–1511, Oct. 1989.
- [54] P. Blockley, D. Gunyan, and J. B. Scott, “Mixer-based, vector-corrected, vector signal/network analyzer offering 300kHz–20GHz bandwidth and traceable phase response,” in *IEEE MTT-S Int. Microw. Symp. Dig.*, Long Beach, CA, USA, Jun. 2005, pp. 1497–1500.
- [55] M. A. Casbon and P. J. Tasker, “Comparison of sampler and VNA based large signal measurement systems (LSNA) under CW and pulsed operation,” in *85th ARFTG Microw. Meas. Conf. Dig.*, Phoenix, AZ, USA, May 2015, pp. 1–3.

- [56] UKAS. Our role, [Online]. Available: <http://www.ukas.com/about/our-role/> (visited on 01/07/2019).
- [57] BIPM. (Nov. 10, 2016). Draft of the ninth SI brochure, [Online]. Available: <http://www.bipm.org/utils/common/pdf/si-brochure-draft-2016b.pdf> (visited on 01/07/2019).
- [58] International Organization for Standardization, *Guide to the expression of uncertainty in measurement*, 1st ed., Geneva, 1993.
- [59] BIPM, IEC, IFCC, ILAC, ISO, IUPAC, IUPAP and OIML, *International Vocabulary of Metrology Basic and General Concepts and Associated Terms (VIM) JCGM 200:2012*, 2012. [Online]. Available: <http://www.bipm.org/utils/common/documents/jcgm/JCGM%20200%202012.pdf>.
- [60] N. Metropolis and S. Ulam, “The monte carlo method,” *J. Amer. Statist. Assoc.*, vol. 44, no. 247, pp. 335–341, Sep. 1949.
- [61] J. Neyman, “Outline of a theory of statistical estimation based on the classical theory of probability,” *Philos. Trans. Roy. Soc. A*, vol. 236, no. 767, pp. 333–380, Aug. 1937.
- [62] A. Gelman, J. B. Carlin, H. S. Stern, D. B. Dunson, A. Vehtari, and D. B. Rubin, *Bayesian Data Analysis*, 3rd ed. Chapman and Hall, 2013, 675 pp.
- [63] D. R. White, “In pursuit of a fit-for-purpose uncertainty guide,” *Metrologia*, vol. 53, no. 4, S107–S124, Jun. 2016.
- [64] R. Kacker, B. Toman, and D. Huang, “Comparison of ISO-GUM, draft GUM supplement 1 and Bayesian statistics using simple linear calibration,” *Metrologia*, vol. 43, no. 4, S167–S177, Aug. 2006.
- [65] R. N. Kacker, “Bayesian alternative to the ISO-GUM’s use of the Welch–Satterthwaite formula,” *Metrologia*, vol. 43, no. 1, pp. 1–11, Nov. 2005.
- [66] R. Kacker and A. Jones, “On use of Bayesian statistics to make the guide to the expression of uncertainty in measurement consistent,” *Metrologia*, vol. 40, no. 5, pp. 235–248, Sep. 2003.
- [67] W. Bich, “Revision of the ‘guide to the expression of uncertainty in measurement’. why and how,” *Metrologia*, vol. 51, no. 4, S155–S158, Jul. 2014.
- [68] C. Elster, W. Wöger, and M. G. Cox, “Draft GUM supplement 1 and Bayesian analysis,” *Metrologia*, vol. 44, no. 3, pp. L31–L32, May 2007.

- [69] K. Klauenberg and C. Elster, “The multivariate normal mean - sensitivity of its objective Bayesian estimates,” *Metrologia*, vol. 49, no. 3, pp. 395–400, Apr. 2012.
- [70] M. Cox and K. Shirono, “Informative Bayesian type a uncertainty evaluation, especially applicable to a small number of observations,” *Metrologia*, vol. 54, no. 5, pp. 642–652, Aug. 2017.
- [71] International Organization for Standardization, *ISO 9000: International standards for quality management*, Genève, Switzerland: International Organization for Standardization, 2015. [Online]. Available: <https://www.iso.org>.
- [72] ——, *ISO 17025: General requirements for the competence of testing and calibration laboratories*, Genève, Switzerland: International Organization for Standardization, 2005. [Online]. Available: <https://www.iso.org>.
- [73] International Bureau of Weights and Measures (BIPM), *The International System of Units (SI)*, 8th ed. 2019. [Online]. Available: <https://www.bipm.org>.
- [74] ——, *A concise summary of the International System of Units, the SI*, 8th ed. 2019. [Online]. Available: <https://www.bipm.org>.
- [75] R. N. Clarke, J. P. Ide, G. R. Orford, and N. M. Ridler, “Draft EAL procedure for the assessment of vector network analysers (VNA), ANAMET report 002,” National Physical Laboratory, Tech. Rep. 002, Sep. 1996, Available from the National Physical Laboratory.
- [76] J. P. M. de Vreede, “Draft procedure for the assessment of vector network analysers (VNA), ANAMET report 019,” National Physical Laboratory, Tech. Rep. 019, Oct. 1998, Available from the National Physical Laboratory.
- [77] ——, “Draft EA guidance document: Assessment of calibrated vector network analysers (VNA), ANAMET report 026,” National Physical Laboratory, Tech. Rep. 026, Aug. 1999, Available from the National Physical Laboratory.
- [78] M. Hiebel, *Fundamentals of Vector Network Analysis*. Rohde & Schwarz, 2008.
- [79] Keysight Technologies. Downloadable vector network analyzer uncertainty calculator, [Online]. Available: <https://www.keysight.com/main/software.jspx?ckey=1000000418:epsg:sud&cc=GB> (visited on 07/16/2019).
- [80] Anritsu. Exact uncertainty calculator, [Online]. Available: <https://www.anritsu.com/en-GB/test-measurement/support/downloads/software/dwl19572> (visited on 07/16/2019).

- [81] Insight VNA calibration and measurement software, [Online]. Available: <https://www.maurymw.com/pdf/datasheets/4T-023.pdf> (visited on 09/22/2019).
- [82] N. M. Ridler and M. J. Salter, “An approach to the treatment of uncertainty in complex S-parameter measurements,” *Metrologia*, vol. 39, no. 3, pp. 295–302, Jun. 2002. [Online]. Available: <https://doi.org/10.1088%2F0026-1394%2F39%2F3%2F6>.
- [83] Keysight Technologies, “Specifying calibration standards and kits for keysight vector network analyzers,” Tech. Rep. 1GP43_0E, Jul. 2016.
- [84] J. A. Jargon, K. C. Gupta, and D. C. DeGroot, “Applications of artificial neural networks to RF and microwave measurements,” *Int. J. of RF and Microw. Computer-Aided Eng.*, vol. 12, no. 1, pp. 3–24, Jan. 2002.
- [85] A. Lewandowski, “Multi-frequency approach to vector-network-analyzer scattering-parameter measurements,” PhD thesis, Warsaw University of Technology, 2010.
- [86] D. K. Rytting, “Network analyzer accuracy overview,” in *58th ARFTG Microw. Meas. Conf. Dig.*, vol. 40, San Francisco, CA, USA, Nov. 2001, pp. 1–13.
- [87] J. Martens, “On quantifying the effects of receiver linearity on VNA calibrations,” in *70th ARFTG Microw. Meas. Conf.*, Tempe, AZ, USA, Nov. 2007, pp. 1–6.
- [88] L. T. Stant, P. H. Aaen, and N. M. Ridler, “Evaluating residual errors in waveguide network analysers from microwave to submillimetre-wave frequencies,” in *IET Colloq. on Millimetre-Wave and Terahertz Eng. & Technol.*, London, U.K.: Institution of Engineering and Technology (IET), Mar. 2016.
- [89] D. Bannister, E. Griffin, and T. Hodgetts, *On the dimensional tolerances of rectangular waveguide for reflectometry at millimetric wavelengths*. National Physical Laboratory, 1989.
- [90] A. Kerr, E. Wollack, and N. Horner, “Waveguide flanges for ALMA instrumentation,” *ALMA Memo*, vol. 278, Nov. 1999.
- [91] A. Kerr, “Mismatch caused by waveguide tolerances, corner radii, and flange misalignment,” *Electronics Div. Tech. Note*, vol. 215, Jan. 2010.
- [92] D. F. Williams, “500 GHz–750 GHz rectangular-waveguide vector-network-analyzer calibrations,” *IEEE Trans. THz Sci. Technol.*, vol. 1, no. 2, pp. 364–377, Nov. 2011.

- [93] H. Li, A. R. Kerr, J. L. Hesler, and R. M. Weikle, “Repeatability of waveguide flanges with worst-case tolerances in the 500–750 GHz band,” in *79th ARFTG Microw. Meas. Conf.*, IEEE, Montreal, QC, Canada, Jun. 2012, pp. 1–8.
- [94] “IEEE standard for rectangular metallic waveguides and their interfaces for frequencies of 110 GHz and above—part 2: Waveguide interfaces,” *IEEE Std 1785.2-2016*, pp. 1–22, Sep. 2016.
- [95] A. Arsenovic, R. M. Weikle, and J. Hesler, “Two port calibration insensitive to flange misalignment,” in *84th ARFTG Microw. Meas. Conf.*, Boulder, CO, USA, Dec. 2014, pp. 1–7.
- [96] M. Garelli and A. Ferrero, “A unified theory for S-parameter uncertainty evaluation,” *IEEE Trans. Microw. Theory Techn.*, vol. 60, no. 12, pp. 3844–3855, Dec. 2012.
- [97] Keysight Technologies, “VNA measurement uncertainty,” Tech. Rep. 5992-3595EN, Jun. 2019.
- [98] METAS. Metas unclib, [Online]. Available: <https://www.metas.ch/metas/en/home/fabe/hochfrequenz/unclib.html> (visited on 07/16/2019).
- [99] M. Wollensack, J. Hoffmann, J. Ruefenacht, and M. Zeier, “VNA tools II: S-parameter uncertainty calculation,” in *79th ARFTG Microw. Meas. Conf.*, Montreal, QC, Canada, Jun. 2012, pp. 1–5.
- [100] R. A. Ginley, “Kicking the tires of the NIST microwave uncertainty framework, part 1,” in *88th ARFTG Microw. Meas. Conf.*, Austin, TX, USA, Dec. 2016, pp. 1–4.
- [101] ———, “Kicking the tires of the NIST microwave uncertainty framework, part 2,” in *90th ARFTG Microw. Meas. Conf.*, Boulder, CO, USA, Nov. 2017, pp. 1–4.
- [102] J. A. Jargon, D. F. Williams, and A. Sanders, “Three-port vector-network-analyzer calibrations using the NIST microwave uncertainty framework,” in *92nd ARFTG Microw. Meas. Conf.*, Orlando, FL, USA, Jan. 2019, pp. 1–4.
- [103] J. N. H. Dortmans, J. T. Quimby, K. A. Remley, D. F. Williams, J. Senic, R. Sun, and P. B. Papazian, “Design of a portable verification artifact for millimeter-wave-frequency channel sounders,” *IEEE Trans. Antennas Propag.*, vol. 67, no. 9, pp. 6149–6158, Sep. 2019.

- [104] D. Gu, X. Lu, B. F. Jamroz, D. F. Williams, X. Cui, and A. W. Sanders, "NIST-traceable microwave power measurement in a waveguide calorimeter with correlated uncertainties," *IEEE Trans. Instrum. Meas.*, vol. 68, no. 6, pp. 2280–2287, Jun. 2019.
- [105] J. A. Jargon, D. C. DeGroot, and D. F. Vecchia, "Repeatability study of commercial harmonic phase standards measured by a nonlinear vector network analyzer," in *62nd ARFTG Microw. Meas. Conf.*, Boulder, CO, USA, Dec. 2003, pp. 243–258.
- [106] P. S. Blockley, J. B. Scott, D. Gunyan, and A. E. Parker, "The random component of mixer-based nonlinear vector network analyzer measurement uncertainty," *IEEE Trans. Microw. Theory Techn.*, vol. 55, no. 10, pp. 2231–2239, Oct. 2007.
- [107] H. C. Reader, D. F. Williams, P. D. Hale, and T. S. Clement, "Comb-generator characterization," *IEEE Trans. Microw. Theory Techn.*, vol. 56, no. 2, pp. 515–521, Feb. 2008.
- [108] D. F. Williams, A. Lewandowski, T. S. Clement, J. C. M. Wang, P. D. Hale, J. M. Morgan, D. A. Keenan, and A. Dienstfrey, "Covariance-based uncertainty analysis of the NIST electrooptic sampling system," *IEEE Trans. Microw. Theory Techn.*, vol. 54, no. 1, pp. 481–491, Jan. 2006.
- [109] P. D. Hale, A. Dienstfrey, J. C. M. Wang, D. F. Williams, A. Lewandowski, D. A. Keenan, and T. S. Clement, "Traceable waveform calibration with a covariance-based uncertainty analysis," *IEEE Trans. Instrum. Meas.*, vol. 58, no. 10, pp. 3554–3568, Oct. 2009.
- [110] Keysight Technologies. (Sep. 2017). Fundamentals of RF and Microwave Power Measurements (Part 3), [Online]. Available: <https://literature.cdn.keysight.com/litweb/pdf/5988-9215EN.pdf> (visited on 08/18/2019).
- [111] Rohde & Schwarz, "Program for measurement uncertainty analysis with Rohde & Schwarz power meters," Tech. Rep. 5989-4840EN, Jun. 2001.
- [112] D. A. Humphreys, P. M. Harris, M. Rodriguez-Higuero, F. A. Mubarak, D. Zhao, and K. Ojasalo, "Principal component compression method for covariance matrices used for uncertainty propagation," *IEEE Trans. Instrum. Meas.*, vol. 64, no. 2, pp. 356–365, Feb. 2015.
- [113] F. Verbeyst and V. Bossche, "VIOMAP, the S-parameter equivalent for weakly nonlinear RF and microwave devices," *IEEE Trans. Microw. Theory Techn.*, vol. 42, no. 12, pp. 2531–2535, Dec. 1994.

- [114] M. Schetzen, *The Volterra and Wiener Theories of Nonlinear Systems*. Melbourne, FL, USA: Krieger Publishing Co., Inc., 2006.
- [115] H. Moodi and D. Bustan, “On identification of nonlinear systems using Volterra kernels expansion on Laguerre and wavelet function,” in *Chin. Control and Decision Conf. (CCDC)*, Xuzhou, China, May 2010, pp. 1141–1145.
- [116] F. Verbeyst and M. Vanden Bossche, “The Volterra input-output map of a high-frequency amplifier as a practical alternative to load-pull measurements,” *IEEE Trans. Instrum. Meas.*, vol. 44, no. 3, pp. 662–665, Jun. 1995.
- [117] F. Verbeyst and M. V. Bossche, “VIOMAP, 16QAM and spectral regrowth: Enhanced prediction and predistortion based on two-tone black-box model extraction,” in *45th ARFTG Microw. Meas. Conf. Dig.*, vol. 27, Orlando, FL, USA, May 1995, pp. 19–28.
- [118] F. Verbeyst, “Using orthogonal polynomials as alternative for VIOMAP to model hardly nonlinear devices,” in *47th ARFTG Microw. Meas. Conf. Dig.*, vol. 29, San Francisco, CA, USA, Jun. 1996, pp. 112–120.
- [119] J. Verspecht, D. Schreurs, A. Barel, and B. Nauwelaers, “Black box modelling of hard nonlinear behavior in the frequency domain,” in *IEEE MTT-S Int. Microw. Symp. Dig.*, vol. 3, San Francisco, CA, USA, Jun. 1996, pp. 1735–1738.
- [120] J. Verspecht, “Everything you’ve always wanted to know about hot-S22 (but we’re afraid to ask),” in *Workshop at the Int. Microw. Symp.*, Seattle, WA, USA, Jun. 2002.
- [121] J. Verspecht, D. Barataud, J. Teyssier, and J. Nébus, “Hot S-parameter techniques: $6 = 4 + 2$,” in *66th ARFTG Microw. Meas. Conf.*, Washington, DC, USA, Dec. 2005, pp. 1–9.
- [122] Verspecht and D. E. Root, “Polyharmonic distortion modeling,” *IEEE Microw. Mag.*, vol. 7, no. 3, pp. 44–57, Jun. 2006.
- [123] J. Verspecht, D. F. Williams, D. Schreurs, K. A. Remley, and M. D. McKinley, “Linearization of large-signal scattering functions,” *IEEE Trans. Microw. Theory Techn.*, vol. 53, no. 4, pp. 1369–1376, Apr. 2005.
- [124] G. Sun, Y. Xu, and A. Liang, “The study of nonlinear scattering functions and X-parameters,” in *Int. Conf. Microw. Millimeter Wave Technol. (ICMWT)*, Chengdu, China, May 2010, pp. 1086–1089.

- [125] C. Widemann, H. Weber, S. Schatz, and W. Mathis, “A comparison of the Volterra series-based nonlinear S-parameters and X-parameters,” in *22nd Int. Conf. Mixed Des. of Integr. Circuits Sys. (MIXDES)*, Torun, Poland, Jun. 2015, pp. 453–457.
- [126] C. Xie, T. Zhang, and D. Liu, “Using X-parameters to model mixers,” in *Int. Conf. Microw. Millimeter Wave Technol. (ICMWT)*, vol. 3, Shenzhen, China, May 2012, pp. 1–3.
- [127] J. Verspecht, J. Horn, L. Betts, D. Gunyan, R. Pollard, C. Gillese, and D. E. Root, “Extension of X-parameters to include long-term dynamic memory effects,” in *IEEE MTT-S Int. Microw. Symp. Dig.*, Boston, MA, USA, Jun. 2009, pp. 741–744.
- [128] D. E. Root, J. Verspecht, and J. Xu, “Closed-form solutions to large-signal PA problems: Wirtinger calculus applied to X-parameters,” in *12th Eur. Microw. Integr. Circuits Conf. (EuMIC)*, Nuremberg, Germany, Oct. 2017, pp. 212–215.
- [129] S. J. Gillespie, D. E. Root, M. Marcu, and P. H. Aaen, “Electrothermal X-parameters for dynamic modeling of RF and microwave power transistors,” in *13th Eur. Microw. Integr. Circuits Conf. (EuMIC)*, Madrid, Spain, Sep. 2018, pp. 353–356.
- [130] Advanced Design System (ADS), Keysight Technologies, [Online]. Available: <https://www.keysight.com/en/pc-1297113/advanced-design-system-ads> (visited on 08/16/2019).
- [131] Microwave Office, NI AWR, [Online]. Available: <https://www.awr.com/software/products/microwave-office> (visited on 08/16/2019).
- [132] D. Gunyan, J. Horn, J. Xu, and D. E. Root, “Nonlinear validation of arbitrary load X-parameter and measurement-based device models,” in *73rd ARFTG Microw. Meas. Conf.*, Boston, MA, USA, Jun. 2009, pp. 1–4.
- [133] S. Woodington, T. Williams, H. Qi, D. Williams, L. Pattison, A. Patterson, J. Lees, J. Benedikt, and P. J. Tasker, “A novel measurement based method enabling rapid extraction of a RF waveform look-up table based behavioral model,” in *IEEE MTT-S Int. Microw. Symp. Dig.*, Atlanta, GA, USA, Jun. 2008, pp. 1453–1456.
- [134] H. Qi, J. Benedikt, and P. J. Tasker, “Nonlinear data utilization: From direct data lookup to behavioral modeling,” *IEEE Trans. Microw. Theory Techn.*, vol. 57, no. 6, pp. 1425–1432, Jun. 2009.

- [135] S. Woodington, R. Saini, D. Williams, J. Lees, J. Benedikt, and P. J. Tasker, "Behavioral model analysis of active harmonic load-pull measurements," in *IEEE MTT-S Int. Microw. Symp.*, Anaheim, CA, USA, May 2010, pp. 1688–1691.
- [136] D. Bespalko, "Modular nonlinear characterization system and large-signal behavioral modelling of unmatched transistors for streamlined power amplifier design," PhD thesis, University of Waterloo, Jan. 2016. [Online]. Available: <http://hdl.handle.net/10012/10179>.
- [137] M. R. Chernick, *Bootstrap Methods: A Guide for Practitioners and Researchers*, ser. Wiley Series in Probability and Statistics. Wiley, 2008. [Online]. Available: <https://books.google.co.uk/books?id=jx5K6IyjhhIC>.
- [138] Agilent. Introduction to Application Development, [Online]. Available: <http://na.support.keysight.com/pna/files/an1408-13.pdf> (visited on 08/16/2019).
- [139] ZX60-14012L datasheet, Mini-Circuits, [Online]. Available: <http://194.75.38.69/pdfs/ZX60-14012L.pdf> (visited on 08/18/2019).
- [140] HMC342LC4 datasheet, Analog Devices, [Online]. Available: <http://www.analog.com/media/en/technical-documentation/data-sheets/hmc342.pdf> (visited on 08/17/2019).
- [141] Keysight Technologies. (Aug. 2014). U9391C/F/G Comb Generators, [Online]. Available: <http://literature.cdn.keysight.com/litweb/pdf/5989-7619EN.pdf> (visited on 08/18/2019).

Appendix A: X-Parameter Extractor Code

The code to extract X-parameters within the MUF was implemented as a post-processor in VB.net. The user is given the choice to perform the extraction using the PNA-X or an algorithm which has been implemented within the post-processor. This algorithm can perform the extraction much faster as it can be run on more powerful hardware than the PNA-X and also parallelised (e.g. on compute clusters). This is useful for uncertainty propagation where large numbers of samples need to be processed.

The code listing below contains the functions used to perform the extraction using the PNA-X. This involves ensuring the measurement files have been transferred to storage which the instrument can access (e.g. a network-mounted drive), and that the PNA-X NVNA DCOM library (available from Keysight) has been registered on the computer executing the code.

```
Private Sub PNAX_Initialize_XP_Extraction(myPNAXAddress As String)
Try
    myNVNA = CreateObject("AgilentNVNA.Application", myPNAXAddress)
    If IsNothing(myNVNA) Then
        Throw New System.IO.FileNotFoundException
    End If
    myNVNA.Preset()
    myNVNA.XparameterEnabled = True
    If myNVNA.XparameterEnabled = False Then
        Throw New System.NotSupportedException
    End If
Catch
    Throw ' Pass exception to caller
```

```

End Try
End Sub

Private Function PNAX_Extract_XPs(myMDIF As MDIF,
myPNAXAddress As String, myLocalPath As String,
myPNAXPath As String) As Object
' Write MDIF file for PNA-X to access
myMDIF.Write(IO.Path.Combine(myLocalPath, "dut.mdf"))
' Perform extraction on PNA-X
Dim success As Boolean = myNVNA.GenerateXParamFromFiles(IO.Path.Combine(
myPNAXPath, "dut.mdf"), IO.Path.Combine(myPNAXPath, "dut.xnp"), False)
If Not success Then
    Throw New System.IO.InvalidDataException
End If
' Read in result from PNA-X
Dim myXNP As New MDIF
myXNP.Read(IO.Path.Combine(myLocalPath, "dut.xnp"))
Return myXNP
End Function

```

The custom X-parameter is implemented in the code listing below. The straightforward “.xnp” file generation and formatting is omitted from the end of the listing for brevity as it contains many boilerplate strings.

```

Private Function MUF_Extract_XPs(myMDIF As MDIF,
normalize_phase As Boolean) As Object

' We can either sweep through AN_1_1 of each stimulus tone and write
' out each block at a time to an xnp file, or build a big array of
' values and then write them out altogether. We use the latter.

' 1. Set blockVAR index to 0
' 1b. Get shape of ET states from first blockVars
' 2. Increment blockVAR index, if valid get values of indepVars

```

' 3. Get block indices of that set of indepVARs
 ' 4. Build index of ET states
 ' 5. Extract X-Parameters using this index
 ' 6. Loop
 ' 7. Write X-Parameters to file

```

Dim blockVAR_index As Integer = 0 ' 1. Set blockVAR index to 0
Dim current_block_VARS As HPList = Nothing
Dim ET_vars As String() = {"ssport", "ssfreq", "ssphase"}

' 1b. Get shape of ET states from first blockVARs
Dim ssports As Integer = 1
Dim ssfreqs As Integer = 1
Dim ssphases As Integer = 1
Dim current_ssport As Double = 1
Dim current_ssfreq As Double = 0
Dim current_ssphase As Double = 1
While True
  current_block_VARS = myMDIF.BlockVARs(blockVAR_index)
  For i As Integer = 0 To current_block_VARS.count - 1
    Dim name As String = current_block_VARS.GetHPName(i)
    Dim value As String = current_block_VARS.GetValueDouble(i)
    If ET_vars.Contains(name) Then
      Select Case name
        Case "ssport"
          If value < current_ssport Then
            Exit While
          End If
          If value > current_ssport Then
            ssports = ssports + 1
            current_ssport = value
          End If
        Case "ssfreq"

```

```

If value > current_ssfreq Then
    ssfreqs = ssfreqs + 1
    current_ssfreq = value
End If
Case "ssphase"
    If value > current_ssphase Then
        ssphases = ssphases + 1
        current_ssphase = value
    End If
Case Else
End Select
End If
Next
blockVAR_index = blockVAR_index + 1
End While

Dim n_X_params As Integer = ((ssfreqs - 1) * ssports * 2 + 1) *
(ssfreqs - 1) * ssports 'XFpk, XSpkql, XTpkql
Dim X_params As New ComplexMatrix(myMDIF.BlockCount, n_X_params)
' We'll trim the rows later
Dim X_param_block_indices(myMDIF.BlockCount) As Integer
' And these rows
Dim X_param_index As Integer = 1
blockVAR_index = 0

While True
    ' 2. Increment blockVAR index, if valid get values of indepVars.
    If (blockVAR_index = myMDIF.BlockCount) Then
        ' We've got through all the stimulus conditions!
        Exit While
    Else
        current_block_VARS = myMDIF.BlockVars(blockVAR_index)

```

```

Dim indepVar_sweep_array (current_block_VARS.count - 4)
    As MDIF_Var_Sweep
Dim j As Integer = 0
For i As Integer = 0 To current_block_VARS.count - 1
    Dim name As String = current_block_VARS.GetHPName(i)
    Dim value As Double = current_block_VARS.GetValueDouble(i)
    ' Unless it 's the ET variables...
    If ET_vars.Contains(name) Then
        Continue For
    End If
    ' Add the indepVar to our sweep object array
    indepVar_sweep_array(j) = New MDIF_Var_Sweep(name, value, value)
    j += 1
Next

' 3.      Get block indices of that set of indepVars
Dim ET_states As Integer() = myMDIF.GetBlockIndexFromVarRanges(
    indepVar_sweep_array)

' 4.      Build index of ET states
Dim ET_index(ssports - 1, ssfreqs - 1, ssphases - 1) As Integer
Dim index As Integer = 0
For ssport As Integer = 0 To ssports - 1
    For ssfreq As Integer = 0 To ssfreqs - 1
        For ssphase As Integer = 0 To ssphases - 1
            ET_index(ssport, ssfreq, ssphase) = ET_states(index)
            index = index + 1
    Next
Next
Next

' 5.      Extract X-Parameters using this index

```

' Fill matrices

```

Dim B_s(ssports - 1, ssfreqs - 1, ssphases - 1) As ComplexMatrix
Dim A_s(ssports - 1, ssfreqs - 1, ssphases - 1) As ComplexMatrix

For ssport As Integer = 0 To ssports - 1
    For ssfreq As Integer = 0 To ssfreqs - 1
        For ssphase As Integer = 0 To ssphases - 1
            Dim block_index As Integer = ET_index(ssport, ssfreq,
                ssphase)
            Dim this_block As RealMatrix = myMDIF.BlockMatrix(
                block_index).CreateRealMatrix
            Dim A As New ComplexMatrix(ssfreqs - 1, ssports)
            Dim B As New ComplexMatrix(ssfreqs - 1, ssports)
            Dim P As Complex
            P = toComplex(this_block.Rarray(0, 1),
                this_block.Rarray(0, 2))
            P = P / Abs(P)
            For port As Integer = 0 To ssports - 1
                For freq As Integer = 0 To ssfreqs - 2
                    ' this_block: freq, A1 real, A1 imag,
                    ' B1 real, B1 imag, A2 real, A2 imag.
                    ' Add one to complex matrix indices because
                    ' they are 1-indexed
                    A(freq + 1, port + 1) = toComplex(
                        this_block.Rarray(freq, port * 4 + 1),
                        this_block.Rarray(freq, port * 4 + 2))
                    B(freq + 1, port + 1) = toComplex(
                        this_block.Rarray(freq, port * 4 + 3),
                        this_block.Rarray(freq, port * 4 + 4))
                    A(freq + 1, port + 1) = A(freq + 1, port + 1) +
                        New Complex(1.0E-17 * (port + 1), 1.0E-17)
                    B(freq + 1, port + 1) = B(freq + 1, port + 1) +

```

```

        New Complex(1.0E-17 * (port + 1), 1.0E-17)

Next

Next

A_s(ssport, ssfreq, ssphase) = A
B_s(ssport, ssfreq, ssphase) = B

Next

Next

Next

' Next step

Dim X_columns As Integer = (ssfreqs - 1) * ssports * 2 + 1 - 1
' -1 as we are fitting XSpk11 and XTpk11 together

Dim X As New ComplexMatrix(ssports * ssfreqs * ssphases - ssphases,
    X_columns) ' Implicit -1 as we don't include ET on A11

Dim Y As New ComplexMatrix(ssports * ssfreqs * ssphases - ssphases)

Dim ET_i As Integer
Dim A0 As New Complex(0, 0)
Dim A0s As New ComplexMatrix(ssfreqs - 1, ssports)
Dim s As New ComplexMatrix(X_columns)

' Calculate A0

Dim OPT_average_A0 As Boolean = False

If OPT_average_A0 Then
    For ET_port As Integer = 0 To ssports - 1
        For ET_phase As Integer = 0 To ssphases - 1
            A0 = A0 + A_s(ET_port, 0, ET_phase)(1, 1) /
                (ssports * ssphases)
    Next

    Next

Else
    A0 = A0 + A_s(0, 0, 0)(1, 1)
End If

```

```

For port As Integer = 0 To ssports - 1
  For freq As Integer = 0 To ssfreqs - 2
    ET_i = 1
    For ssport As Integer = 0 To ssports - 1
      For ssfreq As Integer = 0 To ssfreqs - 1
        If ssport = 0 And ssfreq = 1 Then Continue For
        For ssphase As Integer = 0 To ssphases - 1
          Y(ET_i) = B_s(ssport, ssfreq, ssphase)(freq + 1,
            port + 1)
          X(ET_i, 1) = toComplex(1, 0)
        For a_port As Integer = 0 To ssports - 1
          For a_freq As Integer = 0 To ssfreqs - 2
            If a_port = 0 And a_freq = 0 Then
              X(ET_i, (a_port * (ssfreqs - 1) + a_freq) + 2) =
                (A_s(ssport, ssfreq, ssphase)(a_freq + 1,
                  a_port + 1) - A0) + New Complex(1.0E-17, 1.0E-17)
            Else
              X(ET_i, (a_port * (ssfreqs - 1) + a_freq) + 2) =
                A_s(ssport, ssfreq, ssphase)(a_freq + 1, a_port + 1)
              X(ET_i, (a_port * (ssfreqs - 1) + a_freq) +
                (ssports * ssfreqs - 1)) = Conj(A_s(ssport, ssfreq,
                  ssphase)(a_freq + 1, a_port + 1))
            End If
          Next
        Next
        ET_i += 1
      Next
    Next
  Next
  ' LSE
  s = ((ConjTranspose(X) * X) ^ -1) * (ConjTranspose(X) * Y)

```

```

'XF
'X_params(X_param_index, port * (ssfreqs - 1) + freq + 1) = s(1)
Dim XF As New Complex(0, 0)
XF = B_s(0, 0, 0)(freq + 1, port + 1)
For ET_port As Integer = 0 To ssports - 1
  For ET_freq As Integer = 0 To ssfreqs - 2
    If ET_port = 0 And ET_freq = 0 Then
      XF = XF - s(2 + (ET_port * (ssfreqs - 1) + ET_freq)) *
        (A_s(0, 0, 0)(freq + 1, port + 1) - A0)
    Else
      XF = XF - s(2 + (ET_port * (ssfreqs - 1) + ET_freq)) *
        (A_s(0, 0, 0)(freq + 1, port + 1))
      XF = XF - s(1 + (ET_port * (ssfreqs - 1) + ET_freq) +
        (ssports * (ssfreqs - 1))) * Conj(A_s(0, 0, 0)(freq + 1,
          port + 1))
    End If
  Next
  Next

X_params(X_param_index, port * (ssfreqs - 1) + freq + 1) = XF
For q As Integer = 0 To ssports - 1
  For l As Integer = 0 To ssfreqs - 2
    If q = 0 And l = 0 Then
      'XSpk11 = XS + XT
      X_params(X_param_index, ssports * (ssfreqs - 1) + port *
        (ssfreqs - 1) * ssports * (ssfreqs - 1) + freq *
        ssports * (ssfreqs - 1) + q * (ssfreqs - 1) + 1 + 1) =
        s(2 + (q * (ssfreqs - 1) + 1))
      'XTpk11 = 0
      X_params(X_param_index, ssports * (ssfreqs - 1) + port *
        (ssfreqs - 1) ^ 2 * ssports + freq * ssports *
        (ssfreqs - 1) + q * (ssfreqs - 1) + 1 + 1 +
        (ssfreqs - 1) ^ 2 * ssports ^ 2) = New Complex(0, 0)
    
```

Else

'XS

```
X_params(X_param_index, ssports * (ssfreqs - 1) + port *
(ssfreqs - 1) * ssports * (ssfreqs - 1) + freq *
ssports * (ssfreqs - 1) + q * (ssfreqs - 1) + 1 + 1) =
s(2 + (q * (ssfreqs - 1) + 1))
```

'XT

```
X_params(X_param_index, ssports * (ssfreqs - 1) + port *
(ssfreqs - 1) ^ 2 * ssports + freq * ssports *
(ssfreqs - 1) + q * (ssfreqs - 1) + 1 + 1 +
(ssfreqs - 1) ^ 2 * ssports ^ 2) = s(1 + (q *
(ssfreqs - 1) + 1) + (ssports * (ssfreqs - 1)))
```

End If

Next

Next

Next

Next

X_param_block_indices(X_param_index - 1) = blockVAR_index

X_param_index = X_param_index + 1

blockVAR_index = ET_states(ET_states.Length - 1) + 1

'Jump next loop index to next set of indepVARs

End If

End While

Appendix B: X-Parameter Uncertainty Terms

Below is a sample of the sources of uncertainty included in the evaluations presented in Chapter 5. Many of the sources in the list are repeated, for example line length uncertainty may be included for both the calibration used when measuring the DUT, and for calibrations used previously to characterise those standards. The total number of unique input sources is over 300.

TRL_CIS-C-11 short inner diameter
TRL_CIS-C-11 short outer diameter
TRL_CIS-C-11 16 mm line inner diameter
TRL_CIS-C-11 16 mm line outer diameter
TRL_CIS-C-11 16 mm line length
TRL_thru_w2p_Reproduce
TRL_shorts_w2p_Reproduce
TRL_lines_w2p_Reproduce
PMMP Match_Reproduce
ROMM
ROPU
ZSER
ZCOE
CFER
InsE
noise_Reproduce
Cable_Reproduce
CGMatch_term_Reproduce
CGMatch_unterm_Reproduce
TRL_3.5 TRL flush thru meas_Reproduce

TRL_3.5 TRL shorts meas_Reproduce
TRL_3.5 TRL 16 mm line meas_Reproduce
Phase cal_Reproduce
Power Cal_Reproduce
Inner Conductor Diameter d
Outer Conductor Diameter D
Metal Conductivity Sigma
Length of Offset
Center Conductor Pin Length
Inner Conductor Offset
Center Conductor Pin Diameter
Pin Diameter
Pin Depth
ICDiameter
OCDiameter
MetalCond
LineLength
PinDiameterP1
PinDiameterP2
PinDepthP1
PinDepthP2
PinDepthTotal
CGCHAR_MY020_Reproduce
CGCHAR_MY023_Reproduce
CGCHAR_MY113_Reproduce
CGCHAR_MY114_Reproduce
Load Resistance1
Load Inductance1
open_model_fm45
ZeroLength
CGCHAR_Combine_Reproduce
Shunt Conductance GS
Shunt Capacitance CS

Relative Dielectric Constant Air
Substrate Loss Tangent Air
CGCHAR_Scaling
CGCHAR_SFactor
CGCHAR_Theta
CGCHAR_Teflon
CGCHAR_DCres
CGCHAR_DriftCC
CGCHAR_SRaiian
CGCHAR_LAsym
CGCHAR_GAMMA
CGCHAR_AutoCor
CGCHAR_FieldPen
CGCHAR_BackRefl
CGCHAR_BeamWidth
CGCHAR_DarkCurrent
CGCHAR_SubtractOffset
CGCHAR_LowFrequency
CGCHAR_IgnoreSigMon
CGCHAR_PhaseLinearizeBeforeAvg
CGCHAR_TimeScale
CGCHAR_StageAlignment
CGCHAR_ProbeTipAlignment
CGCHAR_Combined_Reproduce
CGCHAR_BeforeCalibration
CGCHAR_Set1_Combined_Reproduce
CGCHAR_Set2_Combined_Reproduce
CGCHAR_Set3_Combined_Reproduce